NASA CR-132325

INVESTIGATION OF CHEMICAL VAPOR DEPOSITION OF GARNET FILMS FOR BUBBLE DOMAIN MEMORIES

By

P. J. Besser

T. N. Hamilton

October 1973

Prepared under Contract No. NAS 1-11446

Rockwell International Corporation

Anaheim, California

For

LANGLEY RESEARCH CENTER

NATIONAL AERONAUTICS AND SPACE ADMINISTRATION

DR. ROBERT L. STERMER, JR.

Technical Monitor
NAS1-11446
NASA Langley Research Center
Hampton, Virginia 23365

Requests for copies of this publication should be referred to

NASA Scientific and Technical Information Facility
P. O. Box 33, College Park, Maryland 20740

NASA CR-132325

INVESTIGATION OF CHEMICAL VAPOR DEPOSITION OF GARNET FILMS FOR BUBBLE DOMAIN MEMORIES

By

P. J. Besser

T. N. Hamilton

October 1973

Prepared under Contract No. NAS 1-11446

Rockwell International Corporation

Anaheim, California

For

LANGLEY RESEARCH CENTER

NATIONAL AERONAUTICS AND SPACE ADMINISTRATION

CONTENTS

ILLUSTRATIONS

ILLUSTRATIONS (Cont)

TABLES

INVESTIGATION OF CHEMICAL VAPOR DEPOSITION OF GARNET FILMS FOR BUBBLE DOMAIN MEMORIES

By P. J. Besser and T. N. Hamilton
Rockwell International Corporation

1. ABSTRACT

The objective of this program was to establish the important process parameters and control required to grow reproducible device quality ferrimagnetic films by chemical vapor deposition (CVD). Consideration was initially limited to garnet films of the form $Y_{3-z}Gd_zFe_{5-x}Ga_xO_{12}$(YGdGaIG) on $Gd_3Ga_5O_{12}$(GdGaG) substrates.

The initial phase of the program was directed toward the determination of the influence of substrate bulk and surface quality on the magnetic properties of the deposited films. These studies contributed to the establishment of acceptance criteria for substrate boules and wafers. In the course of this effort the mechanism of substrate core and band replication by the films was established.

The best CVD films of bubble domain material ever reported were grown on this contract. The thickness uniformity, compositional uniformity and defect density attained in the CVD samples were comparable to those of films grown by liquid phase epitaxy (LPE).

However, the investigation of the critical parameters in the CVD growth process has led to the conclusion that the required reproducibility of film properties cannot be achieved with individually controlled separate metal halide sources. Therefore, in the last few months of the program the CVD growth effort was directed toward replacement of the halide sources with metallic sources with the ultimate goal being the reproducible growth of complex garnet compositions utilizing a single metal alloy source.

The characterization of the YGdGaIG films showed that certain characteristics of this material, primarily the low domain wall energy and the large temperature sensitivity, severely limited its potential as a useful material for bubble domain devices. Consequently, at the time of the change from halide to metallic sources, the target film compositions were shifted to more useful materials such as YGdTmGaIG, YEuGaIG and YSmGaIG.

The metallic source work proved that uncrazed films of complex garnet compositions could be grown from a single alloy source in an open tube reactor. Unfortunately, time did not permit the optimization of deposition conditions and alloy or film compositions. Although some of the results are promising it has not yet been demonstrated that the alloy source approach is capable of providing the required reproducibility of film properties.

As a separate task on the program a 1024 bit bubble domain digital delay line with a 16μm period and read in-read out capabilities was fabricated and delivered along with a bubble domain memory exerciser.

2.0 INTRODUCTION

2.1 Background

This program was a logical extension of the work performed on an earlier contract, "Investigation of Single-Crystal Ferrite Thin Film" (Ref. 1). Some objectives of that effort were:

(1) To investigate the bubble domain properties of several theoretically promising film compositions and to determine any unique problems or advantages of their fabrication by the CVD method.

(2) To determine the necessary film/substrate matching conditions for growing uncracked, high-quality films of any film composition. A corollary of this was to determine if there was a model or basis for film/substrate matching that would apply to all or most epitaxial garnet compositions.

A wide range of film compositions in the mixed garnet system $Y_{3-z}Gd_zGa_xFe_{5-x}O_{12}$ were studied. At the conclusion of that program the composition with $z = 0.5$ and $x = 1.0$ had been selected as the preferred material. Uncrazed deposits of this composition could be grown on GdGaG which was the best available substrate material at the time. (A situation which is even more predominant today). Based on our available knowledge of the most important device requirements for bubble domain garnet material in June of 1971, it was concluded that YGdGaIG/GdGaG was a potentially useful bubble material film/substrate combination. Therefore, it was selected as the target composition for the present program. The results of Ref . 1 and other developments in the bubble domain materials technology as of late 1971 indicated that it was both timely and necessary to determine and carefully evaluate the critical process parameters and the control necessary to grow reproducible device quality films by CVD.

The bubble domain material situation as it existed in this and other laboratories prior to the start of this program was the following:

(1) A potentially useful film/substrate material combination had been identified for further development.

(2) The deposition conditions for uncrazed films with the proper composition had been established.

(3) The film/substrate lattice matching requirements had been established and were well understood (Ref. 1, 2, 3).

(4) Characterization techniques for both film and substrate evaluation had been developed and were available for use on a routine basis. (Ref. 1 and references therein).

(5) A liquid phase epitaxy (LPE) technique had been reported (Ref. 4) which quickly developed to a more convenient form (Ref. 5) and the film quality was reported to be excellent (Ref. 6).

(6) At the program start it appeared that the CVD and LPE methods were quite competitive. Either or both techniques were being examined in various labs to determine their eventual adaptability to bubble material production.

(7) It was felt that the specific material growth technique which would eventually be used would depend partly on specific device requirements and design, partly on further developments of CVD and LPE toward mass production methods, and partly on further developments in other aspects of the bubble technology.

Although the progress and accomplishments in bubble materials had been very promising, there were still problems that had to be solved and new areas that had to be investigated before the bubble-domain tecnnology could be fully realized. Some of the specific problem areas and subjects that were selected for investigation on this program are described below.

(1) Various substrate "defect" structures had been observed but, in the case of cores and bands, their influence on film properties was undetermined.

(2) The conditions for the growth of "high quality" substrates had been determined but there was no definitive criteria for specifying the quality in a quantitative fashion.

(3) The requirements on substrate surface preparation were not well defined - particularly the relationship of film defect density to substrate surface preparation technique.

(4) Chemical vapor deposition (CVD) had made important contributions to bubble memory technology. However, there were certain problems with this technique, mainly: (1) run-to-run composition control, (2) composition uniformity and (3) defect density.

(5) Material characterization techniques alone did not provide a sufficient evaluation of a material for device usage. It had been concluded that a necessary requirement for bubble domain material characterization is the evaluation of its properties in an operating device. Therefore, one phase of the contract was devoted to the development of a delay line device which would both evaluate the material and demonstrate the feasibility of device requirements for future NASA systems.

One very valuable outcome of this type of closely coupled materials-device evaluation was the conclusion that the characteristics of the YGdGaIG material were not adequate for present device requirements. As a consequence of this finding, the target material was switched to the compositions mentioned in Section 1.0 and samples of LPE material were supplied for the device work.

As a final task on the program, an improved model of a bubble domain memory exercisor developed by Rockwell International was fabricated, characterized, and delivered along with a 1024 bit, 16 μm period bubble domain digital delay line.

2.2 Report and Program Organization

The background, objectives, accomplishments and conclusions of the program are contained in concise form in Sections 1.0 to 3.0, 8.0 and 11.0. A rather complete overview and understanding of the program can be obtained from these sections. The details of the technical effort are presented and discussed in Sections 4.0 through 7.0.

Although an effort was made to avoid redundancy in the material covered in the various sections of the report, this was not always possible or even desirable. It is difficult to meaningfully discuss substrate quality and characteristics or the results of, and rationale behind, changes in film deposition conditions without describing the related film characteristics. Therefore, a certain amount of repetition or intermingling of topics was deemed desirable as making the report more readable in a continuous fashion.

The program was performed almost entirely in the Physical Sciences Department of the Electronics Research Division. Many individuals from several different groups within the department participated in the technical effort and the preparation of the report. In an attempt to assign the proper credit for the various aspects of the program, the names of the principal contributors to each section are shown in parentheses below the heading.

The Magnetic Materials Group, Group Leader: J. E. Mee, had the overall program responsibility with P. J. Besser as Principal Investigator. Film growth (CVD and LPE) and characterization were also performed in this group. The substrate growth, characterization and processing responsiblity was assigned to the Crystal Chemistry Group, Group Leader: S. B. Austerman.

The delay line and memory exercisor effort was performed in the Applied Magnetics Department, Manager: J. L. Archer. The participating groups were Magnetic Circuits, Magnetic Devices and Magnetic Systems with the respective Group Leaders R. F. Bailey, L. R. Tocci and J. E. Ypma.

The authors also wish to acknowledge the contributions of the following individuals in the areas shown:

P. E. Elkins - substrate growth and characterization

L. A. Moudy - substrate characterization

E. C. Whitcomb - LPE film growth

R. D. Henry and R. Mendoza - film characterization.

3.0 REVIEW OF EPITAXIAL GROWTH OF GARNET FILMS
(D. M. Heinz)

3.1 History

The first work on bubble domains was carried out with flux-grown orthoferrite crystals which were a few mils thick (Ref. 7). Since the preferred wafer thickness for maximum device operating margins is half the bubble domain diameter (Ref. 8), as-grown or mechanically polished orthoferrite wafers could adequately fulfill this thickness requirement. With the desire to increase storage density, bubble diameters and hence thicknesses of a fraction of a mil were needed. Magnetic garnet crystals made smaller bubble diameters possible (Ref. 9) but mechanical polishing to thin layers caused excessive breakage. A practical solution to the problem of achieving thin, highly perfect crystals has been to grow epitaxial films of the desired thickness on nonmagnetic substrate wafers.

With a background of epitaxial film growth of ferrites and garnets by CVD in this laboratory, the first known epitaxial bubble domain films were grown in April 1970. The material was gallium-substituted yttrium iron garnet (YGaIG). This breakthrough was first announced in May 1970 (Ref. 10) and a brief account appeared in Applied Physics Letters (Ref. 11). A more complete presentation was made in November 1970 at the 16th Annual Conference on Magnetism and Magnetic Materials (Ref. 12). Following these announcements of highly mobile bubbles in epitaxial YGaIG, there was a great surge of activity in epitaxial bubble garnets. In this laboratory, the CVD work continued with investigations of different film and substrate compositions. A variety of CVD garnets were also investigated at other laboratories including those at Bell Telephone, IBM, RCA, Sperry Rand, Westinghouse, Hitachi, Siemens, U. of Edinburgh and MIT (Refs. 13 to 21).

At the same 1970 Conference on Magnetism and Magnetic Materials, Bell Telephone Laboratory scientists reported on the LPE growth of orthoferrites and garnets using a "tipping" technique (Refs. 22, 4). Due to the very rapid crystal growth produced in this method, these films contained severe compositional gradients. An improved process making use of an isothermal "dipping" technique (Refs. 5, 23) subsequently became the standard LPE method because of the good bubble domain films attainable (Ref. 6) and simplicity of the growth apparatus. All laboratories now working on bubble domain materials utilize this growth technique for magnetic garnet compositions.

3.2 Uniaxial Anisotropy

In a thin plate of magnetic material, with a magnetization of $4\pi M$ and an effective uniaxial anisotropy K_u (producing an easy direction of magnetization perpendicular to the plate), a general requirement for the existence of cylindrical domains with axes perpendicular to the plate is that $K_u \geq 2\pi M^2$ (Ref. 8).

The normal source of the uniaxial anisotropy observed in magnetic materials is the crystal structure of the material. If this structure is conducive to a unique axis of magnetization, as in the hexagonal ferrites and the orthoferrites, the magnitude of the anisotropy constant may be sufficiently large to support bubble domains, (i.e. $\geq 2\pi M^2$) as in orthoferrites and in hexagonal ferrites of lowered magnetization. The basic structure of the nonmagnetic garnets is cubic. Since a material possessing a spontaneous

magnetization cannot be strictly cubic, the magnetic garnets have a slight distortion from the cubic structure. However, this slight distortion does not provide a sufficiently large value of K_u to meet the above requirement.

In magnetic garnets, observations of uniaxial anisotropy have been attributed to two types of phenomena. For one type, the effect is produced by the growth process and is attributed to a pair ordering or a site preference of the rare-earth ions in the garnet structure (Refs. 24 to 26). This growth-induced anisotropy is found in both bulk garnets and LPE films. For the other type, the effect is produced by magnetostriction (Ref. 12). Epitaxial magnetic films are normally in a state of mechanical stress due to a mismatch between lattice constants and thermal expansions of film and substrate (Ref. 2, 3). If the film is magnetostrictive, this stress produces a uniaxial magnetic anisotropy that is superimposed on the bulk, unstrained anisotropy. For a magnetic film with magnetostriction constants and stress of the proper signs, the magnetostrictive contribution tends to make the normal to the film plane an easy axis. This stress-induced anisotropy is found in epitaxial films grown by LPE or CVD.

A major difference between the induced anisotropies is that the growth-induced anisotropy can be completely annealed out, leaving the stress-induced anisotropy unaffected (Ref. 27). Since CVD garnet films are normally grown at temperatures in excess of the annealing temperature for growth-induced anisotropy, the uniaxial portion of the anisotropy in CVD films is solely stress-induced. On the other hand, the anisotropy in LPE films results from a combination of the stress-induced and growth-induced contributions.

4.0 MATERIALS FABRICATION

4.1 Substrates
(H. L. Glass)

4.1.1 Introduction. - The final report under the previous contract (Ref. 1) described in some detail the Czochralski growth of rare-earth gallium garnet single crystals and their fabrication into polished wafers suitable for use as substrates for epitaxial garnet film deposition. That report also described the various types of defects found in the substrates. The bulk defects included: faceted regions (cores), growth bands, iridium inclusions, and dislocations. The substrate polishing procedures left behind a few isolated scratches and a thin, but not well characterized, layer of residual damage. X-ray double crystal reflection topography, also described in the report, showed that the CVD epitaxial films generally replicated all substrate bulk defects and surface scratches. Some evidence was obtained to demonstrate that these replicated defects influenced the magnetic domains in the film.

In view of the existence of these substrate defects and their apparent effects on magnetic properties of the film, the present contract included in its work statement plans for more detailed analysis of defects with the objectives of establishing realistic acceptance criteria for substrate bulk and surface quality. These objectives were viewed as being crucial to the success of bubble domain devices. Therefore, during the period intervening between completion of the previous contract and inception of the present contract, research and development activities were continued under our internally funded bubble program. These internally funded activities lead to considerable progress in characterizing substrate defects and in determining procedures to eliminate them. Furthermore, early in the present contract period, GdGaG crystals of improved quality became available from two commercial suppliers, herein referred to as Vendor A and Vendor B. As a result of these developments, our crystal growth and defect characterization activities under the present contract were reduced. The activities which were continued placed increased emphasis on those defects which persist in even the best quality substrates; namely, surface damage and lattice parameter nonuniformity (growth bands). Characterization of other defects and refinement of substrate preparation techniques were continued as tasks under the internally funded program.

4.1.2 Substrate quality. - Figure 1 is an X-ray double crystal reflection topograph of a substrate wafer prepared from a boule grown in our laboratory at the beginning of the contract period. The X-ray diffraction technique by which this picture was obtained is a slight refinement of the method which was used during the previous contract for examining wafers with films (Ref. 1, 29). Although the defects revealed by topography can also be observed by other methods (optical microscopy, chemical etching), the topographic method provides a more detailed graphic display.

The wafer seen in figure 1 exhibits all of the common defects of Czochralski grown GdGaG: faceted regions (central core), growth bands, iridium inclusions (arrow), as well as a few surface scratches. Although no growth dislocations appear, there is evidence of dislocation loops surrounding the iridium inclusion (Ref. 30). Growth dislocations have been investigated in some detail (Ref. 31). These dislocations can be prevented by maintaining a crystal/liquid interface which is convex toward the melt (Ref. 32); however, in <111> growth, an excessively convex interface may lead

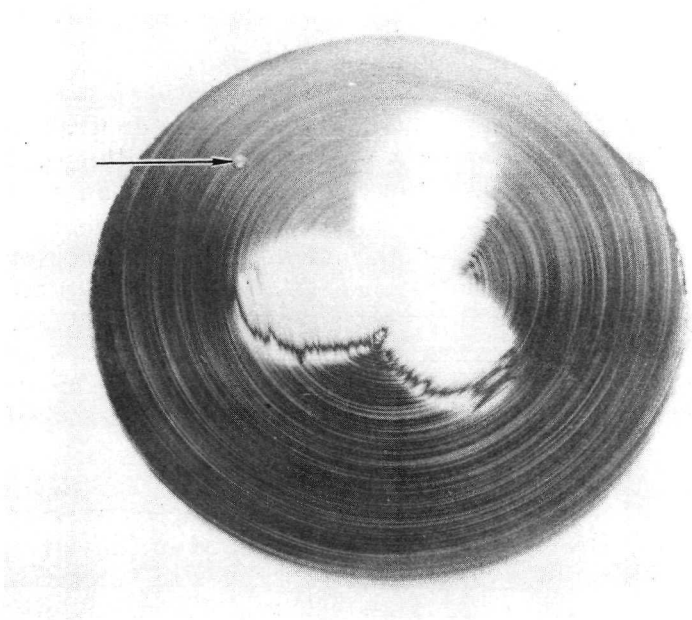

Figure 1. - (842) FeKα X-ray Double Crystal Reflection Topograph of <111> GdGaG Substrate Wafer from In-House Boule (Magnification - 6X)

to facet development (Ref. 33) which produces a core as in figure 1. A highly curved interface also results in very sharp growth bands. Interface shape is controlled mainly through boule rotation rate. The incidence of iridium inclusions can be minimized by control of thermal gradients and by using an atmosphere containing only a few percent O_2 (Ref 34).

Figures 2 and 3 are topographs of wafers representative of the materials supplied by Vendor A and Vendor B, respectively. Figure 2 indicates that the boule had been grown with a nearly flat interface, since there is no core and the growth bands are broad and diffuse. This batch of substrate wafers exhibited the least severe growth banding observed to date. Unfortunately this wafer also exhibits the rather large circular defects. These defects run the length of the boule. They are also visible by optical microscopy with crossed polarizers and by chemical etching as circular arrays of asymmetric etch pits. It is believed that these circular defects are giant helical dislocations although it is possible that they are stacks of dislocation loops. This batch of substrates was obtained from Vendor A in the form of polished wafers. A number of deep scratches are present. Profilometer measurements showed that the surface deviated appreciably from flatness; typically, a 6 μm decrease in elevation was measured between the center of the wafer and a point 6 mm from the center. This is considered to be unacceptable for device fabrication.

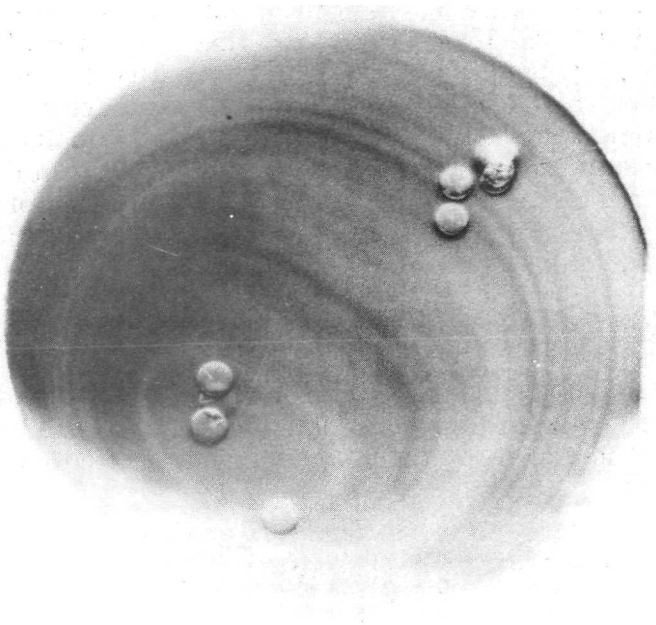

Figure 2. - (842) FeKα X-ray Double Crystal Reflection Topograph of <111> GdGaG Substrate Wafer from Vendor A. (Magnification - 6X)

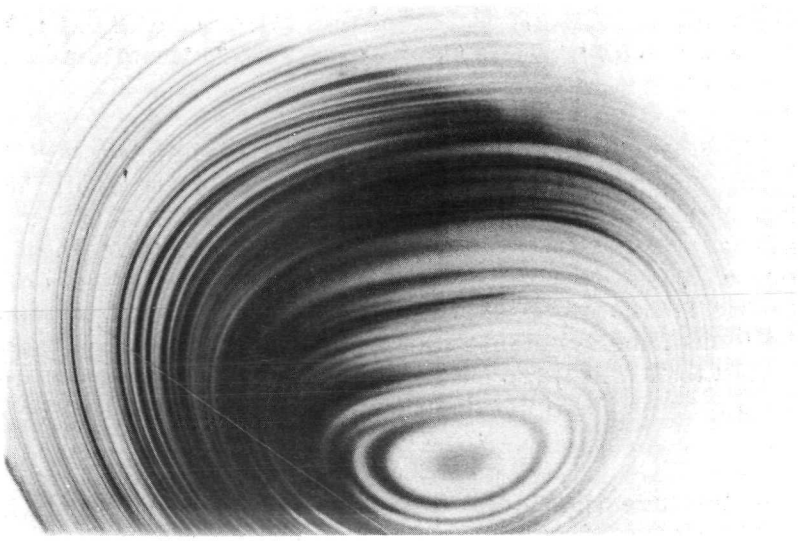

Figure 3. - (842) FeKα X-ray Double Crystal Reflection Topograph of <111> GdGaG Substrate Wafer from Vendor B. (Magnification -6X)

The wafer seen in figure 3 was polished in our laboratory from material supplied by Vendor B. The topograph shows that the material is free of faceted regions and, at this low magnification, free of obvious inclusions or dislocations. At higher magnifications a few localized defects were observed. Chemical etching and optical microscopy of wafers in this batch indicated a density of 1-5 localized defects per square centimeter. The growth banding is sharper than that seen in figure 2, but slightly more diffuse than that in figure 1. The surface of the wafer contains quite a few shallow scratches. The one very long scratch which is prominent in the figure is almost certainly due to mishandling after polishing was completed. It should be noted that this wafer was of larger diameter than those shown in figures 1 and 2 so that only a portion of the wafer is recorded in figure 3.

As has already been mentioned, and as may be inferred from figure 3, the only defects which occur with sufficient frequency to be of concern are growth bands and surface damage (including scratches). Considerable attention was focused on these two types of defects.

4.1.3 Lattice parameter variations. - Three distinct types of lattice parameter variations have been observed in Czochralski grown GdGaG; macroscopic, facet, and growth band. The macroscopic variations correspond to differences in lattice parameter from boule-to-boule and, possibly, along the length of an individual boule. X-ray powder diffraction measurements yielded lattice parameter values in the range 12.382Å to 12.383Å for the materials supplied by the vendors and values slightly less than 12.382Å for the crystals grown in our laboratory. These macroscopic variations fall within the range reported in the literature (Ref. 34) for similar single crystals.

X-ray double crystal diffraction studies of faceted regions were initiated during the previous contract and continued as part of our internally funded effort. By the combination of topography and diffraction profile analysis, it was determined that faceted regions in Czochralski grown GdGaG always have a larger lattice parameter than the unfaceted regions. The magnitude of this difference is 0.001Å to 0.002Å (Ref. 35). There also are small scale lattice parameter variations within the faceted regions.

Since the macroscopic and facet types of lattice parameter variation are preventable, they are not of great concern. However, they are more easily investigated than growth bands. Furthermore, since all three types of variation are apparently due to slight differences in composition, observations of the effects of macroscopic and facet variations will lead to a better understanding of the effects of banding. The relation between boule lattice parameter and melt composition has been investigated (Ref. 34) and the effect of the substrate mean lattice parameter on the epitaxial films is well established (Ref. 2). It was, therefore, deemed desirable to analyze the effects of faceted regions on the epitaxial films and, inferentially, the effects of growth bands.

The results of the investigation of the effects of faceted regions have been published as Ref. 36, a copy of which is appended to this report. The essential conclusions of the investigation are:

(1) The substrate faceted regions, which have a slightly larger lattice parameter than the unfaceted regions, are replicated in the film by the difference in film stress which results from the difference in film/substrate lattice parameter mismatch.

(2) As a result of the stress difference, the magnetic domain wall energy of the film is larger inside the faceted region than outside. This indicates that it would be more difficult to propagate a domain into the core than out of it and that the operating margins of bubble generators would be different in the two regions.

(3) Since growth bands in the substrate, like faceted regions, are lattice parameter fluctuations, similar effects on film properties are expected unless the banding is diffuse and/or the lattice parameter variation is small.

4.1.4 Surface damage. - The X-ray topography studies carried out under the previous contract (Ref. 1) produced some evidence for the existence of a thin damaged layer on polished substrate surfaces. The thickness of this layer was estimated to be about 1 μm. This result was not unexpected since the polishing was performed by mechanical methods. Somewhat surprisingly, the films were observed to replicate substrate defects even though the defects presumably were beneath the damaged layer.

During the present contract period, chemical etching studies of substrate surface damage were undertaken. The thickness of the damaged layer was determined by the constant etch rate method. This technique is based upon the concept that damaged surfaces etch faster than undamaged surfaces. Etch rates are determined by performing the chemical etching in a sequence of steps with measurements of the quantity of material removed being carried out between steps. The thickness of the material which must be removed before the etch rate approaches a constant value is a measure of the depth of surface damage. The precision of the determination is about ±0.5 μm. Etch rate measurements were performed on wafers from the batch which inluded the substrate shown in figure 3. The etchant was hot phosphoric acid. The results indicated depths of damage in the range of 1-2 μm. This is in agreement with the estimates from X-ray diffraction.

Improvements in polishing procedures have resulted in the preparation of flat wafers with scratch-free surfaces on a routine basis. The use of Syton (Monsanto Corp.) as the final polishing abrasive followed by rigorous cleaning produces a surface of high quality. Generally, these Syton prepared wafers receive a chemical polish in hot phosphoric acid just prior to CVD film growth. The films grown on such wafers show no evidence of magnetic defects arising from substrate surface damage. In view of this result, detailed analysis of surface damage was deemed unnecessary.

4.1.5 Acceptance criteria. - Based in part upon the work done under this contract, specifications for GdGaG boules and wafers have been developed. These criteria are realistic in terms of the quality attainable by present technology and in terms of the requirements for satisfactory yield of device quality films.

(1) Boule Specifications

a) latice parameter: 12.383 ± 0.001Å
b) boule axis: within two degrees of [111]
c) faceted regions: none
d) inclusions: maximum of one per lineal centimeter
e) dislocations: maximum of 10 per cm^2 over entire cross-section surface or maximum of 5 per cm^2 over a contiguous area exceeding one-half the total cross-section area
f) lattice parameter variations: not to exceed 0.0005Å across any boule cross-section; variations in growth bands not to exceed ± 0.0003Å

(2) Wafer Specifications

All wafers are to be prepared from boules which comply with the above boule specifications.

a) surface orientation: within two degrees of (111)
b) thickness variation: ± 25 μm
c) inclusions: none visible at 100X
d) dislocations: same as boule specification e
e) flatness of deposition surface: within one fringe of sodium light except within 0.5 mm of wafer periphery
f) finish of deposition surface: Syton polished and cleaned. Scratch-free when viewed at 120X with Nomarski interference microscope.
g) finish of reverse surface: inspection polish with Linde A abrasive or equivalent.

4.2 CVD Film Growth From Metal Halide Sources
(T. N. Hamilton, P. J. Besser, D. M. Heinz)

The growth of good quality, low imperfection epitaxial complex garnet films has been demonstrated using the CVD technique. The major problem plaguing this technique has been a lack of film composition reproducibility. Therefore the bulk of this CVD film growth effort has been concentrated on improving the film composition reproducibility.

The CVD furnaces used for this work were developed in this laboratory and have the T-type configuration as shown in figure 4. These reactors have been designed to accept a chemical charge sufficient to last for seven to eight hours which is the normal run series period. The procedure followed for a typical series is as follows: The anhydrous metal chloride chemicals are loaded into the vertical leg of the T furnace with each chemical positioned in its respective thermal zone. The reactant gases, O_2 and $HC\ell$, and the inert carrier gas, (He) are turned on so as to purge the system and achieve temperature equilibrium. After approximately one-half hour, the deposition conditions are tested. (A typical set of deposition parameters are shown in table I.) A fused silica test plate is positioned for 15 minutes in the deposition zone which is the first eight inches downstream of the crux of the T. The deposit on this plate is visually examined for proper garnet zone length and growth rate. If proper conditions exist, garnet substrates are loaded into the furnace. The substrates are positioned on a fused silica tray and placed into the upstream end of the reactor T. Five minutes are allowed for the tray and substrates to attain temperature and for the system to purge. The substrate tray is then pulled into the downstream deposition zone by a position rod manipulated from the downstream or exhaust end of the reactor tube. At the end of the deposition period, the substrate tray is pushed to the upstream end using the downstream manipulator rod. The tray is then removed from the furnace through the upstream port. Another tray is then placed in the furnace for the second deposition period. This substrate loading and unloading procedure is continued throughout the run series.

A detailed study of the deposition parameter interactions was not carried out during this contract period, due to our concentration on improving the source chemical input reproducibility of this system. A reaction parameter overview is therefore presented below.

The overall reaction which occurs in this deposition system may be written as

$$RC\ell_3(g) + ZC\ell_3(g) + O_2(g) \rightarrow R_2O_3(s) + RZO_3(s) + R_3Z_5O_{12}(s) + Z_2O_3(s) + C\ell_2(g)$$

where R is one or more of the rare earths or yttrium and Z is iron and/or gallium. (For convenience in handling, $FeC\ell_2$ is actually used as a source chemical rather than $FeC\ell_3$ but the iron is readily converted to the higher oxidation state.) The solid reaction products will grow epitaxially on appropriate seed crystals when these crystals are positioned in the appropriate growth zone and will deposite as polycrystalline material on the fused silica reactor tube and substrate holders. The reaction products deposit in orderly zones with decreasing rare earth content as shown in figure 5. (The position of the support tray, and a substrate for garnet deposition are also shown.) The length and position of each of the product zones is largely controlled by the ratio of the iron and gallium chlorides to the rare earth chlorides ($FeC\ell_2$+$GaC\ell_3$/$RC\ell_3$) introduced into the reaction. As this ratio decreases, the tendency toward the deposition of ortho-

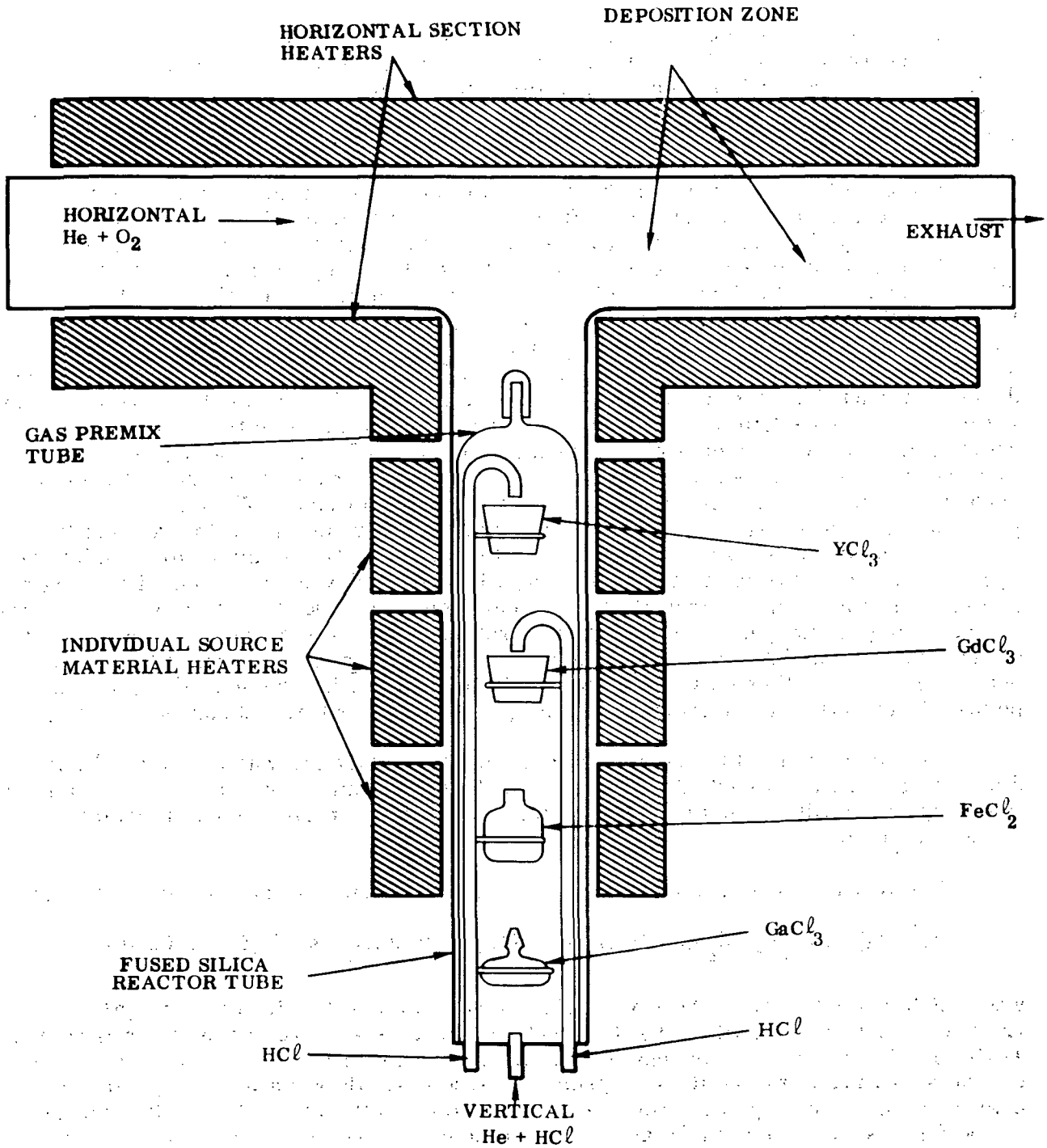

Figure 4. – Standard "T" Reactor

TABLE I. – TYPICAL DEPOSITION CONDITIONS FOR YGdGaIG IN A STANDARD T REACTOR USING FOUR CHLORIDE SOURCES

Chemicals/Parameters	Transport Rates cc/min	gm/hr	Temperature °C
$GaC\ell_3$	4.2	2.0	190
$FeC\ell_2$	23.3	8.0	925
$YC\ell_3$	1.3	0.7	1050
$HC\ell$ over $YC\ell_3$	150		
$GdC\ell_3$	0.3	0.2	1000
$HC\ell$ over $GdC\ell_3$	50		
He Vertical	14,500		
$HC\ell$ Vertical	250		
Deposition Temperature			1150
He Horizontal	4,775		
O_2 Horizontal	55		
Deposition Rate	6 μm/hr		

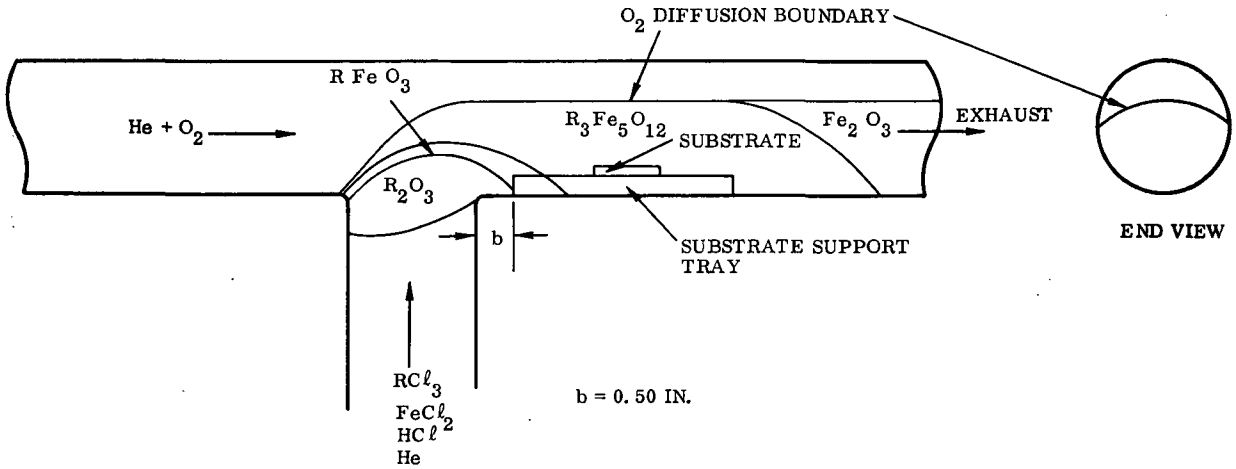

Figure 5. — Product Zone Configuration With Deposition Conditions Adjusted for Garnet Growth

ferrites ($RFeO_3$) and R_2O_3 increases. As the ratio increases, the tendency is toward the deposition of increasing amounts of garnet and iron oxide. By adjusting this ratio, conditions can be established for the growth of garnet or orthoferrite films without substantial changes in any other growth conditions.

Oxygen, $HC\ell$ and He flow rates are adjusted to control the garnet growth rate and to position the garnet product zone at the film deposition zone. The $HC\ell$ flow also inhibits the premature reaction of the very reactive rare earth chlorides. Good garnet growth conditions can be established using a wide range of O_2 flow rates when the O_2 flow is compensated for with an appropriate $HC\ell$ flow rate. An increase in the O_2 flow will cause the product zones to shift in an upstream direction and/or may cause excessive Fe_2O_3 to deposit in the deposition zone. Good deposition conditions may again be established with an increase in the $HC\ell$ flow. An $HC\ell$ flow increase will cause the product zones to move in a downstream direction and reduce the amount of Fe_2O_3 deposition. Changes in the O_2 and $HC\ell$ flows may require small compensating changes in the source chemical inputs to re-establish a desired garnet composition.

The garnet deposition temperature is primarily determined by the reactivity of the source chemicals involved. From free energy considerations, the very high reactivity of the rare earth chlorides with O_2 at lower temperatures dictates that a deposition temperature near 1200 C be used. At these elevated temperatures the $FeC\ell_2$ reactivity is substantially lower than the reactivity of the rare earth chlorides. To compensate for the reactivity difference, a high $FeC\ell_2/RC\ell_3$ chemical transport ratio is required to establish garnet growth conditions. As the deposition temperature is lowered from

1100°C, the transport ratio must be reduced, even to maintain a shrinking garnet product zone. As the deposition tempe rature is raised from 1100°C, the transport rates must be increased to maintain reasonable garnet growth rates. The optimum growth temperature region has therefore been determined to be between 1075 and 1175°C. At these temperatures, the garnet deposition zone length can be maximized without requiring excessive source chemical transport rates.

Many garnet films of near identical film thickness are required for device applications. A large constant growth rate garnet zone is therefore necessary for the deposition of garnet films on several GdGaG substrates during one deposition period. The garnet growth rate will gradually decrease, in a downstream (horizontal) direction, over the length of the garnet deposition zone due to the consumption of reactant chemicals. The growth rate will also decrease from the O_2 diffusion boundary in a downward (vertical) direction. The combination of these two growth rate trends results in a decreasing growth rate in a downward downstream direction as shown in figure 6. Consequently the horizontal substrate support configuration shown in figure 5 is not conducive to good thickness uniformity along the flow direction. However, a three-inch long constant growth rate zone has been achieved with the use of a 18 deg tilted substrate trav. Uniform thickness garnet films have been grown on GdGaG substrates placed on the 18 deg tilted tray with the downstream end of the tray tilted up as shown in figure 7.

The area of film thickness uniformity is one factor which determines the usable area of any single wafer for device applications. The smooth flow of deposition gasses over the GdGaG substrated is disturbed by the substrate edges causing turbulence which results in an increased growth rate and thickness buildup at the film edges. Recessing the substrates in an alumina plate has been successful in eliminating the edge thickness buildup. A small decrease in the garnet growth rate over the entire substrate surface also results with the use of the recessed holder.

Composition reproducibility in a standard T-type reactor is dependent on the control over the evaporation rates of the metal halide source materials. In the initial YGdGaIG growth experiements, four metal halide sources were stacked in the vertical leg of a standard T reactor (figure 4). Each halide source was positioned in an individual thermal zone. The use of four metal halide sources, $YC\ell_3$, $GdC\ell_3$, $FeC\ell_2$ and $GaC\ell_3$, required a wide range of source temperatures: The highest temperature of 1050°C was for $YC\ell_3$ and the lowest of 190°C was for $GaC\ell_3$. Control over the evaporation rate (transport rate) of each of the source chemicals was dependent on the thermal zone uniformity, thermal zone separation and temperature reproducibility. These source temperature requirements were not achieved using the standard T reactor; therefore, composition reproducibility was less than ideal.

A modified T furnace was designed and built to satisfy the metal halide source material thermal requirements. As shown in figure 8, this furnace has four vertical chambers, each separately controlled and thermally isolated. One of the four vertical chambers is a low temperature region (wire wound resistor heaters) for the control of $GaC\ell_3$. The other three vertical chambers are high temperature regions (silicon carbide glo-bar heated) for the control of $YC\ell_3$, $GdC\ell_3$ and $FeC\ell_2$ source chemicals. Successful garnet deposition conditions were established in this new furnace for the growth of YGdGaIG films using four halide source chemicals. (See table II).

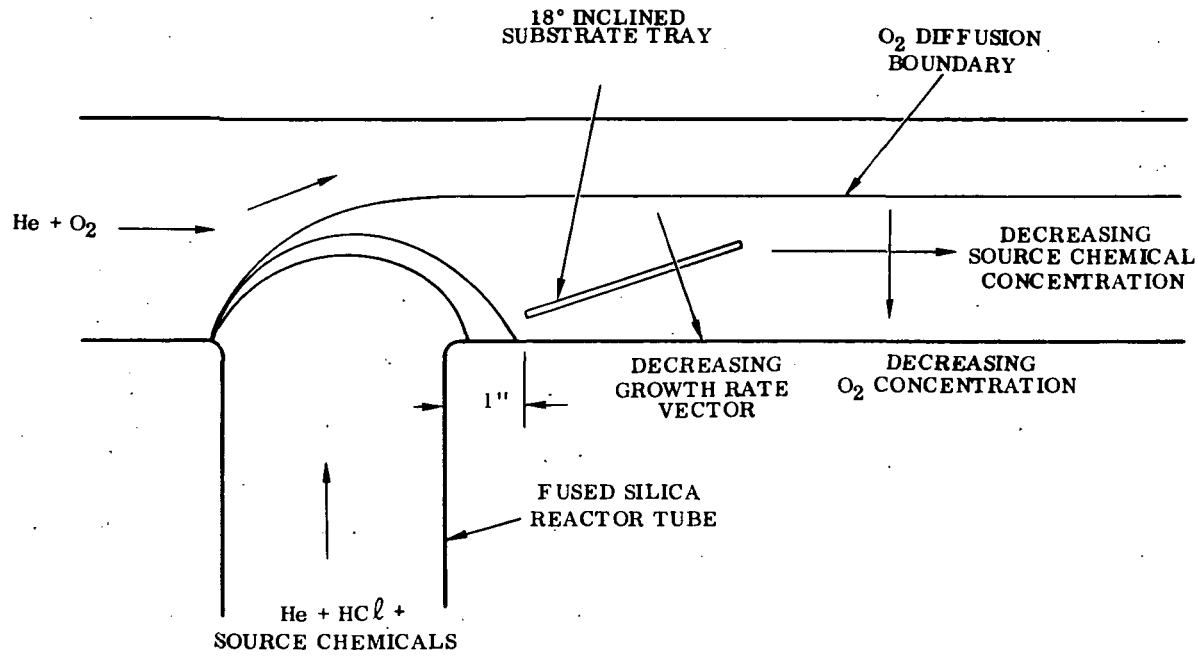

Figure 6. – Factors Affecting Growth Rate in a "T" Reactor

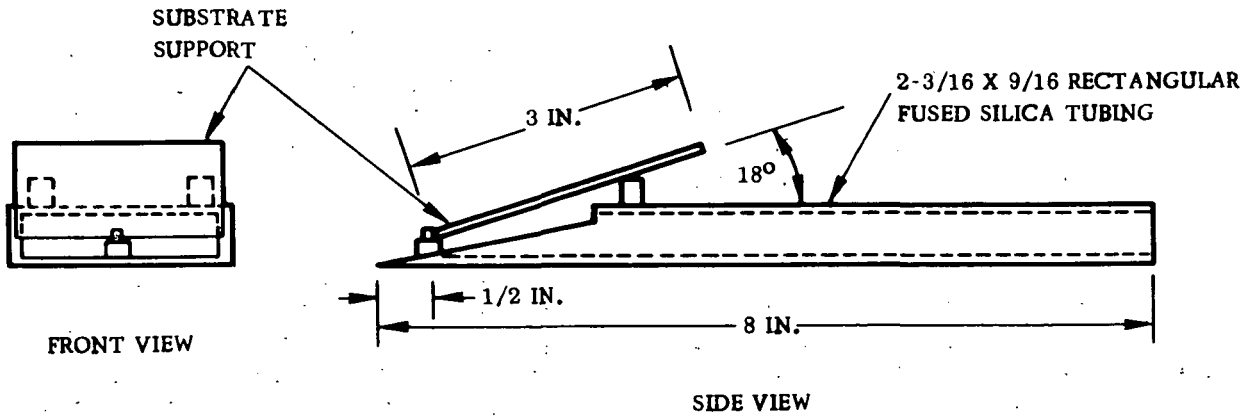

Figure 7. – Inclined Substrate Tray

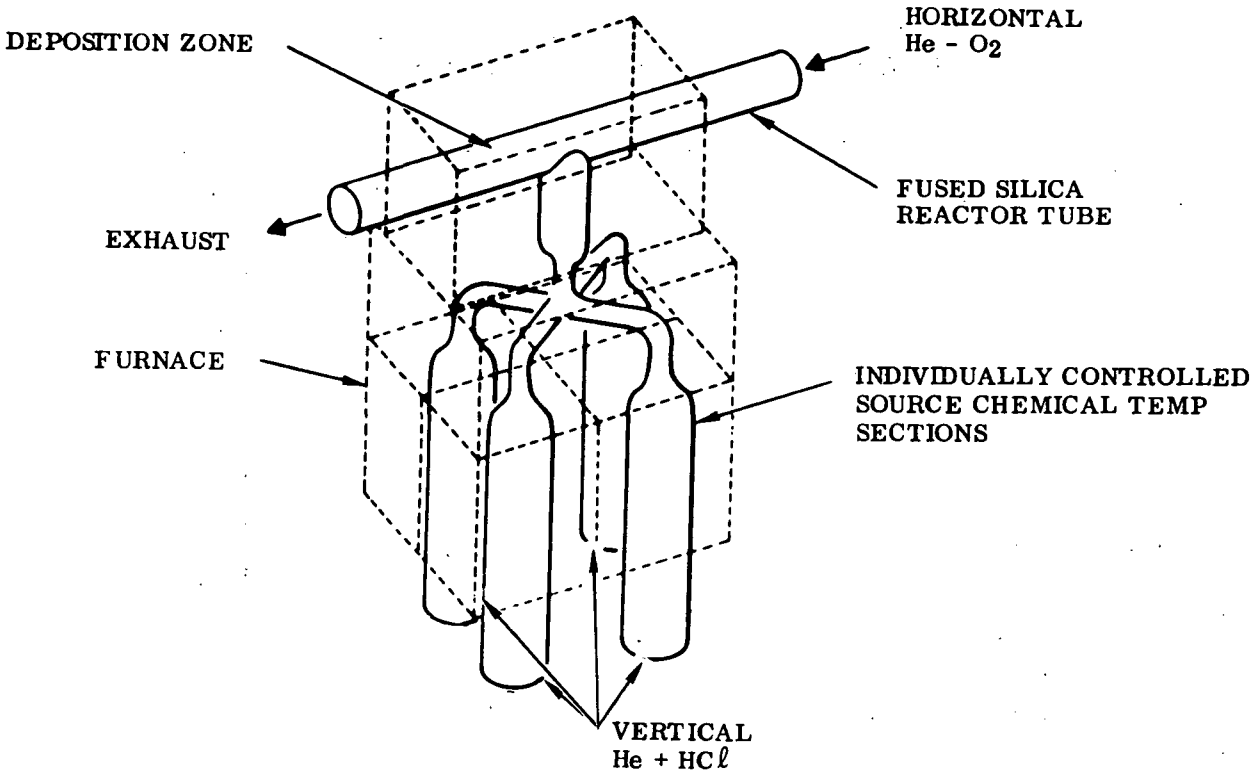

Figure 8. – Four-port "T" Reactor

A problem which arose as a direct result of the furnace redesign was a film compositional gradient transverse to the flow of deposition gases. Films grown during these growth experiments had compositional gradients with the gallium content increasing toward the right side of the deposition zone (looking downstream). The gallium chloride source was also located on the right side of the furnace. The compositional gradient was therefore judged to be due to poor source chemical gas mixing. To solve this malady, the fused silica reactor tube was redesigned to incorporate a gas mixer as shown in figure 9. The secondary gas mixer section was previously the only mixing area. The innovation is the addition of the primary mixing section. This primary mixer was positioned in the reactor tube where the source gases are brought together. Better gas mixing was achieved which resulted in improved compositional uniformity. Typical results before and after the incorporation of the mixer are described in Section 5.1. A side effect of the incorporation of this mixer was the tendency of the gallium source orifice (2mm I.D.) to plug after about one week of operation. This plugging was prevented by purging the reactor overnight with HCℓ. There were no noticeable deteriorations effects on the deposition conditions due to this purge.

After many deposition experiments, it became evident that adequate control over the evaporation rate of the low temperature volatile $GaC\ell_3$ could not be achieved. Some typical film property reproducibility data using an all chloride source system, is in Section 5.1, table VIII.

TABLE II. – TYPICAL DEPOSITION CONDITIONS FOR YGdGaIG IN THE FOUR PORT FURNACE USING FOUR CHLORIDE SOURCES.

Reactor Section	Chemicals	cc/min	°C	gm/hr
Port No. 1	$GaC\ell_3$	4.2	190	2.0
	$HC\ell$ Vertical	100		
	He Vertical	2650		
Port No. 2	$FeC\ell_2$	23.3	925	5.0
	$HC\ell$ Vertical	100		
	He Vertical	5000		
Port No. 3	$YC\ell_3$	1.3	1050	0.7
	$HC\ell$ over $YC\ell_3$	150		
	He Vertical	2650		
Port No. 4	$GdC\ell_3$	0.3	1000	0.2
	$HC\ell$ over $GdC\ell_3$	50		
	He Vertical	2650		
Horizontal Section	O_2 Horizontal	55		
	He Horizontal	6000		
Deposition Temperature			1150	

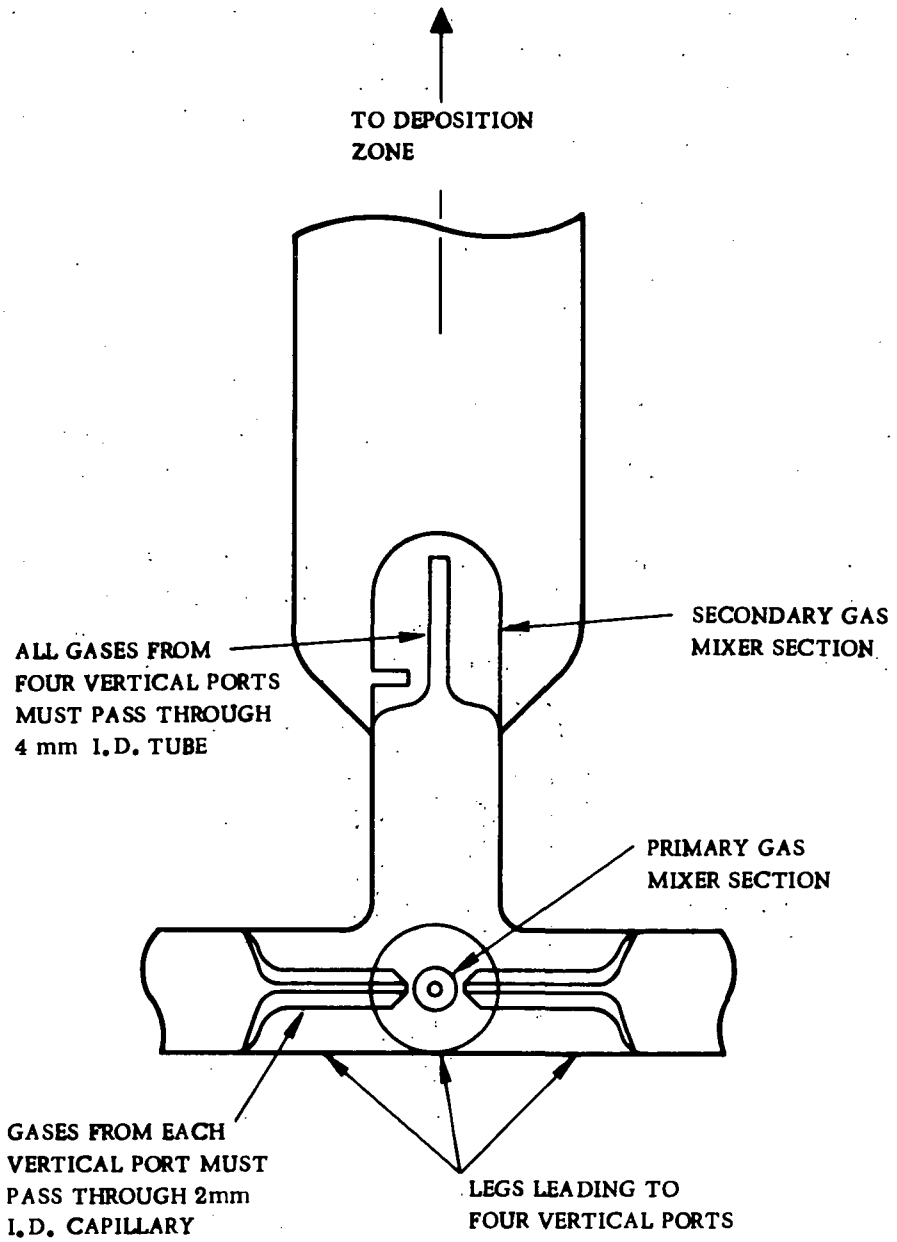

Figure 9. —Gas Mixer Installed in Four-Port Furnace

The gallium source section of the four port furnace was modified to facilitate the in situ production of $GaC\ell$ (Ref. 37) using gallium metal and $HC\ell$ gas. Gallium metal was placed in a fused silica container and positioned in a 900 °C chamber where $HC\ell$ gas was injected over the molten metal as shown in figure 10. The $HC\ell$ gas flow was accurately controlled by an Applied Materials Mass Flow Controller. Using this technique the rate of $GaC\ell$ production was relatively unaffected by small temperature fluctuations. The control over the $GaC\ell$ input into the reaction was greatly improved using this in situ production technique.

Over a period of several hours of run time, the transport rates of $FeC\ell_2$ and $YC\ell_3$ would gradually decrease due to the partial depletion of these chemical charges, thereby causing a gradual reduction in the iron and yttrium content of the deposited YGdGaIG films. Programmers were installed on the $FeC\ell_2$ and $YC\ell_3$ temperature controllers which would increase these source temperatures over the period of the run. The temperature program rates which best compensated for the $FeC\ell_2$ and $YC\ell_3$ chemical charge loss were 1.25 and 1.5 C/hr., respectively. The use of these temperature programmers and in situ $GaC\ell$ production resulted in an improvement in film property reproducibility. Examples of film reproducibility before and after these changes are presented in Section 5.1.

Despite the improvements in run-to-run reproducibility of CVD films using metal halide sources, the modified T with programmer controls did not provide adequate compositional control for device needs. Thus the use of individual source chemicals was abandoned in favor of a single, pre-mixed chemical source.

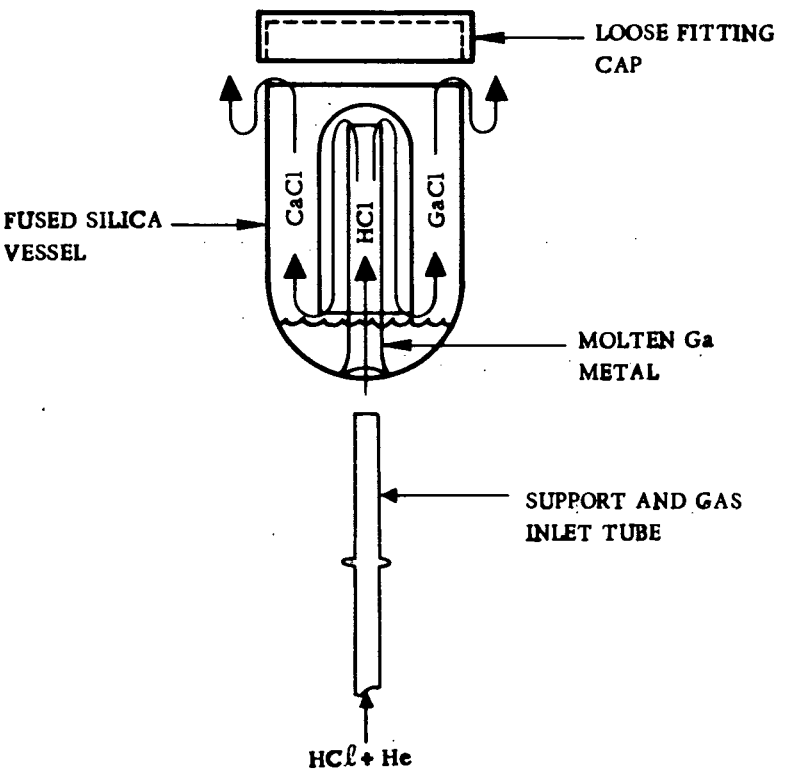

Figure 10. – In Situ $GaC\ell$ Production Vessel

4.3 CVD Film Growth from Metal Alloy Sources
(T. N. Hamilton, P. J. Besser, D. M. Heinz)

Critical control of the evaporation rates from several sources has been the unattainable requirement for reproducible CVD films. Reduction in the number of sources would reduce the number of critical controls required. As the ultimate reduction, a single chemical source which yielded the necessary concentration of the constituent chemicals would eliminate the difficult problem of maintaining constant evaporation rates from multiple sources.

As a first step toward reducing the number of sources, experiments were carried out some years ago in this laboratory (Ref. 1, p. 37) and elsewhere (Ref. 13) utilizing a mixture of rare earth halides in a single source crucible. The concept was to rely on the relative concentrations and partial pressures to maintain a constant transport ratio. Unfortunately, noticeable fractionation occurred in the course of several runs which caused the film composition to shift with time. Thus this technique cannot be employed unless the constituents have similar vapor pressures at the source temperature.

Recent CVD work at MIT has made use of a single source (Ref. 21). In this case, the source is an alloy which is attacked by a regulated flow of $C\ell_2$ to produce volatile chlorides of the garnet constituents in the same manner as gallium was used to produce $GaC\ell$. The transport rates are not temperature dependent and the relative rates are fixed by the alloy composition. Transport rates are constant for long runs provided that the alloy is homogeneous. Since the alloy may be made up of a number of elements, the deposited garnet may be quite complex. Although the reported alloy work was performed at reduced pressures, no problems were anticipated in adapting this technique to our atmospheric pressure system. Garnet deposition experiments using metal alloy sources were carried out in a standard T reactor (figure 4) using the run procedures previously described. A Tylan Mass Flow Controller was added to the reactor gas control system, to control the $HC\ell$ or $C\ell_2$ gas flow directed over the alloy source. The metal alloy sources were contained in fused silica crucibles similar to those used for the gallium metal source (figure 10). These quartz crucibles were adequate when used at temperatures above 1100°C but were subject to attack and breakage, by unevaporated chlorides, when temperatures below 1100°C were used.

The metal alloys were vacuum arc melted at the Science Center Division of Rockwell International. Inverting and remelting each alloy 12 times was the procedure used to achieve the desired melt homogeniety. In the course of developing techniques for making these alloys, some but not all these were prepared to within ±0.1 wt. % of our composition and homogeniety specifications. The preparation of the metallic constituents before melting and the handling of the alloys after melting was carried out in inert atmosphere glove boxes to minimize the oxidation of the rare earth metals. (A comparable procedure is necessary for handling the anhydrous metal chlorides previously used.) When oxidation occurred it resulted in the creation of a $ROC\ell$ powder residue in the fused silica crucible after each deposition experiment. This $ROC\ell$ powder residue can cause film imperfections if carried in the gas stream to the seed surfaces.

Chlorine gas was found to be more efficient at reacting with the metal alloy sources and inhibiting the oxidation of the metal chlorides than was $HC\ell$ gas. Therefore, $C\ell_2$ rather than $HC\ell$, was used in these alloy source deposition experiements. Due

to this greater efficiency, a considerable reduction in the vertical $C\ell_2$ flow and a considerable increase in the O_2 flow, compared with the $HC\ell$ and O_2 flows previously used, was required to achieve garnet growth. These new conditions, as listed in table III were used for the first series of depositions using metal alloy sources. These conditions were used for the growth of epitaxial YIG, YEuGaIG and YGdTmGaIG films on GdGaG substrates.

The YEuGaIG films grown, using YEuGaFe source alloys, were deficient in europium and gallium content. The films were severely crazed due to the lattice mismatch caused by the europium deficiency. The deficiency of europium in the deposited films was found to be due to insufficient europium in the metal alloy source material (table IV). The europium metal would boil off during arc melting with the other alloy constituents, due to its boiling point being lower than the melting points of yttrium or iron (table V). Pre-melting the europium and gallium together was unsuccessful in preventing the loss of europium during vacuum arc melting with yttrium and iron. The YEuGaIG growth experiments were terminated due to the inability to fabricate an adequate alloy source material in the available contractual time period.

Epitaxial YGdTmGaIG films were grown using the deposition conditions listed in table III with YGdTmGaFe source alloys No. 1 and No. 2. These films were also low in gallium content as was experienced with the YEuGaIG depositions. Efforts to increase the gallium content of the films by simply increasing the gallium content of the alloy source were unsuccessful. The limit to the amount of gallium that would remain alloyed with the other alloy constituents, at the source temperature of 1150 °C, was exceeded with YGdTmGaFe alloy No. 2. A new set of deposition conditions were therefore sought which would allow more gallium to be incorporated in the films with less gallium required in the source alloy. These deposition conditions are listed in table VI. The incorporation of more gallium in the deposited films, using these new deposition conditions, results from the reactivity of $FeC\ell_2$ being more responsive to parameter changes than the reactivity of $GaC\ell$. The decreased O_2 concentration therefore resulted in less iron being incorporated in the films.

Two YGdTmGaFe alloys (No. 3 and 4) were fabricated with reduced gallium content (table IV). Successful YGdTmGaIG depositions were made using these alloys with the deposition conditions shown in table VI. Under these deposition conditions, small adjustments in the O_2 flow rate were made to achieve the required film gallium content.

Depositions of YSmGaIG films on GdGaG substrates were also made using a YSmGaFe metal alloy with the conditions shown in table VI. These films had excessive samarium content due to excessive samarium in the metal alloy (table IV). Insufficient time remained to adjust the composition of this alloy for further experimentation.

The detailed characteristics of the films grown from these metal alloy sources and the relationship of film properties to the deposition conditions are covered in Section 5.0. In summary, it has been possible to obtain uncrazed deposits of complex bubble domain garnet compositions using the metal alloy sources. Time did not permit the optimization of alloy compositions or deposition conditions to the point where the question of compositional reproducibility from an alloy source could be definitely answered one way or another.

TABLE III. – INITIAL DEPOSITION CONDITIONS USING METAL ALLOY SOURCES

Deposition Parameter	Flow Rate cc/min.	Temperature ^{o}C	Transport Rate gm/hr
Alloy Temperature		1150	
Alloy Transport Rate			~5.0
$C\ell_2$ over Alloy	30		
He over Alloy	200		
$C\ell_2$ Vertical	60		
He Vertical	14,000		
Deposition Temperature		1150	
O_2 Horizontal	1,300		
He Horizontal	5,700		
Deposition Rate		6μm/hr.	

TABLE IV. – COMPOSITION OF METAL ALLOY SOURCES

	Element	Alloy Requested wt %	Chemical Analysis wt %
YFe No. 1	Y	90.0	
	Fe	10.0	Not Requested
YEuGaFe No. 1	Y	7.6	7.6
	Eu	2.4	.1
	Ga	15.6	16.4
	Fe	74.4	76.0
YEuGaFe No. 2	Y	6.2	5.9
	Eu	1.9	0.3
	Ga	21.9	22.1
	Fe	70.0	71.7
YGdTmGaFe No. 1	Y	3.0	3.0
	Gd	1.9	1.7
	Tm	5.8	6.0
	Ga	21.3	21.2
	Fe	68.1	68.2
YGdTmGaFe No. 2	Y	2.8	2.5
	Gd	2.9	2.6
	Tm	5.0	7.3
	Ga	26.3	30.0
	Fe	63.1	57.7
YGdTmGaFe No. 3	Y	2.9	2.7
	Gd	2.9	2.5
	Tm	5.0	4.9
	Ga	18.2	15.6
	Fe	71.0	74.4
YGdTmGaFe No. 4	Y	4.3	3.9
	Gd	6.9	7.0
	Tm	9.9	10.0
	Ga	15.2	15.2
	Fe	63.7	63.8
YSmGaFe No. 1	Y	8.7	
	Sm	2.6	
	Ga	17.0	Not Requested
	Fe	71.7	

All rare earth metals were 3N+ pure with respect to rare earth impurities. The Fe and Ga were 4N pure with respect to any impurities.

TABLE V. - MELTING AND BOILING POINTS OF ALLOY SOURCE CONSTITUENTS

Metal	Melting Point (^{o}C)	Boiling Point (^{o}C)
Ga	30	2237
Eu	826	1439
Fe	1536	3000
Y	1509	2927
Tm	1545	1727
Gd	1312	3000
Sm	1072	1900

TABLE VI. - IMPROVED DEPOSITION CONDITIONS USING METAL ALLOY SOURCES

Deposition Parameter	cc/min.	^{o}C	gm/hr.
Alloy Temperature		1150	
Alloy Transport Rate			~5.0
Cl_2 over Alloy	30		
He over Alloy	200		
Cl_2 Vertical	20		
He Vertical	14,000		
Deposition Temperature		1150	
O_2 Horizontal	75		
He Horizontal	6,500		
Deposition Rate	6μm/hr.		

4.4 LPE Film Growth
(R. G. Warren)

The liquid phase epitaxy (LPE) magnetic garnet film growth as done in this laboratory is essentially the isothermal method first reported by Levinstein et al. (Ref. 5). This utilized the $PbO-B_2O_3$ flux system and deposition occurs while the melt is held at a temperature lower than the saturation temperature.

The equipment used for LPE film growth is as follows. The melt is contained in a 250 ml platinum crucible which rests on a pedestal in the geometric center of the furnace. The furnace is a modified laboratory three-zone diffusion furnace that will accommodate a 4-1/2 in. O.D. alumina liner. The furnace sits in the vertical position. The three zone furnace feature permits control of the temperature profile of the melt as well as the substrate preheat zone located above the melt. A platinum baffle is positioned approximately half way between the melt surface and the top of the furnace where an alumina top baffle is located. These baffles minimize heat loss out of the top opening of the furnace. Both of the baffles have holes through their center large enough to allow passage of the substrate and holder through to the melt for deposition.

Located at the top opening of the furnace is an exhaust scavenger unit to prevent escape of the toxic PbO vapors into the work area. The above equipment is positioned just below the work surface of a class 100 laminar flow clean bench and access to the furnace is through an opening in the clean bench table top thus providing a clean environment for substrates and films both before and after film growth. A unit which provides mechanical action to insert and withdraw the substrate in and out of the melt and also to provide rotation of the stubstrate during film growth is attached to the side of the laminar flow unit.

The melts are prepared from the appropriate oxides for the desired film composition. Several of the melt component molar ratios must be carefully controlled to provide films of the proper composition and quality. The molar ratio $\frac{Fe_2O_3}{(RE)_2O_3}$ controls the particular phase that will be deposited. If the ratio is too small some orthoferrite phase is present in the films and results in film defects. A ratio that is too great will produce a magnetoplumbite phase. In the above ratio the $(RE)_2O_3$ indicates the rare earth oxides as well as Y_2O_3. A ratio range which provides good garnet film quality is 20-25 to 1. Also to be considered are the film/melt distribution coefficients of the rare earth and gallium ions for the specific flux system. None of the values are unity although under our deposition conditions most of the values for the rare earths are close to one. If the desired composition contains gallium, the value of $\frac{Fe_2O_3}{Ga_2O_3}$ is approximately 12 and is strongly affected by film growth rate. The solute concentration,

$$\frac{(RE)_2O_3 + Fe_2O_3 + Ga_2O_3}{(RE)_2O_3 + Fe_2O_3 + Ga_2O_3 + PbO + B_2O_3}$$

primarily controls deposition temperature for a specific degree of supersaturation and a typical value is 0.09 or 9 mole percent. The $\frac{PbO}{B_2O_3}$ ratio used is the 50:1 weight ratio or an approximate mole ratio of 16:1. The constituent oxides are weighed and premelted

into the crucible. The crucible is then placed in the LPE furnace and heated at 1200°C for a minimum of four hours to insure total solvation as well as obtaining melt homogeneity. The temperature is then decreased and the saturation temperature determined. For the above ratios this temperature is approximately 925°C. Deposition is generally performed at a temperature 8°C below the saturation temperature.

A typical growth sequence is described below. The polished GdGaG substrates are cleaned with hot detergent in an ultrasonic bath, rinsed in hot deionized water and blown dry in filtered N_2. About 8μm of substrate material is then removed from the surface in a molten salt bath of $PbO-B_2O_3$. This results in a very clean damage-free surface. The wafer is placed in a precleaned platinum holder which supports the sample in a horizontal position. The substrate is lowered into the furnace slowly to avoid thermal shock until it is one inch above the melt surface where it is held for approximately one minute to thermally equilibrate. The substrate is then lowered into the supersaturated melt and substrate horizontal rotation begun in the range of 30 to 100 RPM. This rotation insures uniform film thickness and composition across the substrate except for about a 1/8 in. border, which is wafer edge effect. Deposition is continued in this manner until the desired film thickness is obtained. Typical growth rates are 0.2 to 0.3μm per minute for a total deposition time in the order of 15 minutes. At the end of deposition the substrate is raised just above the melt surface and spun at near 300 RPM to throw off any flux still remaining. The sample is then slowly raised out of the furnace, again avoiding thermal shock, and allowed to cool. The sample, still in the holder is placed in a hot 50-50 acetic acid-H_2O solution and then in 20 percent nitric acid solution to clean and remove retained flux. The sample is finally washed in hot deionized water and blown dry.

5.0 FILM CHARACTERIZATION
(P. J. Besser and D. M. Heinz)

The previously mentioned intimate relationship between growth conditions/techniques and film characteristics is clearly evident in the organization of this section. It has seemed most convenient and logical to separate the discussion of film characterization into three major categories depending upon the growth technique utilized. The most extensive discussion is devoted to the characteristics of deposits grown in the multiple source reactor. These deposits were the YGdGaIG composition and each cation was supplied from a separate source cup. Initially, all the sources were metal halides but the previously described conversion to Ga metal was made part way through the program. The second category of film characterization deals with the deposits grown from a single metal alloy source. The compositions grown in this phase of the program were YIG, YEuGaIG, YSmGaIG and YGdTmGaIG. The final category is the properties of the LPE films grown for the delay line development effort. Film materials studied were YGdTmGaIG and two compositions of YEuTmGaIG. As a sub-topic of the LPE evaluation, the variable temperature characteristics of some bubble materials were considered to provide the basis for selection of suitable compositions for the alloy source work.

The various film parameters determined are listed in table VII along with the technique by which they were obtained and the glossary of symbols used.

An excellent review and description of characterization techniques for bubble materials has been published by Shaw (Ref. 38). All of the techniques mentioned in table VII are discussed in that report and in Ref. 1.

The primary parameters which were used to monitor the run-to-run and day-to-day changes of film properties are domain observations (usually w), film thickness, Neel temperature and film-substrate lattice mismatch. The Ga content of the film can be determined from T_N and in conjunction with the $\Delta a^{\perp}$ measurement, published lattice constant data and a simple stress model (Ref. 2, 3), this information allows one to calculate the film composition of a gallium substituted iron garnet with no more than two different rare earth ions. (Although it is not strictly correct to do so, yttrium is classified as a rare earth ion throughout much of the report). Examples of this procedure for obtaining composition are given in the final report of the previous contract (Ref. 1). Electron beam microprobe analysis was also used to determine film compositions, particularly those of the YGdTmGaIG material.

5.1 CVD Films Grown from Individual Cation Sources

In the CVD growth of complex metal oxides there is frequently a variation in film thickness and composition along the direction of gas flow. However, the early deposits of YGdGaIG also showed an unexpected variation in domain size transverse to the flow direction. Neel temperature measurements on opposite sides of films with a non-uniformity of w transverse to the flow direction showed that T_N was considerably lower on the side having the larger domains, indicating a higher Ga content, hence lower $4\pi M_S$ there. Invariably the domain size was larger on the side of the reactor from which the $GaC\ell_3$ was introduced so that it appeared that improved source material mixing was required. Under the initial growth conditions, some h and w variation along the flow direction was also evident. Examples of the variations observed is shown in figures 11 and 12. The sample designation in the figures is one adopted internally to identify

TABLE VII. – FILM PARAMETERS AND CHARACTERIZATION METHODS

Parameter	Symbol	Units	Measurement Technique
1. Thickness	h	microns (μm)	Infrared interference
2. Thickness uniformity	-	-	Photograph fringe pattern under monochromatic light, $\lambda = 5890$Å
3. Demagnetized domain width	w	microns (μm)	Photomicrograph of domain pattern
4. Bubble collapse field	H_{col}	oersteds (Oe)	Domain observations-polarizing microscope with calibrated field coils
4a. Collapse field spread (normal to hard bubbles)	δH_{col}	oersteds (Oe)	Domain observations-polarizing microscope with calibrated field coils
5. Magnetization	$4\pi M$	Gauss (G)	Calculate from h, w, H_{col} and domain theory
6. Characteristic length	ℓ	microns (μm)	Calculate from h, w, H_{col} and domain theory
7. Wall energy	σ_w	ergs/cm^2	Calculate from h, w, H_{col} and domain theory
8. Defect density	-	no./cm^2	Oscillating bias field technique
9. Neel temperature	T_N	^oC	Variable temperature AC optical modulation
10. Exchange constant	A	ergs/cm	Calculate from T_N and FMR measurements of A in YGaIG.
11. Anisotropy constant	K	ergs/cm^3	Calculate from $\sigma_w = 4(AK)^{1/2}$
12. Film-substrate lattice mismatch, $(a_s^{\perp} - a_f^{\perp})$	$\Delta a^{\perp}$	Angstroms (Å)	X-ray diffraction rocking curves, double crystal diffractometer
13. Film Lattice constant	a_f	Angstroms (Å)	Calculate from $\Delta a^{\perp}$ and stress model (Ref. 3).
14. Bubble domain velocity	v	cm/sec	Bubble translation in a field gradient.
15. Coercive force	H_c	oersteds (Oe)	Calculate from threshold field for bubble translation.
16. Composition	-	-	Determine from T_N, $\Delta a^{\perp}$ and literature data; also electron beam microprobe analysis.

TABLE VII. (CONT)

Parameter	Symbol	Units	Measurement Technique
17. Compositional uniformity	-	-	Measure T_N,H_{col} and w at several locations-calculate $4\pi M$, ℓ and σ_w.
18. Domain Wall Mobility	μ_w	cm/sec/Oe	Take slope of velocity-field characteristic.
19. Field difference across a domain diameter	ΔH	oersteds (Oe)	Calculate from geometry of field-producing conductors and the domain size.

the reactor used, the run number and the location of the seed in the deposition zone. The first digit identifies the CVD reactor which in this case is the four port reactor No. 4. The next three digits are reserved for run (deposition) numbers; e.g., 4-001 is the first deposition in reactor 4. The suffix digit designates the location of the seed in zones of the garnet growth region. Each zone is 1 in. long and is measured from the front of the substrate support tray. (See figure 5) For example, 4-001-2 and 4-001-5 would be samples placed 2 in. and 5 in. from the front of the support tray during the first run in reactor 4.

Domain size measurements were made at the five locations indicated on sample 4-042-2.5. (figure 11) Although the dimensions of the sample are small, there is only a slight variation along the flow direction but a very dramatic one in the transverse. Neel temperature measurements on samples similar to 4-042-2.5 typically show that T_N is ~15 C lower at point 5 than at point 4.

An example of the extent of domain size variation over larger dimensions along the flow direction is shown in the domain photographs of figure 12. It can be seen that there is a dramatic difference in the domain size. Film characterization showed that the Ga/Fe ratio is increasing in the downstream direction. (table VIII)

The film thickness in zones 2.5 and 5 shows that the growth rate also decreases along the length of the garnet deposition region. In this run the deposition temperature was constant within ±0.5 C along the 6 in. garnet deposition zone and the seed support

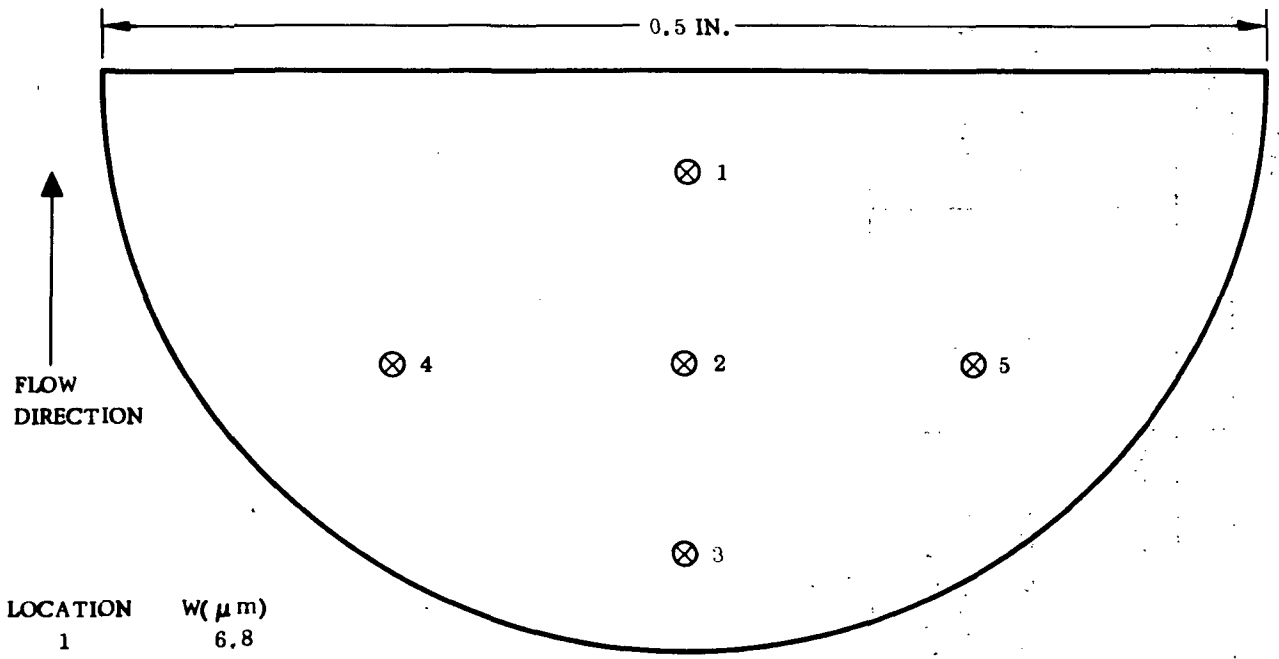

LOCATION	W(μm)
1	6.8
2	6.8
3	6.6
4	5.6
5	9.6

Figure 11.– Variation of Demagnetized Domain Width with Position on Sample 4-042-2.5

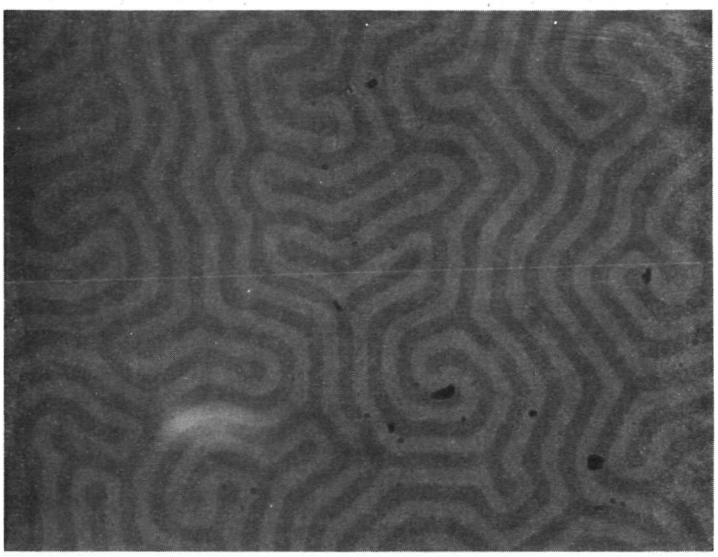

A. Zone 2.5

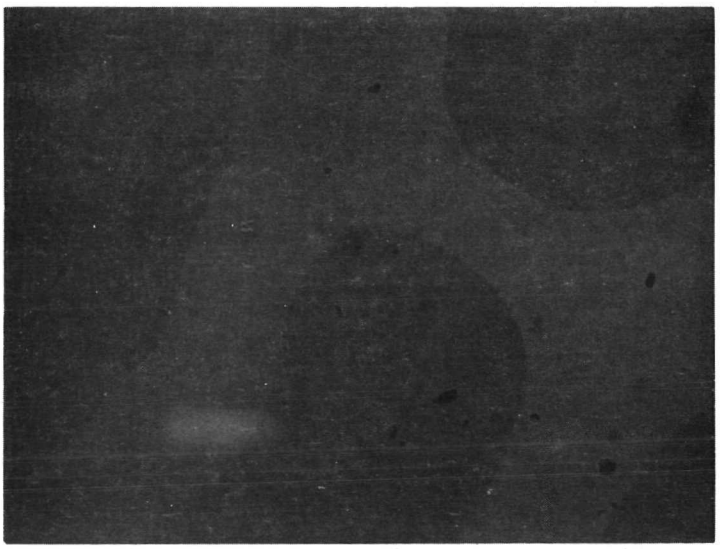

B. Zone 5

Figure 12.—Domain Size Variation with Location in Garnet Deposition **Zone** - Run 4-056 (Magnification - 400X)

TABLE VIII. - RUN-TO-RUN AND ZONAL VARIATION IN FILM THICKNESS AND NEEL TEMPERATURE FOR FILMS GROWN FROM HALIDE SOURCES

Sample	h (μm)	T_N (°C)
4-056-2.5	3.88	136
4-056-5	2.64	127
4-057-2.5	3.90	125
4-057-5	2.48	130
4-058-2.5	4.00	133
4-058-5	2.90	141
4-059-2.5	4.69	146
4-059-5	2.84	149

tray was horizontal. The results of attempts to achieve uniformity of composition and growth rate by adjusting the deposition zone temperature and temperature profile are also shown in table XIII. In run 4-057 there was a ~20°C decrease in temperature over a 6 in. region along the flow direction. In run 4-058 the temperature differential was increased to ~30°C and in 4-059 the 30 deg decrease was maintained but the endpoint temperatures were each lowered 10°C in an effort to increase the growth rate in all zones. It can be seen that the introduction of the temperature gradient actually reversed Ga gradient but the growth rate remained substantially lower in zone 5. Also the lowering of the baseline temperature in 4-059 did not produce the desired increase in growth rate.

Another characteristic of these initial deposits was a lack of reproducibility of domain size (hence composition) from run-to-run and day-to-day even under supposedly identical deposition conditions. Characterization of the samples revealed that T_N was varying substantially indicating that the Ga/Fe ratio was fluctuating considerably over the course of successive depositions. Monitoring of the halide source transport rates suggested that the $GaC\ell_3$ transport rate was erratic and the decision was made to evaluate the reproducibility of Ga transport using a metal source and reacting $HC\ell$ with it. At the same time a new mixing chamber was being designed to solve the transverse non-uniformity problem.

Although the film uniformity and reproducibility were unsatisfactory, it was concluded that these problems did not preclude work on the task of correlating film properties with substrate quality, properties and surface preparation. As stated in Section 4.1, the level of effort required in this area was not as large as anticipated at the program start due to the tremendous rate of advancement of the substrate growth, characterization and surface preparation technology.

Since all of the significant aspects of the substrate related work on this program are covered in Section 4.1 and the Appendix, there will be no further discussion of that work in this section.

During the course of the film/substrate interaction studies reactor No. 4 was converted from the $GaC\ell_3$ to the metallic Ga source. Several series of runs were then made to check the run-to-tun and day-to-day reproducibility of the film Ga content and other film properties. Every attempt was made to achieve identical conditions of source and deposition zone temperatures, gas flow rates, seed location, characterization location, etc. in each series of runs. Some typical results are shown in tables IX. and X. Most of the essential characteristics of the depositions from the four separate sources ($FeC\ell_2$, $GdC\ell_3$, $YC\ell_3$ and Ga) are evident in the data of these two tables. Consider first the series shown in table IX. It was frequently the case that the growth rate of the first run of the day, 4-082-3 and 4-086-3, was lower than that of subsequent runs of the same day. The reproducibility of growth rates from the second deposition on was usually quite good. The reproducibility of T_N for the 4-08X series is a considerable improvement over that obtained with the $GaC\ell_3$ source. However, while these variations are not large on either an absolute or percentage basis, they are unsatisfactory for the requirements of bubble domain materials. The results of a more detailed examination of a series of films are contained in Table X. Here again the growth rate reproducibility is excellent - as good or better than that presently obtained by the LPE method. The reproducibility of T_N in the first three films is within the measurement accuracy and that of w is close to it. However, in the fifth run of the day (4-109-3 was on an experimental substrate) T_N dropped considerably reflecting an increase in Ga content and resulting in the increase in w. This increase in Ga/Fe ratio at the end of a day's runs was a typical occurrence - suggesting a fall-off of the $FeC\ell_2$ transport or an increase of Ga transport. Another difficulty is revealed by the $\Delta a^{\perp}$ data. Although the Ga/Fe ratio was essentially constant during the first three runs, $\Delta a^{\perp}$ declined in magnitude indicating an increase in the Gd/Y ratio in the films. This trend continues into sample 4-110-3 even though the increased Ga/Fe ratio there would have a tendency to increase $\Delta a^{\perp}$.

TABLE IX. - VARIATIONS IN GROWTH RATE AND T_N AFTER CONVERSION TO Ga METAL SOURCE

Sample	Date Grown	Growth Rate (μm/hr)	T_N (^oC)
4-082-3	7/20/72	2.68	131
4-083-3	7/20/72	3.12	129
4-084-3	7/20/72	2.97	130
4-085-3	7/20/72	2.97	131
4-086-3	7/21/72	2.45	135

The conclusions drawn from characterization of such series of films, along with source material transport data, were that the $FeC\ell_2$ and $YC\ell_3$ transport rates were declining over the course of a day, probably due to the drop in the level of material in the source cups.

The installation of the new mixing chamber produced a great improvement in the uniformity of film properties transverse to the flow direction. Measurements of w were made on sample 4-190-2 at three locations which were along a line perpendicular to the flow direction. The locations were at the film center and 0.5 cm to each side of

TABLE X. - CHARACTERISTICS OF CONSECUTIVE DEPOSITS MADE ON THE SAME DAY - REACTOR 4, Ga METAL SOURCE

Sample	Growth Rate (μm/hr)	w (μm)	T_N (°C)	$\Delta a^{\perp}$ (Å)
4-106-3	3.26	5.1	138	+0.0168
4-107-3	3.36	4.6	138	+0.0153
4-108-3	3.31	4.8	139	+0.0102
4-110-3	3.29	7.1	133	+0.0088

center and identical values of w = 4.5μm were obtained at each place, in dramatic contrast to the results in figure 11. One side effect of the use of the new mixing chamber, the need for HCℓ cleaning of the reactor overnight was discussed in Section 4.2, but deserves special mention in the characterization section since it appears to have reduced the incidence of "fall-out" defects in the CVD films. The lowest defect densities ever reported on CVD bubble garnet materials were obtained on this program. These will be reported later in this section.

After the modification of reactor 4 to include the new mixing chamber a new series of depositions were made to determine the day-to-day and run-to-run reproducibility of film composition and properties. It was found that even films grown in successive runs on the same day under identical conditions of source temperatures, gas flow rates and deposition zone temperatures show a gradual change in film properties. Characterization data from four such runs are shown in table XI. The increase in domain size results primarily from the increase in the Ga content of the films and the corresponding reduction in $4\pi M$. The increase in Gd content also contributes to the reduction in magnetization but partially compensates for the reduction in film lattice constant caused by the Ga increase. The values of X and Z were determined from measured values of T_N and $\Delta a^{\perp}$ according to the method of Ref. 3. Thus the results again show that the Fe/Ga and Y/Gd ratios decrease from run to run. It was concluded that this decrease is due to a reduction in the transport rate of the $FeC\ell_2$ and $YC\ell_3$ with time as a consequence of the drop in the level of the materials in the source cups. This problem arises because the transport rates of the yttrium and iron chlorides are much larger than those of the gadolinium and gallium chlorides. In an attempt to overcome this problem programmable controllers were attached to the $YC\ell_3$ and $FeC\ell_2$ source zones so that the source temperatures can be raised slowly during the course of a day's run.

The data in table XII was obtained on three successive runs in which the $YC\ell_3$ and $FeC\ell_2$ source temperatures were being increased at 2°C/hour. Although the run-to-run reproducibility of the Fe/Ga ratio is improved over the series in table XI, and the direction of the Gd/Y ratio change was reversed it was obvious that further experiments were needed to determine the proper program rate for each source material.

Interspersed with the many reproducibility runs were experiments directed toward improving the thickness uniformity across a substrate, and attaining a constant growth rate and film composition along the length of the garnet deposition zone. Certain

TABLE XI. - DATA ON FILMS GROWN WITH CONSTANT SOURCE TEMPERATURES

Sample	w (μm)	$4\pi M$ (gauss)	$\Delta a^{\perp}$ (Å)	X (Ga)	Z (Gd)
4-176-2	4.4	154	0.0107	1.01	0.507
4-177-2	4.7	143	0.0110	1.06	0.525
4-178-2	5.3	126	0.0115	1.08	0.525
4-179-2	5.7	118	0.0121	1.11	0.529

TABLE XII. - DATA ON FILMS GROWN WITH $FeC\ell_2$ AND $YC\ell_3$ SOURCE TEMPERATURES INCREASED AT $2^{o}C$/HR

Sample	w (μm)	$\Delta a^{\perp}$ (Å)	X (Ga)	Z (Gd)
4-202-2	2.7	0.0114	0.93	0.46
4-203-2	3.3	0.0132	0.96	0.44
4-204-2	2.9	0.9130	0.94	0.44

techniques and approaches which were developed during these studies were utilized in the final reproducibility series runs in reactor 4. Therefore, it is germane to present these results before going on to the final discussion of reproducibility. The question of individual film thickness uniformity will be considered first. Figure 13 shows the interference pattern obtained in monochromatic light (λ = 5890 Å) on sample 4-134-3. The substrate is 0.030 in. thick and 0.50 in. in diameter and was supported on a flat horizontal support tray (see figure 5). It can be seen that there is a definite edge effect - the film being thickest at the perimeter of the substrate. The gas direction is indicated by the arrow. The fringe-to-fringe spacing corresponds to a thickness variation of 0.13μm. Such a thickness uniformity is quite typical of samples which are horizontal and elevated above the surface of the surrounding support plate. Figure 14 shows the effect of recessing the substrate in an alumina plate so that its upper surface is at the same height as the surrounding surface. It can be seen that this produces a considerable change in the thickness uniformity. By making the thickness of the surrounding plate greater than that of the substrate, the film thickness at the edge can be made less than that at the center. Additionally, it has also been found that greater areas of uniformity are obtained as the substrate diameter increases. The best film thickness uniformity was obtained on 1 in. diameter substrates that were inclined 18^{o} from the horizontal by use of the tray shown in figure 7. An example of a film grown in this fashion is shown in figure 15. This uniformity is as good as that obtainable by LPE methods. The striations perpendicular to the flat are on the backside (non-epi) surface of the substrate and are a result of the chemical polish (Ref. 39).

Use of an inclined tray also had the effect of reducing the growth rate difference between zones that had been previously discussed. Films grown 2 in. apart on such an

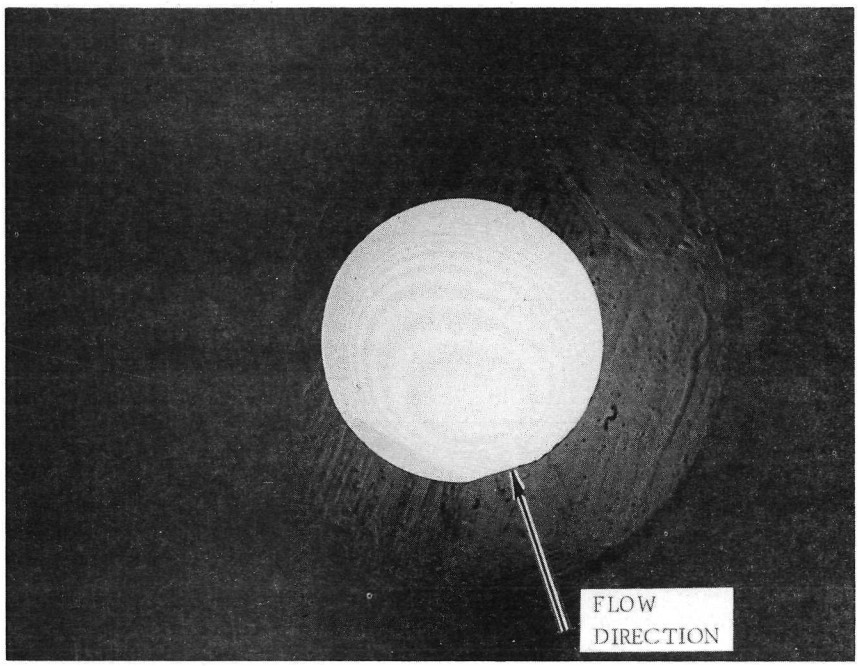

Figure 13.—Thickness Uniformity of Sample 4-134-3. (λ = 5890Å) Substrate Horizontal - Not Recessed. Substrate Diameter = 0.50 In.

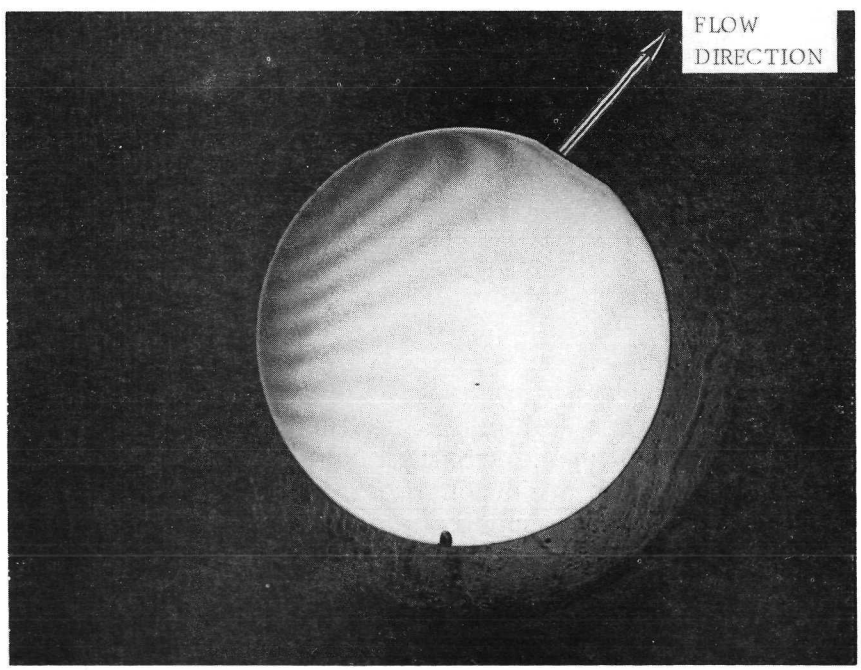

Figure 14.—Thickness Uniformity of Sample 4-137-3 (λ= 5890Å) Substrate Horizontal and Recessed Into Alumina Plate of Equal Thickness. Substrate Diameter = 0.75 In.

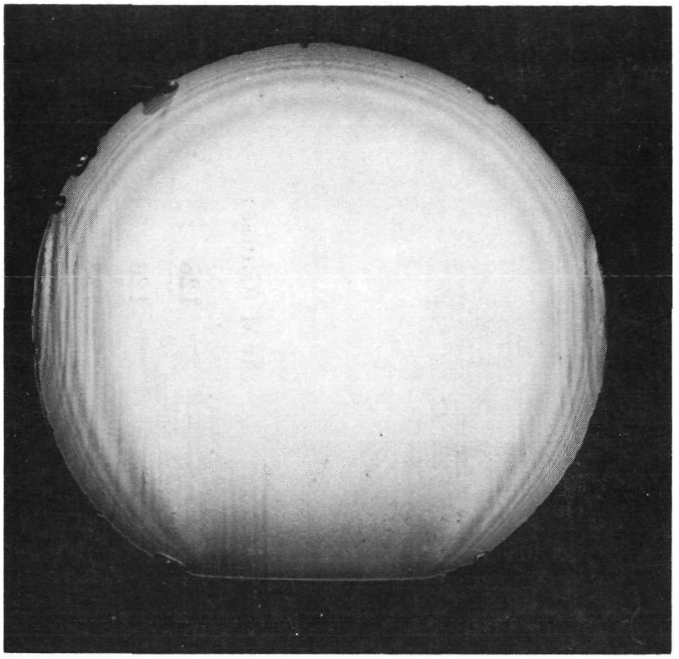

Figure 15.– Thickness Uniformity of CVD Sample 4-261-3 ($\lambda = 5890$Å)

inclined tray were 3.6μm (front) and 3.5μm (rear) thick. In LPE samples the composition is sensitive to the growth rate and good compositional uniformity results when good thickness uniformity is achieved. Thus an LPE sample having the thickness profile such as that shown in figure 15 would also have essentially constant film properties over the uniform thickness area. In CVD samples the composition does not seem to be as sensitive to growth rate and one can observe some variation in properties even within the region bounded by a single fringe. An example of CVD film property uniformity data is contained in figure 16. Bubble collapse measurements were made at seven locations indicated on the thickness uniformity photograph. The differences in w values at the locations were within the reproducibility of the measurement. The magnetization values calculated from these data (correcting for thickness differences) are also included in the figure. (This sample is 1 in. in diameter and the area of characterization is ~1.25 cm^2.) It can be seen that $4\pi M$ is slightly lower near the flat, which is the upstream end of the seed, leading to the slightly reduced values of H_{col} in this area - points 1 and 2. The uniformity of H_{col} at locations 2 through 7 is quite good and demonstrates dramatic improvement in both longitudinal and transverse (to flow) uniformity from the initial deposits.

After some additional experiments with different combinations of source temperature program rates a five-run reproducibility series (4-260 to 4-264) was made in reactor 4 under the best attainable conditions for this type of reactor configuration. The reactor was HCℓ cleaned overnight. All of the substrate wafers were obtained from the same boule, supplied by Vendor B. The substrates were chemically polished in H_3PO_4 and rigorously cleaned prior to insertion in the reactor. Each seed was placed on the inclined tray. The Ga source was metallic and the Y, Gd and Fe sources were halides. Both the $YC\ell_3$ and $FeC\ell_2$ source temperatures were programmed to increase at 1.25°C/hour.

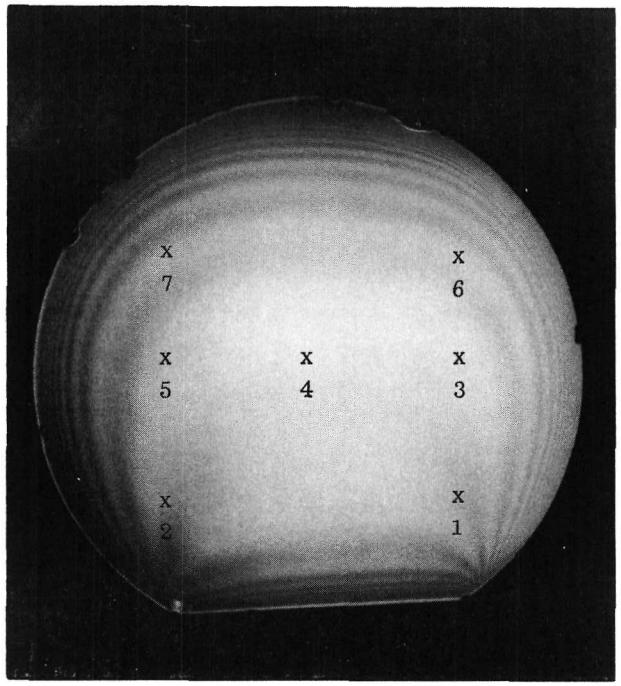

Location	H_{col} (Oe)	$4\pi M$ (Gauss)
1	57.1	128
2	56.5	126
3	60.3	133
4	62.0	137
5	59.8	134
6	60.1	134
7	61.2	137

Figure 16.–Variation of Collapse Field and Magnetization - Sample 4-242-2

The characterization results on the five-run series are shown in table XIII. The measurement location was the center of the film in each case. Film thickness was uniform to within 0.13 m over 80 percent of each wafer. The variation in absolute thickness from film to film is less than 5 percent which is within the accuracy of the measurement technique.

TABLE XIII. - CHARACTERISTICS OF FIVE CVD GaYGdIG FILMS - GROWN CONSECUTIVELY ON THE SAME DAY

Sample No.	4-260-2	4-261-2	4-262-2	4-263-2	4-264-2
Thickness (μm)	4.5	4.3	4.4	4.5	4.5
Domain Width (μm)	4.7	4.6	4.5	4.8	5.7
Collapse Field (Oe)	74	71	80	68	60
Magnetization (Gauss)	145	143	156	138	135
Characteristic Length (μm)	0.54	0.55	0.51	0.60	0.72
Wall Energy (Ergs/cm^2)	0.089	0.089	0.098	0.091	0.10
Neel Temperature (^{o}C)	152	152	152	151	150
Defects (Best 1 cm^2)	2	5,6 (2 areas)	Many polishing scratches	5	31

Examination of the other data in table XIII reveals that the variation in the listed parameters (excluding defects) is less than 20 percent for the first four samples but sample 4-264 shows a considerable deviation from the others in a number of its properties. The collapse field H_{col} is the parameter most sensitive to changes in film properties. The point-to-point uniformity of H_{col} is quite good on any given sample, the typical variation being 1 or 2 Oe over a 1cm^2 area. As an example, data taken at five locations on 4-261 covering a 1cm x 1cm area centered at the film center are given in table XIV. The locations are the center and four corners of the square area. The composition uniformity on such individual samples is well within present requirements and quite comparable to that of LPE deposits.

The defect densities in samples 4-260, 4-261 and 4-263 are the best ever reported for CVD films. The cause of the large increase in defects in 4-264 is not known. In any event it appears that the target of <10 defects/cm^2 can be achieved by the CVD process as well as by LPE.

Measurements of domain velocity and mobility were obtained by the method of bubble translation in a field gradient. (Ref. 40) The results shown in figure 17 are typical of the CVD films of YGdGaIG listed in table XIII. The initial slope of the velocity - field characteristic is very steep, but the velocity appears to saturate at a value of 1700 cm/sec for field differences of >3 Oe. Thiele (Ref. 8) has shown that the bubble velocity in a field gradient is given by $v = \frac{\mu w}{2} (\Delta H - \frac{8}{\pi} H_c)$.

TABLE XIV. - VARIATION OF PROPERTIES OVER 1CM^2 AREA OF CVD SAMPLE 4-261-2

Location	1	2	3	4	5
h (μm)	4.28	4.28	4.28	4.28	4.28
w (μm)	4.84	4.85	4.84	4.84	4.84
H_{col} (Oe)	67.6	66.5	66.4	67.9	67.5
4πM (Gauss)	145	143	142	145	145
ℓ (μm)	0.57	0.57	0.57	0.57	0.57
σ_w (erg/cm^2)	0.095	0.093	0.092	0.096	0.095

The values of μ_w and H_c derived from the data of figure 17 are 1800 cm/sec/oe and 0.16 oe, respectively. Both of these values are quite respectable for bubble domain materials, particularly the high mobility. However, it is misleading to quote a mobility value in view of the severe nonlinearity in the v -ΔH curve since the velocity at ΔH=6 oe is essentially the same as at 2Oe. Such nonlinear behavior is frequently typical of materials with very low ferromagnetic resonance damping constants (Ref. 41).

The three samples 4-260, 4-261 and 4-263 represent the best CVD bubble domain material so far produced. However, examination of the data in table XIII reveals two problem areas:

1. The run-to-run reproducibility of film properties, although vastly improved since the program start, is still not satisfactory (and the day-to-day reproducibility is less satisfactory). The main problem appears to be changes in the transport rates of the halide sources due to temperature fluctuations and depletion of source cups. The need to control four independent sources whose transport rates are temperature dependent is the basic difficulty.

2. The wall energy of the GaYGdIG material is rather low for present device requirements. It appears that it would be desirable to go to a different composition in order to increase the wall energy.

The above considerations and the report of successful YGaIG deposition from an alloy source (Ref. 21) lead to the decision to explore the feasibility of using a single metal alloy as the cation source.

Throughout the course of the work on film deposition using the separate sources, several samples were selected for device work. These samples are listed in table XV.

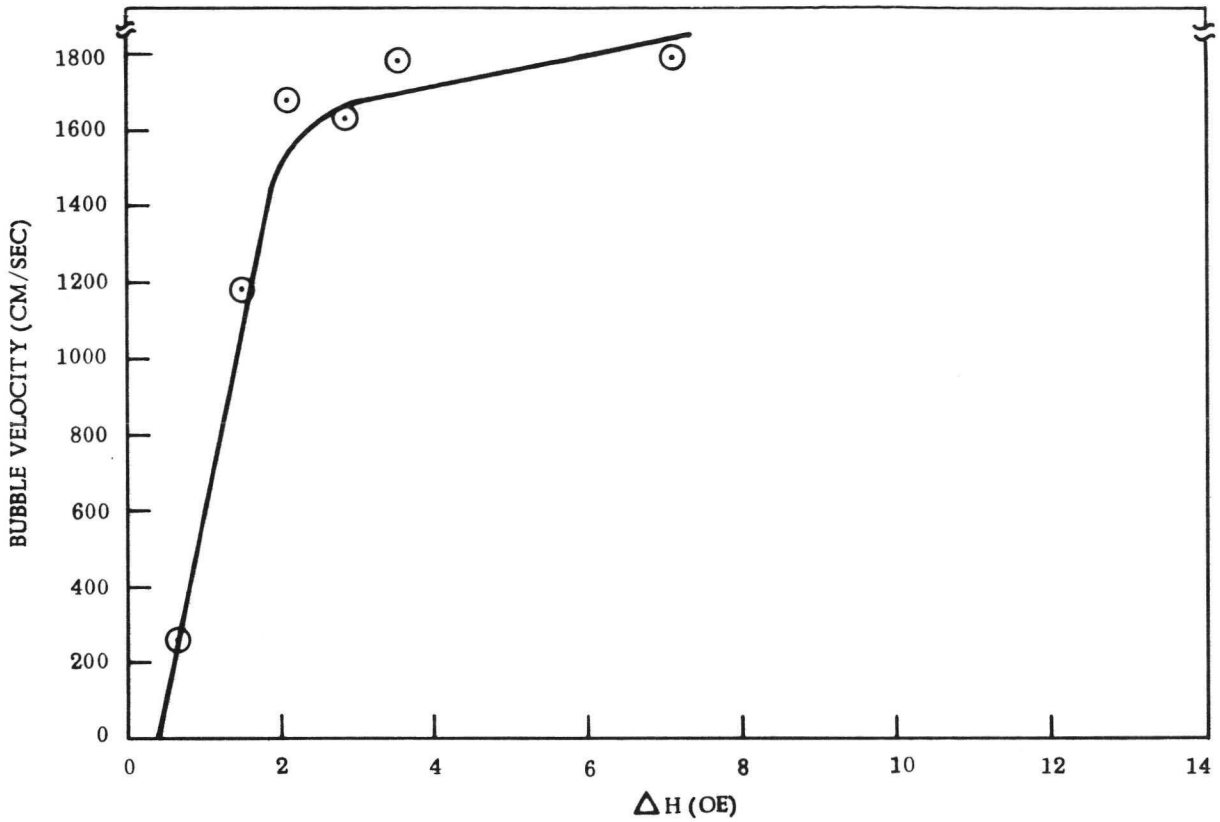

Figure 17.– Bubble Domain Velocity as a Function of the Field Difference Across the Domain Diameter for YGdGaIG Film Grown by CVD

TABLE XV. - PROPERTIES OF CVD FILMS USED FOR DEVICE WORK

Sample	4-061-3	4-068-3	4-194-2	4-246-2	4-260-2
h (μm)	3.4	4.2	5.1	4.6	4.3
w (μm)	4.4	5.3	5.2	6.0	4.8
H_{col} (Oe)	63.5	54.7	73.3	52.1	67.6
$4\pi M$(G)	149	126	147	123	144
ℓ (μm)	0.54	0.65	0.59	0.75	0.56
σ_w (ergs/cm^2)	0.10	0.08	0.10	0.09	0.09

In all cases the wall energy is ≤ 0.10 ergs/cm^2. In the device work on these samples it was found that reliable operation could not be achieved due to problems of spurious domain nucleation. Therefore LPE samples with higher σ_w were used for the completion of the device work.

5.2 CVD Films Grown from Alloy Sources

The film composition selected as the goal of the alloy source CVD growth effort was $Y_{1.7}Eu_{0.65}Tm_{0.65}Ga_{1.0}Fe_{4.0}O_{12}$. The bases for this choice were the better temperature stability and possibly higher wall energy of this material compared to GaYGdIG. Attainment of a higher wall energy however, would require the achievement of some growth-induced anisotropy in the CVD deposits. The following plan of action was adopted for film growth. It was decided to begin the alloy source work by growing YIG to establish some baseline deposition parameters. Following successful YIG growth the next attempt was to be with a YEuGaIG to determine whether Eu could actually be transported. This composition has the additional advantage that it may be possible to obtain some growth-induced anisotropy at the CVD growth temperature. (Ref. 42) If the YEuGaIG were successfully deposited, work would proceed to the final YEuTm composition. If Eu could not be successfully transported the target composition would be shifted to $Y_{1.07}Gd_{0.76}Tm_{1.17}Ga_{0.8}Fe_{4.2}O_{12}$.

As described in Section 4.3, YIG films were successfully grown on {111} GdGaG using the YFe alloy source. These samples were uncrazed and had the parallel plate domain structure typical of YIG/GdGaG. The samples were riddled with point imperfections which were thought to result from particulate fallout of $YOC\ell$ during film growth. A value of $\Delta a^{\perp}$ of +0.0125Å was measured on sample 3-529-2 yielding a film lattice constant of 12.376A, which is the accepted value for YIG. Data on this sample and other deposits from alloy sources is shown in table XVI. Optical transmission measurements on these CVD films showed them to have considerably less absorption near the ~0.5μm edge than LPE YIG films - which presumably have some Pb and/or Si incorporated from the flux.

Several deposits were made from YEuGaFe alloy No. 1. (table IV) All of these films were crazed and $\Delta a^{\perp}$ measurements yielded a film lattice constant of ~12.370Å. The films had vertical domains with w ≈ 1.5μm and the H_{col} was in excess of 360 Oe. The gallium content estimated from the T_N's was x ≈0.45. This gallium content along with the $\Delta a^{\perp}$ values suggested that very little Eu was present in the films. The presence of Eu in the films was confirmed by electron beam microprobe analysis but the amount was considerably lower than the desired value. The low Ga and Eu contents are consistent with the high $4\pi M$ (w small, H_{col} large) and the crazing due to the large lattice mismatch.

Thus, the characterization of films deposited using the YEuGaFe alloy source showed that they were lower in Eu and Ga than the target composition of the alloy source. The Ga content of the film was low by a factor of ~2 which is not unreasonable since the desired alloy composition was estimated from transport data on the halide sources. However, the Eu content of the film was ~1/20 of the desired value and at first raised some concern that it would indeed be very difficult to obtain Eu transport. Chemical analysis of the source alloy, however, showed that it also was a factor of ~20 too low in Eu and in fact the relative amount of Eu in the film is close to that in the alloy.

The probable cause of the low Eu content of the alloy is evident from the data in table V. Of the various constituents of the metal alloys, Eu has the lowest boiling point. This in itself would not be too serious except for the fact that its boiling point is below the melting points of Y, Fe and Tm. It is thought that the Eu boiled off during

TABLE XVI. - CHARACTERIZATION DATA ON CVD FILMS GROWN FROM ALLOY SOURCES

Run	Deposit	Source	h(μm)	w(μm)	T_N(°C)	$\Delta a_{\perp}$(Å)	Composition
3-530-2	YIG	YFe#1	9.3	-	-	+0.0125	$Y_3Fe_5O_{12}$
3-532-2	YEuGaIG	YEuGaFe#1	4.6	1.5	230	+0.0229	$Y_{2.97}Eu_{0.03}Fe_{4.55}Ga_{0.45}O_{12}$
3-533-2	YEuGaIG	YEuGaFe#1	4.5	1.6	233	-	
3-535-2	YEuGaIG	YEuGaFe#1	5.1	1.7	236	-	
3-536-2	YEuGaIG	YEuGaFe#1	5.7	1.8	230	-	
3-538-2	YEuGaIG	YEuGaFe#2	4.3	1.6	214	+0.0249	
3-539-2	YEuGaIG	YEuGaFe#2	4.2	1.6	214	+0.0214	$Y_{2.95}Eu_{0.05}Fe_{4.44}Ga_{0.56}O_{12}$
3-542-2	YGdTmGaIG	YGdTmGaFe#1	5.1	2.1	212	+0.0342	$Y_{1.17}Gd_{0.48}Tm_{1.36}Ga_{0.58}Fe_{4.42}O_{12}$
3-543-2	YGdTmGaIG	YGdTmGaFe#1	5.5	2.5	205	+0.0357	
3-544-2	YGdTmGaIG	YGdTmGaFe#1	5.5	2.1	214	+0.0334	
3-545-2	YGdTmGaIG	YGdTmGaFe#1	5.1	2.0	233	+0.0325	
3-551-2	YGdTmGaIG	YGdTmGaFe#2	4.8	-	-	+0.0193	
3-552-2	YGdTmGaIG	YGdTmGaFe#2	3.3	2.1	211	+0.0079	$Y_{0.99}Gd_{0.83}Tm_{1.18}Ga_{0.59}Fe_{4.41}O_{12}$
3-553-2	YGdTmGaIG	YGdTmGaFe#2	-	in-plane	233	-	
3-558-2	YGdTmGaIG	YGdTmGaFe#3	4.9	1.8	218	+0.0206	
3-559-2	YGdTmGaIG	YGdTmGaFe#3	4.4	2.0	216	-	$Y_{1.24}Gd_{0.50}Tm_{1.26}Ga_{0.55}Fe_{4.45}O_{12}$
3-560-2	YGdTmGaIG	YGdTmGaFe#3	4.3	1.9	219	-	
3-561-2	YGdTmGaIG	YGdTmGaFe#3	4.6	1.9	222	-	
3-562-2	YGdTmGaIG	YGdTmGaFe#3	4.5	1.8	226	-	
3-567-2	YGdTmGaIG	YGdTmGaFe#3	3.6	large	145	+0.0352	$Y_{1.28}Gd_{0.60}Tm_{1.12}Ga_{1.04}Fe_{3.96}O_{12}$
3-568-2	YGdTmGaIG	YGdTmGaFe#3	3.4	28	169	+0.0348	$Y_{1.30}Gd_{0.56}Tm_{1.14}Ga_{0.94}Fe_{4.06}O_{12}$
3-570-2	YSmGaIG	YSmGaFe#1	-	in-plane	-	-0.0078	$Y_{2.21}Sm_{0.79}Ga_{1.18}Fe_{3.82}O_{12}$
3-575-2	YSmGaIG	YSmGaFe#1	-	in-plane	-	-	$Y_{2.30}Sm_{0.70}Ga_{1.05}Fe_{3.95}O_{12}$
3-578-3	YGdTmGaIG	YGdTmGaFe#4	4.3	3.7	139	-	
3-579-3	YGdTmGaIG	YGdTmGaFe#4	4.8	4.3	142	+0.0038	$Y_{1.01}Gd_{1.01}Tm_{0.98}Ga_{1.06}Fe_{3.94}O_{12}$
3-580-3	YGdTmGaIG	YGdTmGaFe#4	4.1	4.0	143	-	
3-584-5	YGdTmGaIG	YGdTmGaFe#4	3.8	5.9	186	+0.0024	$Y_{0.94}Gd_{0.94}Tm_{1.12}Ga_{0.76}Fe_{4.24}O_{12}$

the vacuum arc melting process of alloy formation. In an attempt to circumvent this problem a gallium-europium alloy was made and this alloy was arc melted with the Y and Fe. An alloy of the backup material, YGdTmGaFe, was also made up. In each of these alloys the Ga content was raised to increase the amount in the film.

Film depositions made using YEuFeGa alloy No. 2 had a low Eu content as experienced with alloy No. 1. The efforts to minimize the Eu loss by pre-melting the Eu and Ga, before arc melting with Y and Fe, were unsuccessful. Experiments using Eu alloys were terminated due to the shortness of time and the complexity of other alloying techniques.

The first YGdTmGaIG films were grown using YGdTmGaFe alloy No. 1. The composition of the alloy source and films grown from this source are shown in tables IV and XVI. All of the films grown using YGdTmGaFe alloy No. 1 were severely cracked. This is due to having the rare earth ratios off from the target $Y_{1.07}Gd_{0.76}Tm_{1.2}$ value resulting in a low film lattice constant. Adjustments in the alloy composition were calculated and a second alloy was ordered and received. The first good run from YGdTmGaFe No. 2 had very low magnetization, suggesting either excess Ga or Gd. The sample was also crazed which indicated that the Ga excess was more likely. The second deposit 3-552-2 was uncrazed, with $\Delta a^{\perp} = +0.079$Å, $w = 2.1\mu m$ and $T_N = 211$ C. The reduced $4\pi M$ (i.e., w) and $\Delta a^{\perp}$ indicated a considerable reduction in Ga content from 3-551-2, although the deposition conditions were the same. This trend continued in 3-553-2 which had $T_N = 233$ C. These changes and examination of the residual alloy removed from the source cup suggested that the Ga was segregating out of the alloy at deposition temperature.

The film 3-552-2 was extremely significant since it was the first uncrazed bubble composition grown from an alloy source. Microprobe analysis showed the composition to be close to target but slightly high in Gd and low in Ga and Y.

A third YGdTmGaFe alloy was requested and made up. This sample had a Ga/Fe ratio lower than that of alloy No. 1, hopefully to eliminate any preferential Ga segregation. A series of runs were then made with alloy No. 3 to study the effect of changing O_2 and $C\ell_2$ flow rates on the film composition. Runs 3-558-2 through 3-562-2 showed little change in film properties, (w and T_N) despite large changes in O_2 rate. The problem of insufficient Ga in the film still persisted. However, the deposition conditions of 3-567-2 (see table VI) produced a deposit with an excess of Ga and a low $4\pi M$. Increasing the O_2 flow rate by 10 cc/min had a dramatic effect on Ga content - increasing T_N by 15°C to 150°C for 3-568-2. However, both these deposits were severely crazed, $\Delta a^{\perp} \approx 0.035$Å, indicating that the rare earth ratios were considerably off target. This was confirmed by the compositional analysis shown in table XVI. Based on these results the fourth and final YGdTmGaFe alloy was ordered.

Due to a delay in the Tm metal delivery, a YSmGaFe alloy was made up before the YGdTmGaFe alloy No. 4. The films grown from the YSmGaFe alloy had in-plane magnetization suggesting that the Sm content was too high. This was confirmed by the negative $\Delta a^{\perp}$ and the microprobe analysis as shown in table XVI.

The Ga content was encouragingly close to the target value. It had been hoped that this composition would provide a temperature-stable alternative to the previously abandoned YEuTmGaIG material. Unfortunately, time did not permit a second alloy with adjusted YSm ratio to be made.

Four films grown from YGdTmGaFe alloy No. 4 are shown in table XVI. The deposits were uncrazed indicating the adjustment in rare earth ratios of the alloy had produced the desired result of reducing the film/substrate lattice mismatch. However the low Neel temperatures of 3-578-3 through 3-580-3 suggested that $4\pi M_S$ was negative, i.e., the magnetization of the rare earth and octahedral iron sublattices exceeded that of the tetrahedral iron sublattice. This was confirmed by Faraday effect domain observations in an applied field and comparison with a reference sample. Adjustment of the deposition conditions to reduce the Ga content did produce a positive magnetization sample 3-584-5, but also shifted the garnet zone downstream drastically. All of these deposits are uncrazed and the $\Delta a^{\perp}$ values confirm the low lattice mismatch. In fact, the mismatch is too small, resulting in a low wall energy in 3-584-5 ($\sigma_W = 0.06$ ergs/cm^2). These results indicated that another adjustment in the alloy composition should be made to reduce the Ga/Fe ratio, decrease the ratio of gallium and iron to rare earth constituents and reduce the Gd content slightly. This would have the effect of producing films near the target composition of $Y_{1.07}Gd_{0.76}Tm_{1.17}Ga_{0.82}Fe_{4.18}O_{12}$ under deposition conditions that would give a good garnet zone in the desirable deposition region of the reactor. Unfortunately time did not allow the alloy fabrication and film deposition.

The fact that this final alloy No. 4 was selected from only one previous data set, i.e., the No. 3 alloy results at the deposition conditions of 3-567-2 and 3-568-2, is encouraging and establishes confidence that the suitable alloy composition and deposition conditions could be arrived at in a relatively short time. Film 3-584-5 is reasonably close to the target composition, the main problem being the excess Gd content. Reduction of the Gd content will have two beneficial results, increasing $4\pi M_S$ and increasing $\Delta a^{\perp}$ and hence, σ_W.

Some domain and material parameters of selected alloy source deposits are shown in table XVII. In particular it appears that under these growth conditions this composition will also have wall energies in the 0.10 to 0.15 ergs/cm^2 range even with the maximum allowable lattice mismatch. The higher $4\pi M_S$ of 3-578-3 relative to 3-579-3 and 3-580-3 is consistent with its slightly lower T_N, indicating a higher Ga content (for negative $4\pi M_S$).

Although the T_N data on 578, 579 and 580 suggests that the Ga content of the films is decreasing it is apparent that the Ga content of the alloy is still too high and the deposition conditions were obviously not optimized. The rare earth ratios of the films appear to be less sensitive to changes in deposition conditions than the Ga/Fe ratio as judged by results on 3-567-2, 3-568-2, 3-570-2, 3-575-2, 3-579-3 and 3-584-5. However, there is not enough data to determine whether or not the rare earth constituents of the alloy undergo selective chlorination as a series of runs progresses. Thus the question of film reproducibility from the alloy source remains unanswered.

TABLE XVII. - DOMAIN AND MATERIAL PARAMETERS ON ALLOY SOURCE SAMPLES OF YGdTmGaIG

Sample	3-568-2	3-578-3	3-579-3	3-580-3	3-584-5
w(μm)	28	3.7	4.3	4.0	5.9
H_{col}(Oe)	7.5	83.6	76.0	75.5	36
$4\pi M_S$ (gauss)	77	152	141	147	95
ℓ(μm)	2.2	0.38	0.45	0.44	0.76
σ_w (ergs/cm^2)	0.10	0.069	0.071	0.76	0.06

5.3 LPE Films

Bubble domain films of three different compositions were grown by the LPE method described in Section 4.4 and were utilized for the development of a 1024 bit delay line with a 16μm period. These samples are listed in table XVIII along with some static material parameters. All of the films with the exception of Nos. 1 and 4 were ion implanted to suppress hard bubbles. The unimplanted samples were intended for use only under quasi-static conditions. The implantation conditions and collapse field spread data are given in table XIX. The post-implant characteristics were essentially the same as the pre-implant values shown in table XVIII with the exception of the collapse field spread and the slight shift in collapse field reported by Smith. (Ref. 43). The device delivered on the contract (see Para 6.4.1) was made from sample 6.

Comparison of the data in table XVIII with that reported for the CVD films in the previous sections shows that the most significant difference between the two types of samples is in the wall energy values. The growth induced anisotropy which is obtained at the lower LPE growth temperatures produces a large increase in the wall energy and allows the use of a large $4\pi M_S$ to obtain a given domain size. In terms of the static properties at 25°C there is little difference between the three compositions listed. The mobility values are also quite similar for each material. However, the Eu-containing compositions have vastly superior temperature stability in comparision to the Gd-containing films. This superior temperature stability is shown clearly in figures 18 and 19. It can be seen that the limits of the bubble stability range are essentially independent of temperature in the 0-50°C range for the YEuTm compound whereas they vary considerably for the YGdTm material. Therefore considerable bias field temperature compensation would be required to obtain variable temperature operation with the latter composition.

The mere existence of an acceptably wide stability range is not sufficient to insure that adequate device operation can be obtained over a given temperature range. This point is illustrated in figure 19 where the collapse and runout diameters of the two materials are shown from 0°C to 50°C. Although the bias field can be adjusted to maintain a constant diameter bubble from 0 C to 50°C in the YGdTmGaIG it is unlikely that reliable device performance could be obtained over this range because this diameter is close to the collapse value at 0°C and close to the runout value at 50°C. The

TABLE XVIII. - CHARACTERISTICS OF LPE FILMS

Sample	Composition	h(μm)	w(μm)	$4\pi M_S$ (Gauss)	ℓ(μm)	σ_w(ergs/cm^2)
1	$Y_{1.07}Tm_{1.17}Gd_{0.76}Ga_{0.8}Fe_{4.2}O_{12}$	2.9	5.8	197	0.78	0.24
2	"	4.0	5.8	210	0.74	0.26
3	$Y_{1.70}Eu_{0.65}Tm_{0.65}Ga_{1.06}Fe_{3.94}O_{12}$	3.4	5.9	195	0.78	0.23
4	"	4.5	5.4	225	0.65	0.26
5	"	5.2	5.7	223	0.67	0.26
6	"	5.4	5.8	215	0.67	0.25
7	"	4.1	5.4	208	0.67	0.23
8	$Y_{2.14}Eu_{0.56}Tm_{0.3}Ga_{1.1}Fe_{3.9}O_{12}$	4.5	5.5	196	0.67	0.20
9	"	4.8	5.9	182	0.73	0.19

TABLE XIX. - ION IMPLANTED LPE FILMS

Sample	Ion	Energy (KeV)	Dosage (cm^{-2})	δH_{col} at 25°C (Oe)	
				Before	After
2	H^+	75	2×10^{16}	43	<1
3	H^+	25	3×10^{16}	32	<1
5	H^+	25	3×10^{16}	29	<1
6	H^+	25	3×10^{16}	28	<1
7	H^+	25	3×10^{16}	29	<1
8	H^+	25	2×10^{16}	26	<2
9	Ne^+	80	2×10^{14}	26	<1

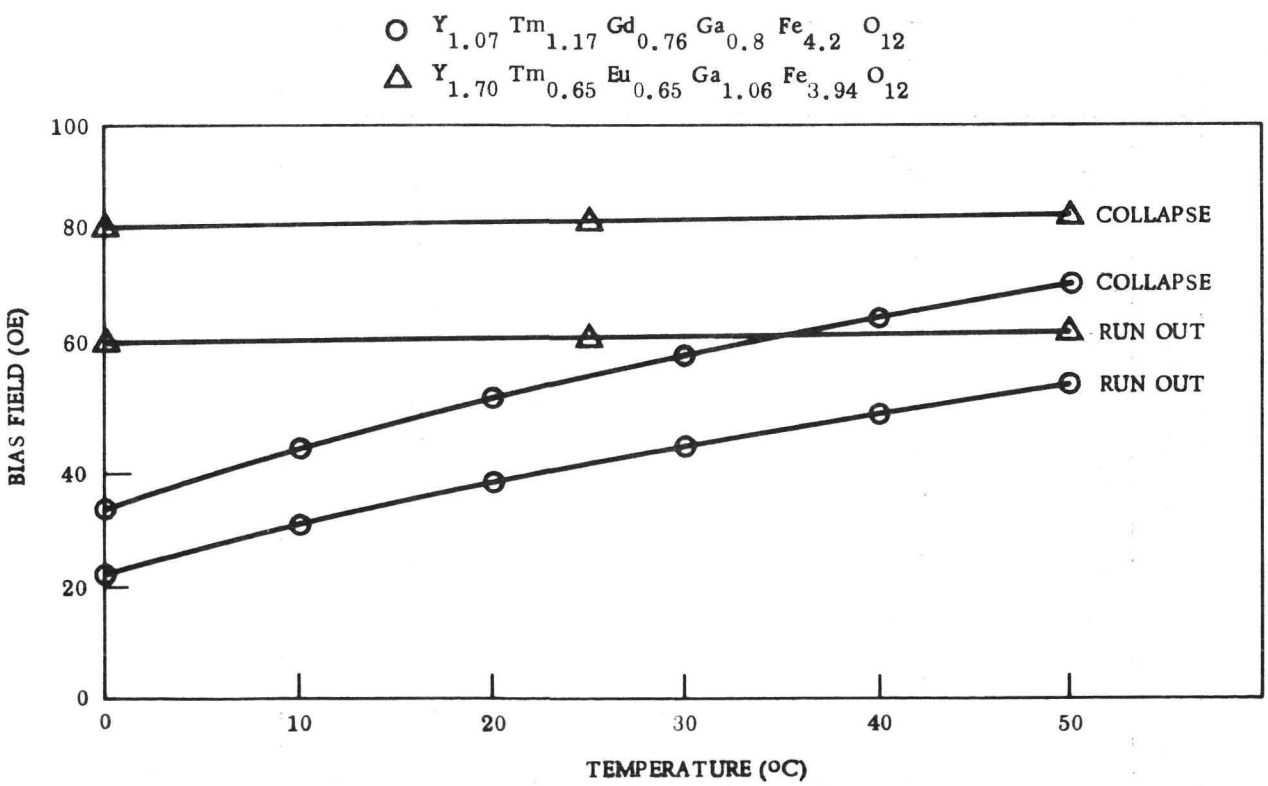

Figure 18. - Temperature Variation of Bubble Stability Range

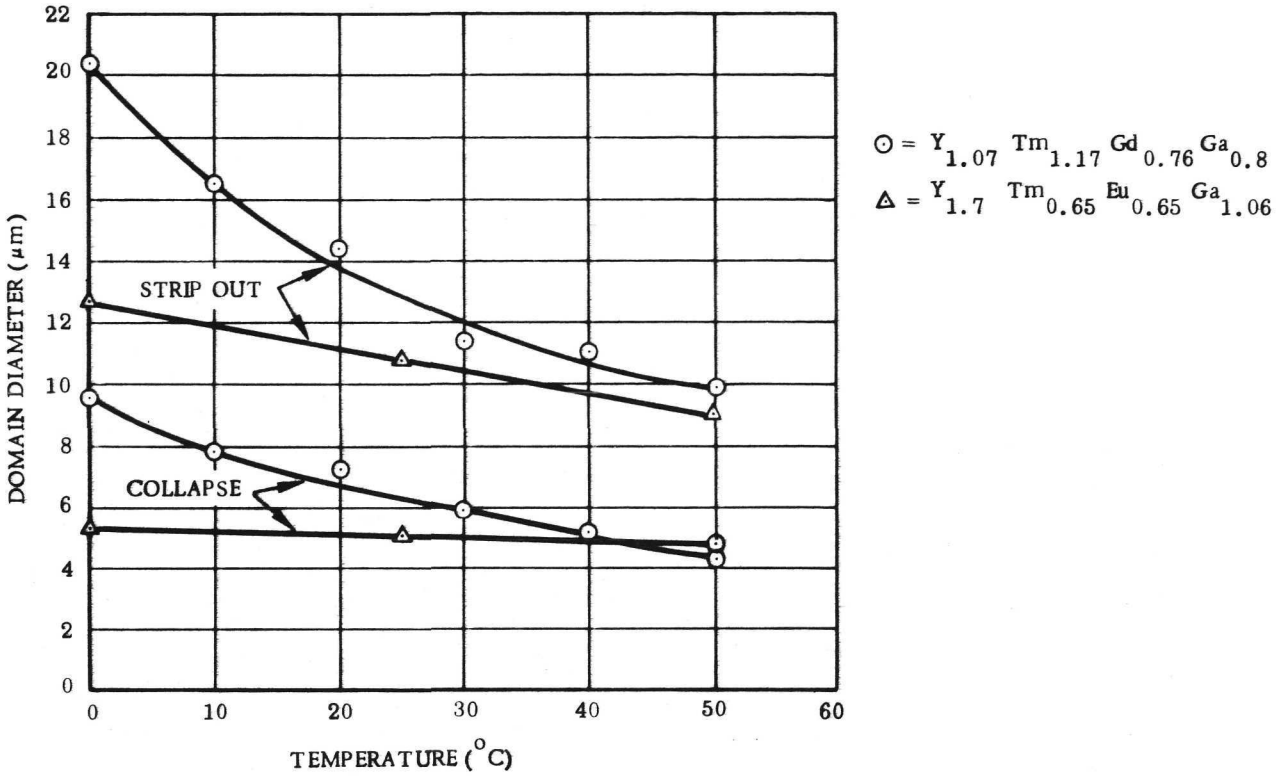

Figure 19. - Domain Diameter at Collapse and Stripout vs Temperature

device structure can no doubt accommodate some variation in diameter from the optimal value but it would seem that variable temperature operation with the YGdTm material would almost certainly result in degraded device margins. In the case of the YEuTm composition, however maintaining the 25°C mid-range diameter to 0°C and 50°C would still allow operation near the middle of the static stability range at these temperatures.

It is these temperature stability considerations which led to the selection of YEuTmGaIG as the initial target composition for the alloy source work. Although no data has been presented, the YSmGaIG also has quite good temperature stability in the 0-50 C range and this was the basis for its selection as an alternate composition for the alloy source CVD work.

5.4 Comparison of CVD and LPE Films

The strengths and weaknesses of the CVD and LPE growth techniques must be judged on how well the epitaxial films meet bubble device requirements. As presently employed, CVD growth takes place as a result of the reaction between volatile metal halides and oxygen, while LPE growth takes place from a supersaturated solution of metal oxides in a lead oxide flux system. Highly-polished, scratch-free wafers of (111)GdGaG are used as substrates for epitaxial growth. (Experimental details of the growth techniques are given in the next Section.) Comparisons between the performances of the two techniques are presented in order of importance to bubble device work.

(1) Composition uniformity (and hence magnetic property uniformity) across a garnet film is of prime importance for fabricating a bubble device. Both growth techniques can produce films of uniform composition.

(2) Run-to-run compositional reproducibility is necessary for assembly of a memory system wherein a number of garnet films are used in the same bias field magnet. LPE films can be prepared within close tolerances but CVD films are not sufficiently reproducible at this time.

(3) A low density of defects which pin bubble domains is required in order to fabricate large shift registers. (Considerable reduction in defect densities by both techniques resulted from the introduction of commercially-grown GdGaG during 1972.) Low defect density films have been produced by both techniques, but LPE has more often yielded very low defect-count films. CVD substrate wafers must be meticulously cleaned prior to deposition for there is no cleaning action at the start of the run; by contrast, LPE substrate wafers experience the purging action of the flux as they are lowered into the melt so that the process is more forgiving of inadequate surface cleaning.

(4) Film thickness uniformity across a garnet film determines the area useful for device patterns. Except for edge and holder effects, both techniques have produced films with large useful areas.

(5) Run-to-run film thickness reproducibility is necessary when a number of identical films are to be prepared. Both techniques have produced films within tight thickness tolerances.

(6) The bubble domain wall energy, σ_w, must be large enough so that uncontrolled nucleation and/or annihilation does not occur during normal device operation. Since $\sigma_w = 4\sqrt{AK_u}$ in a uniaxial material (where A is the exchange constant), the wall energy is determined by the uniaxial anisotropy. As discussed earlier, CVD garnet films have only stress-induced anisotropy whereas LPE films normally have a larger growth-induced anisotropy. Thus the wall energies attainable by CVD are lower than those attainable by LPE which may make CVD films of marginal value in some device structures.

(7) The rate at which garnet films can be deposited on substrate wafers is also of importance in evaluating growth techniques. Typical growth rates by LPE are two to four times those for CVD. However, the CVD process has the potential for simultaneous deposition on several wafers or ultimately for a continuous in-line process. The LPE method (as presently envisioned) is limited to batch deposition on several wafers.

(8) The potential for the incorporation of contaminating ions in garnet films is another measure of the growth techniques. Lead ions from the flux have been identified in LPE films (Ref. 28) but the very small lead content of films grown for bubble domain device use has not caused any deleterious effect. No foreign ions have been found in CVD garnet films.

(9) A final consideration in comparing the growth techniques is their versatility for growing films of different compositions (within the general constraint of the limits of film-substrate lattice constant mismatch). The LPE technique appears to be capable of growing any garnet composition of potential interest while the CVD technique is limited to compositions which may be produced by volatile constituents.

Considerable progress has been made in CVD and LPE techniques during the course of this program; however, the results with CVD have not been so dramatic. The LPE technique currently provides films which are similar to or better than CVD in every comparison area. The CVD technique has been found wanting in compositional reproducibility, wall energy, reproducibility of low defect counts and versatility of composition.

6.0 MAGNETIC BUBBLE DELAY LINE
(J. L. Williams)

The objective of this effort was to demonstrate the feasibility of a 1000 bit delay line with a 16 μm bit period (~2 x 10^6 bit per in.^{2}) with CVD or LPE garnet films having 4-5 μm bubble diameters. It was expected that the device would consist of elements known in the field and that the experimental analysis effort would be expended on device fabrication and integration at the 16 μm period level.

6.1 Delay Line Technology

The basic unit for a magnetic bubble delay line is a simple serial propagation track. Within the delay line, programmed information consists of a series of bubble and no bubble sites. This requires the ability to control the generation of the bubbles, the ability to move the bubbles along a periodic structure at a controlled rate, and finally the ability to detect the presence or absence of the bubble at a specific location. Bubble domain motion can be induced by the application of localized magnetic field gradients. These gradients can be produced by (1) conductor loops placed on the film surface (Ref. 44); (2) by the field access technique employing soft magnetic materials (permalloy overlaid on the film surface (Ref. 45); or (3) by combinations of conductors and soft magnetic materials. In propagation by current loops, adjacent loops are energized by opposing currents, repelling the bubble from one loop and attracting it to the other. However to achieve the packing densities expected, fabrication of current loops by standard photolithographic techniques is not easily achievable. The conductors would be on the order of 1 to 3 μm wide and are required to be continuous at every point with sufficient thickness to minimize over all resistance and electromigration effects (Ref. 46). These requirements tax the practical limits of photolithographic processes.

The standard photolithographic process is suitable to implement the field access technique and thus is used for most magnetic bubble domain devices. In the field access mode of propagation, the uniform inplane rotating field polarizes the permalloy propagation pattern; thereby creating localized poles which, if the pattern is correctly designed, produce a field gradient at the bubble position causing motion along a prescribed path (Refs. 47 and 48).

Two distinct patterns were selected for the device propagating element. Figure 20a shows a typical T-bar element and figure 20b depicts the Y-bar design. The two individual elements were arranged to provide a delay line of 1024 bits.

Two methods of bubble generation/annihilation were also tested. Figure 21 shows a typical loop annihilator and loop generator. The loop annihilator can function in one of two ways. As a domain enters the loop the conductor is activated by a current pulse which raises the bubble sustaining (z) bias field locally. If this field is greater than the bubble collapse field, the domain will be annihilated. This method is most commonly used at this time. A second method is to apply a current pulse which reduces the z bias field and holds the domain within the loop. The pulse is on for 180 deg of rotating field at which time the pole of the propagation element within the loop becomes

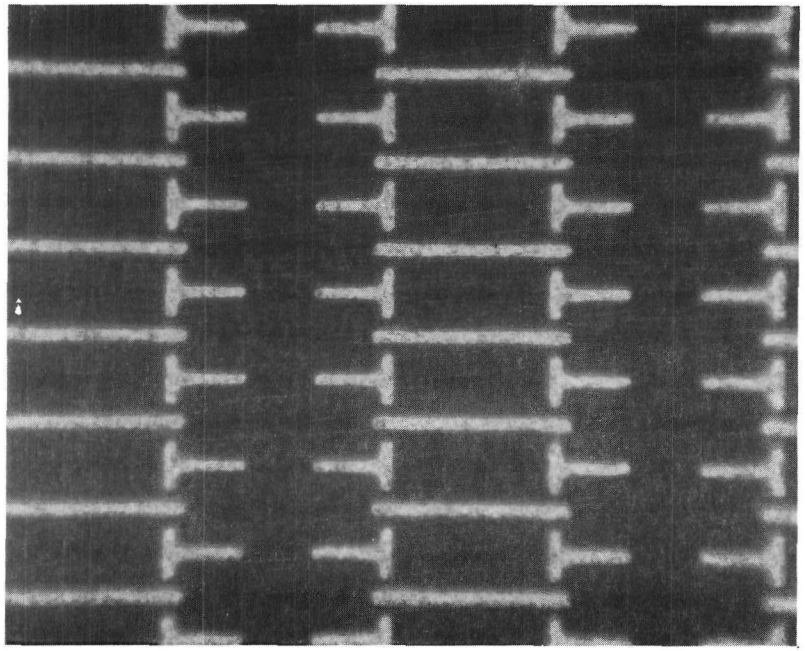

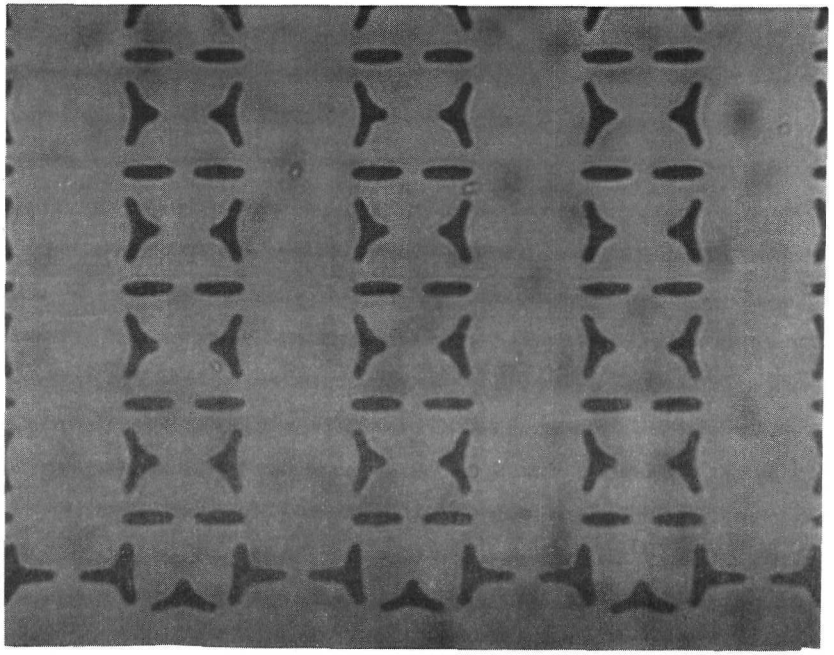

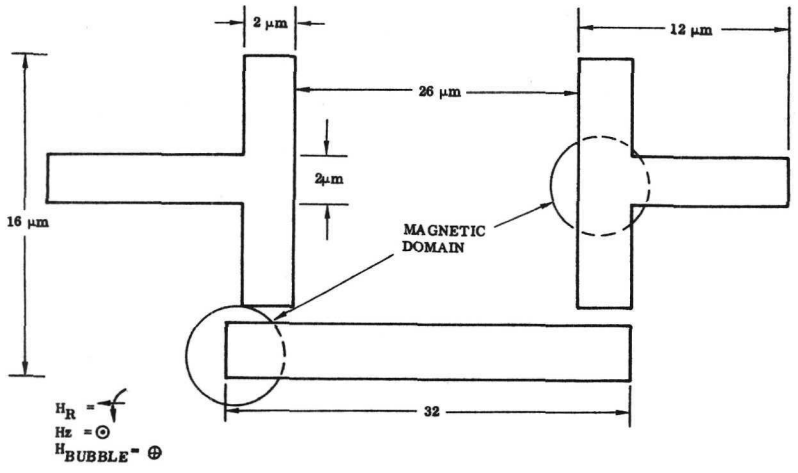

Figure 20a. – Typical T-Bar Elements

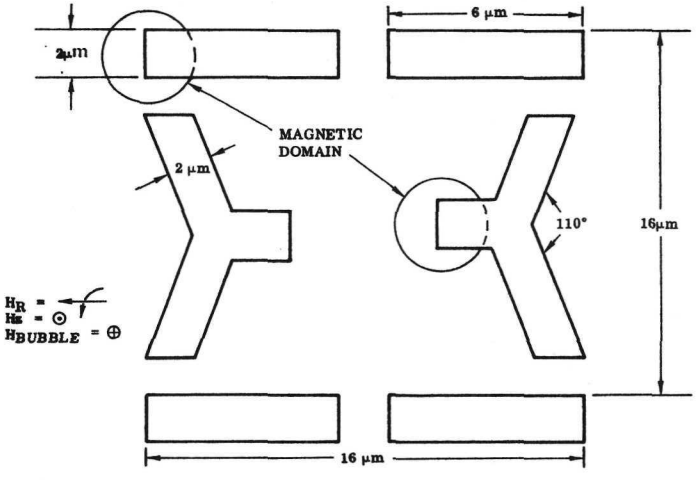

Figure 20b. – Typical Y-Bar Elements

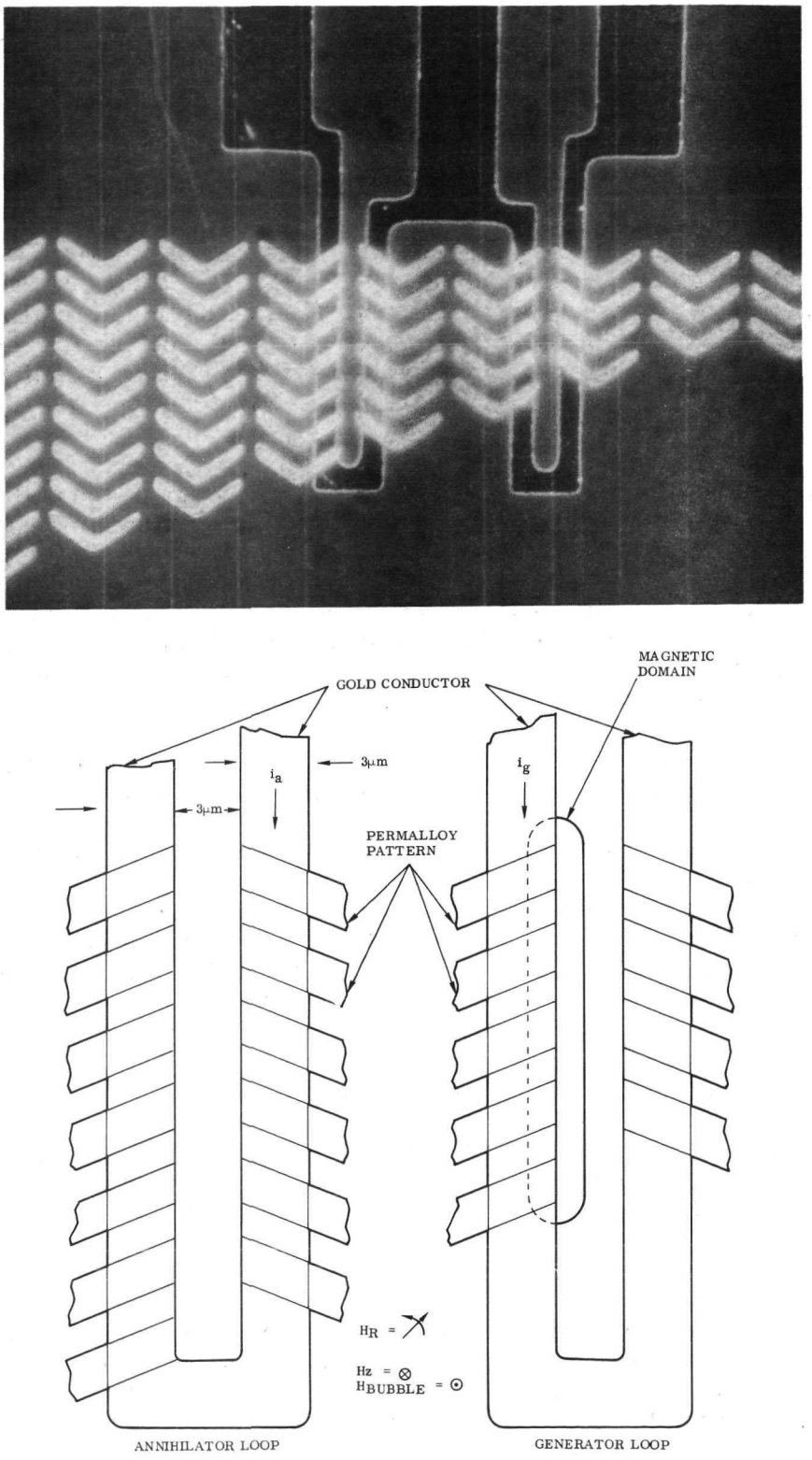

Figure 21. – Typical Loop Annihilator and Generator

unfavorable and collapses the domain. A small, short duration current can also be applied at this time to aid the collapse. The loop generator accomplishes generation by domain nucleation. Unlike the keyhole or other replicate generators no seed bubble is required. In this case the current pulse creates a domain wall at the surface and propagates it through the material until at least a half bubble is formed. After this point the full bubble is the stable condition and the domain wall propagates itself through the remaining film thickness.

The passive annihilator (figure 22) employs a current switch to remove the domain from the storage track and into the annihilator. As a propagating domain passes adjacent to the conductor, a current pulse is applied, creating a magnetic field gradient normal to the conductor which causes the bubble to move from one side of the conductor to the other side. The domains are allowed to either merge with existing domains or are collapsed between competing domains (i.e., domains competing for the same pole).

The keyhole generator operates by taking advantage of the ability of the bubble domains to stretch outward from a disk (figure 23). The domain beneath the disk is attracted by the adjacent bar. Although the bar has insufficient pole strength to completely free the domain from the disk, it will cause the domain to stretch out. As the stretched domain passes beneath the conductor loop, the loop is antivated to create a highly localized field within the loop which aids the z bias and collapses the domain within the loop. The replicated domain propagates into the main line track as a new bubble while the disk retains the seed domain.

The smallness of the bubble (4-6 μm) requires a relatively efficient detector and one that is both simple in design and can be easily fabricated in conjunction with the other device components. The magnetoresistance effect (Refs. 49 and 50) has proven to be most practical. Detection of small bubbles has been successfully accomplished by employing bubble stretching techniques. By stretching the bubble the total flux available for detection is increased allowing larger, more efficient detector elements. One type of stretcher detector is shown in figure 24, the so called Chinese character detector. The three consecutive bars in the propagation pattern stretch the bubble along the propagation direction as it passes the detector element. This element is designed to reduce the demagnetizing effect producing a greater signal. The bubble must however, increase its velocity as it passes through this detector creating a possible frequency limitation. An alternative method is to stretch the domain normal to the propagation track. The chevron stretches shown in figure 25 accomplishes this as well as increasing the bubble size some 10 to 12 times. All detectors are designed in a bridge configuration with the active detector being an integral part of the track and a dummy or reference detector adjacent to the track.

6.2 Delay Line Fabrication Techniques

The fabrication of a field access, magnetic bubble domain device normally requires the deposition of at least three metal thin films. These films are: (1) a 200 Å to 400 Å permalloy film for the magnetoresistive detector, (2) a 2000 Å to 4000 Å gold film for the control loops and interconnects and (3) a ~4000 Å permalloy film for the propagation structure. The order in which these metals are deposited and the means used to define the patterns can have a substantial effect on the magnetic properties of the films.

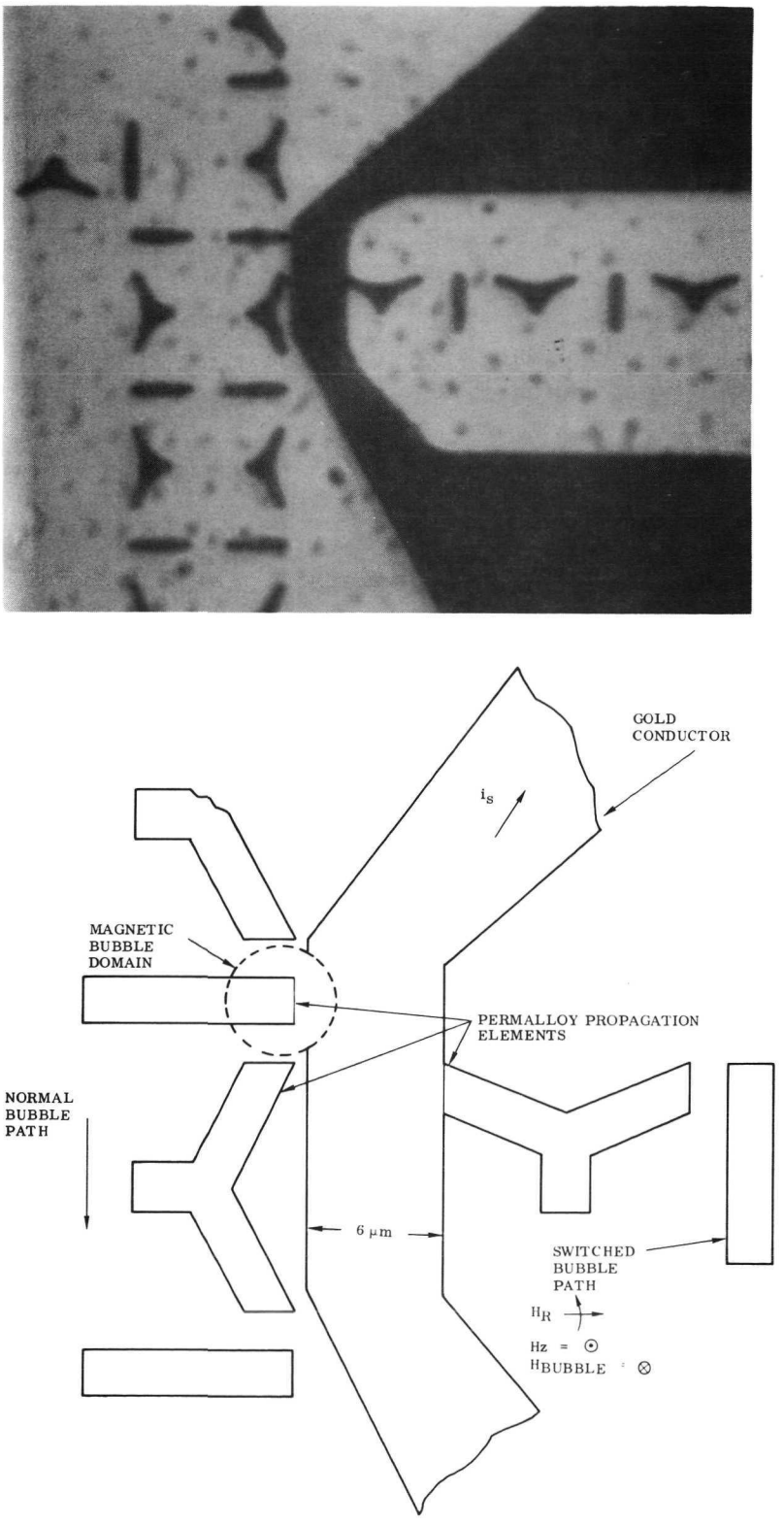

Figure 22. – Typical Unidirectional Transfer Switch

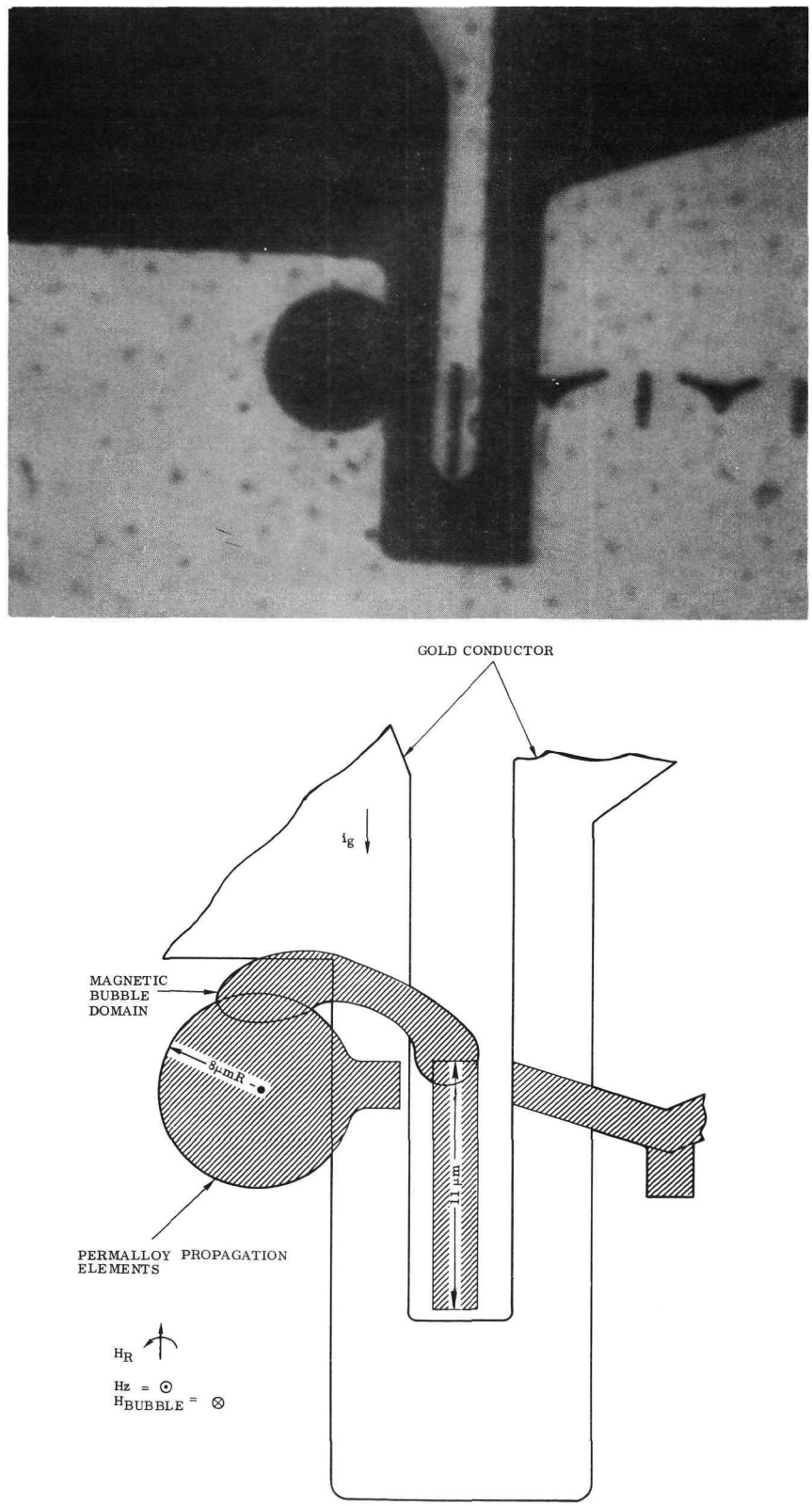

Figure 23. – Typical Splitter-Disk Generator

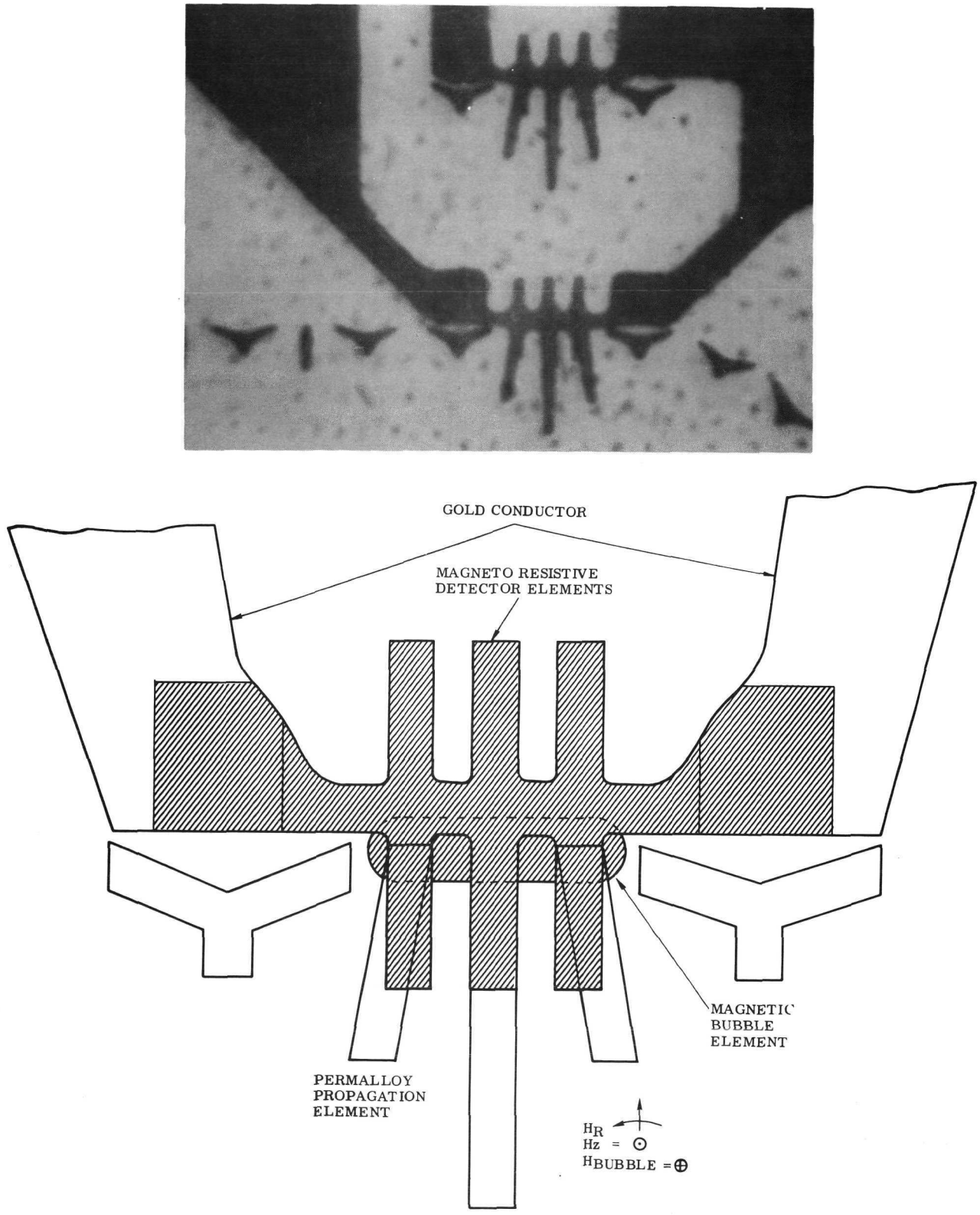

Figure 24. – Three-Element Chinese Character Detector

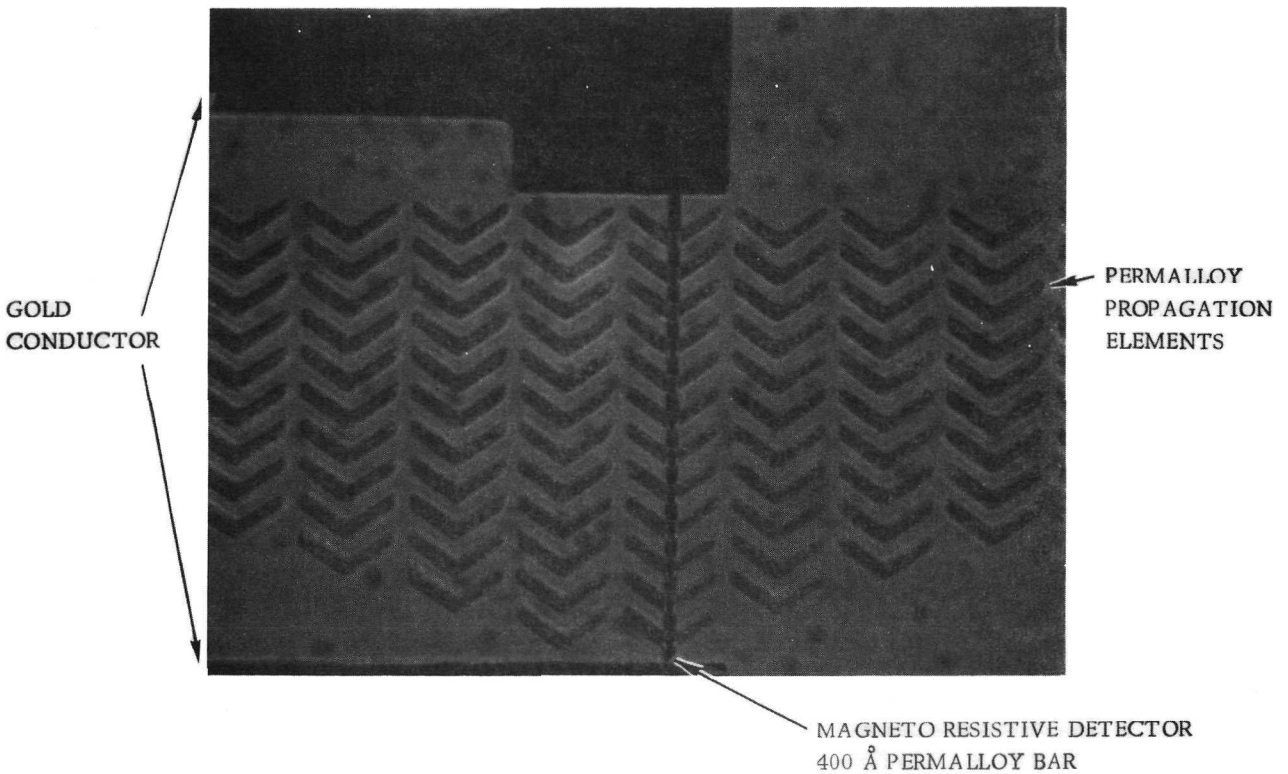

Figure 25. – Twelve-Element Chevron Stretcher Detector

While it was not the objective of this effort to study the methods of bubble domain device fabrication, an overview of device fabrication is presented for completeness.

Sputter deposition, in the rf mode, has been found to be a suitable technique for all the films used in device fabrication. Physical vapor deposition employing electron beam heating is an alternative mode for gold deposition and has the advantage that the substrate remains relatively cool during deposition. The substrate temperature has been found to have a variety of effects on the magnetic properties of the permalloy films.

By monitoring the magnetic and physical properties of the thin films, the deposition and fabrication parameters may be controlled to produce desired results. The measured properties include magnetic moment, anisotropy and coercivity fields, film stress, sheet resistivity, composition, and thickness. All these film parameters, with the exception of composition, have been found to be strong functions of the deposition parameters. (Ref. 51).

The delay lines were primarily processed on Dow Corning 7059 5/8 in. glass squares which were mated to garnet films to form overlay devices. Due to the critical dimensions involved, processing yields were poor when devices were processed on garnet, and thus the on-glass method was used. The garnet material used for overlays was diced into 100 mil square dice. These dice were then checked for defects and the selected units were bonded to the on-glass device with Aron Alpha or Eastman 910 adhesive. To minimize contact separation, the garnet die was applied under

sufficient pressure to produce a uniform fringe pattern of two or less fringes of λ = 5890 Å light. The completed devices were cemented to a terminal board and either ultra-sonically bonded with Aℓ wire or thermal compression pulse bonded with Au wire (figure 26).

6.3 Delay Line Evaluation and Testing

The operating margin of a device is a measure of its performance under various operating conditions. By plotting the X-Y in-plane drive field along the abscissa and the Z axis field on the ordinate and verifying device operation at various settings of X-Y and Z fields, the stability range or margin is determined. The actual margin curve represents the region where at a given drive field reliable operation will occur. At Z field values above the margin, bubble collapse causes errors and below, the bubble will strip out into serpentine domains. Two methods of establishing the margin were used. Both were performed at 25 kHz.

6.3.1 Gated testing. – The gated test mode provides a visual method of obtaining the margins at high frequency. The device to be evaluated is placed in a coil set on a microscope stage. The z axis bias is adjusted to support bubble domains. Various bubble patterns are written into the delay line. The X-Y field is then gated on for a preset number of cycles or clock pulses. When the number of clock pulses is equivalent to the bit capacity of the closed loop delay line, the bubbles will return to its initial position and will appear to stand still. This stroboscopic action allows the bubbles to be observed even though while in transit they can not be observed. The gated testing provides the first operational screening of the device.

6.3.2 Continuous testing. – Continuous drive testing requires the use of a detector. The device is in its final form and is tested under a full operational condition. The applied drive field and Z bias field are adjusted until stable propagation of various bubble patterns is achieved. This is determined by displaying the full register contents on an oscilloscope trace that is synced to one full delay line strobe pulse. When stable operation occurs, the bubble outputs are stationary on the display. Once propagation is achieved, the annihilation and generation circuits are characterized.

6.4 Deliverable Items

6.4.1 1024 bit delay line device. – The deliverable device consists of a 1024 bit, Y bar delay line that was reduced from a 24 μm period pattern by a 2/3 x reduction (figure 27). Propagation with the Y bar pattern has been achieved in both the continuous and gated modes. Operating margins for the device overlayed on a 70 mil by 70 mil die of sample No. 6 (table 18) are shown in figure 28. The element separation requires both a high drive field and slightly larger bubbles. The bubble diameter that operates best on these devices is about 5.5 μm diameter. The larger bubble diameter accounts for the narrowing of the margin from the single bit value. Generation is accomplished by a keyhole type generator and has a threshold pulse of 100 ma at 1 μsec. Annihilation is performed by a switch which transfers the bubble from the track to the annihilator at a threshold of 100 ma at 0.25 μsec. The detector element is a Chinese character type. The detector, annihilator and generator are shown in figure 29. The operating margins are shown in figure 30. Curve A is the gated margin and has an 8 Oe margin. Curve B is the complete operating margin. That is, the margin that includes all element margins (annihilator and generator).

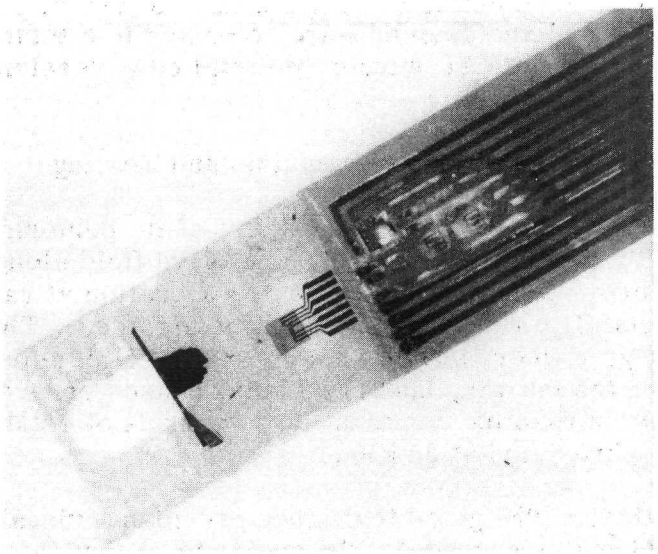

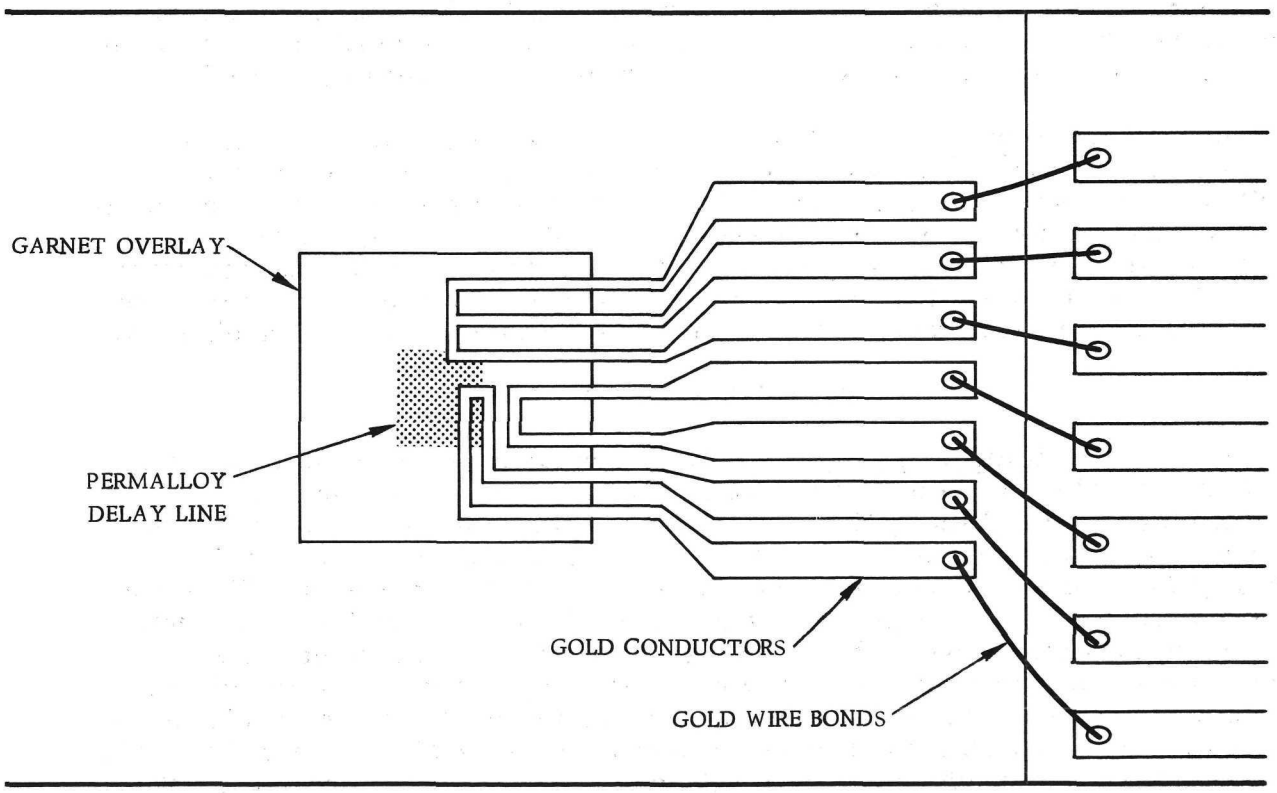

Figure 26. – Delay Line Mounted to Test Terminal Board.
Overlay Device, Au Bond Leads

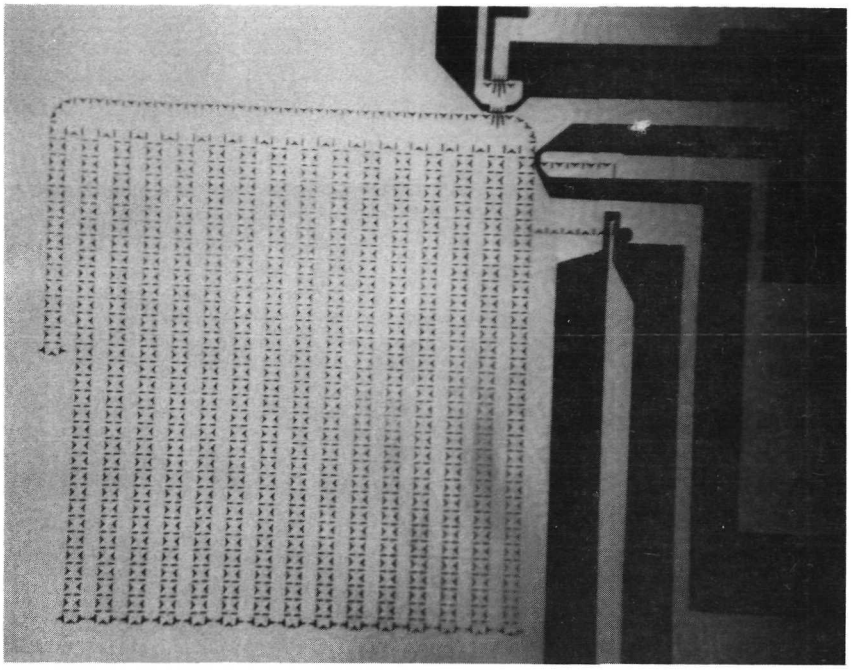

Figure 27.- 1024 Bit Y-Bar Delay Line, 16 μm Period

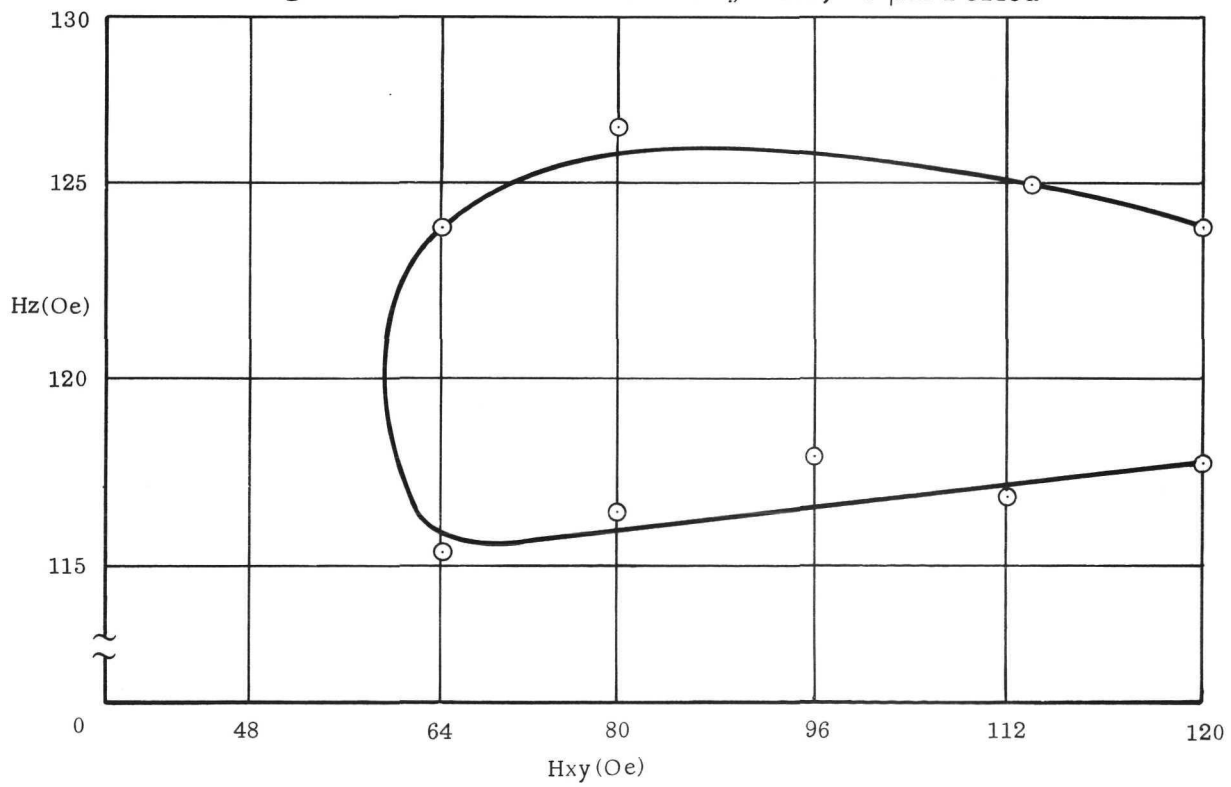

Figure 28.-Propagation Margins, Y-Bar Delay Line

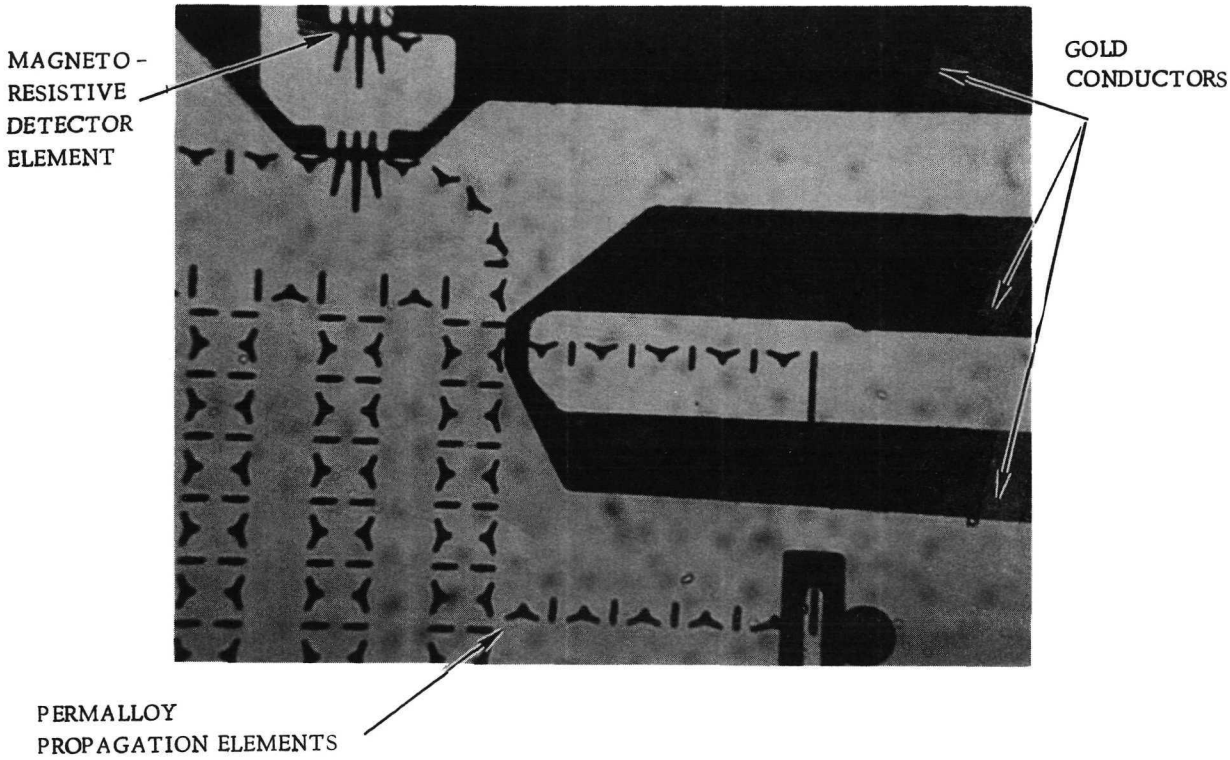

Figure 29. – Detector, Annihilator and Generator Region

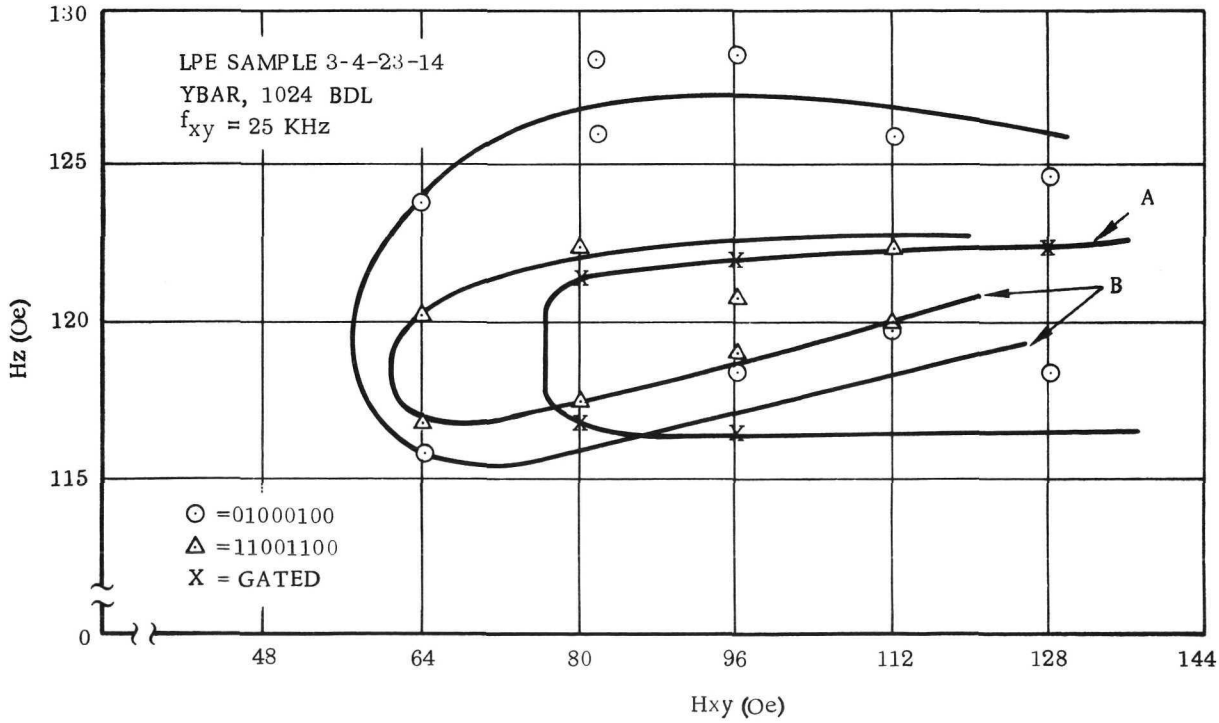

Figure 30. – Device Operating Margins

The slope of the lower limit is the result of the change in operating temperature by the higher coil currents. Figure 31 shows the relationship of the rotating field and the annihilator generator. The radial axis is the z bit for a nominal X-Y field and threshold pulses on both elements. All margins were taken at 25 kHz with the deliverable coil set. These margins reflect annihilation and generation only and are wider (greater Hz variation) than the total device operating margins.

6.4.2 Deliverable coil set. – Figure 32 shows the deliverable coil set. The xy field coil consists of two, two-layer coils wound orthogonally. The layers are then connected in either series or parallel configurations. The field coils are then placed inside a support structure containing the z bias coils. The z bias is derived from a split solenoid or Helmholtz coil and is mutually orthogonal to the drive fields. The coil leads are terminated in a standard connector. The device is inserted in the slot formed by the field coils and is placed in the magnetic center of the coil. To determine the magnetic center of the coils, characterization plots of the fields are made. Figure 33 represents the bias field distribution in the coils of figure 32. The uniform field area is determined and the device is mounted on the terminal board accordingly.

6.5 Alternate Delay Line Study

6.5.1 T-bar delay line. – A 1024 bit delay line consisting of a T-bar propagation element, a loop annihilator, and loop generator and a chevron stretch type detector was fabricated as a 16 μm period device (figure 34). Special design effort was extended

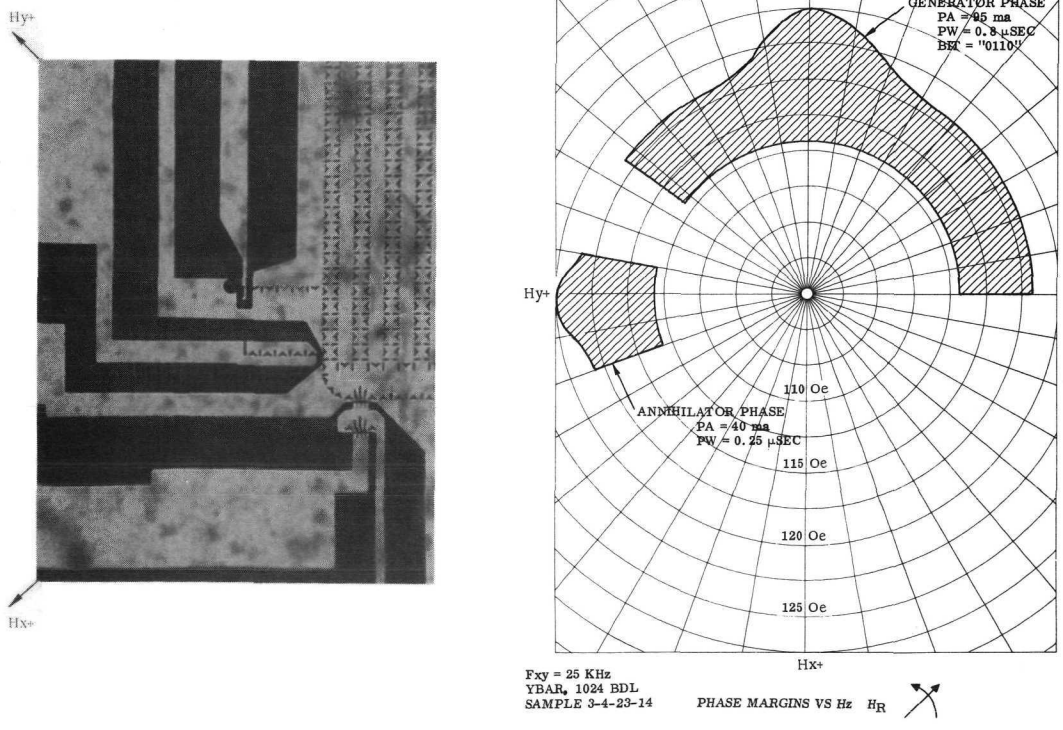

Figure 31.- Annihilator/Generator Phase Plots

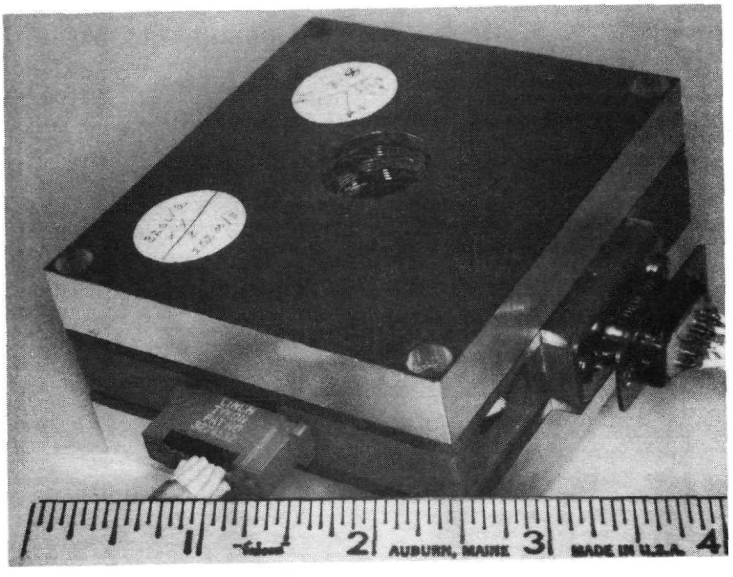

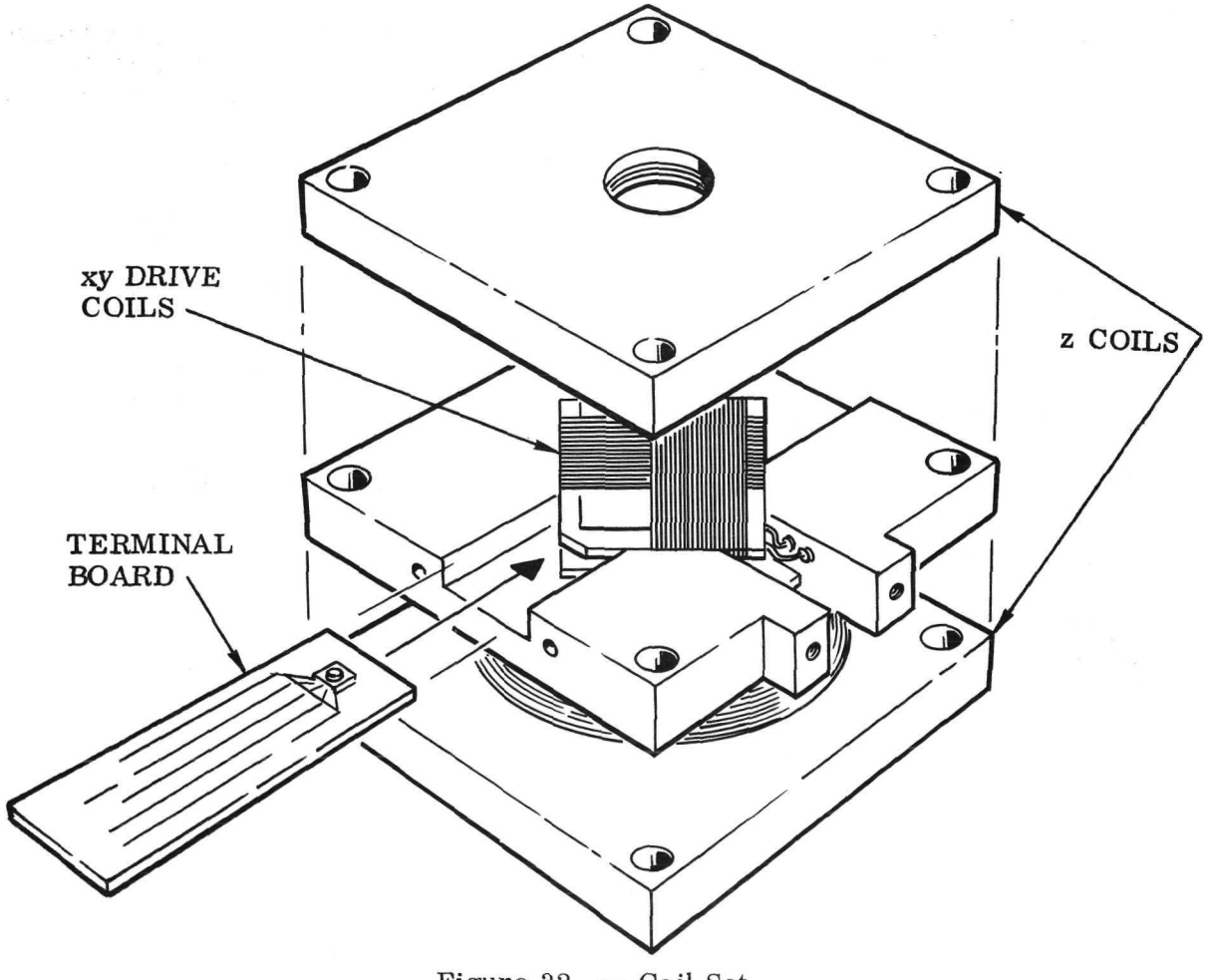

Figure 32. — Coil Set

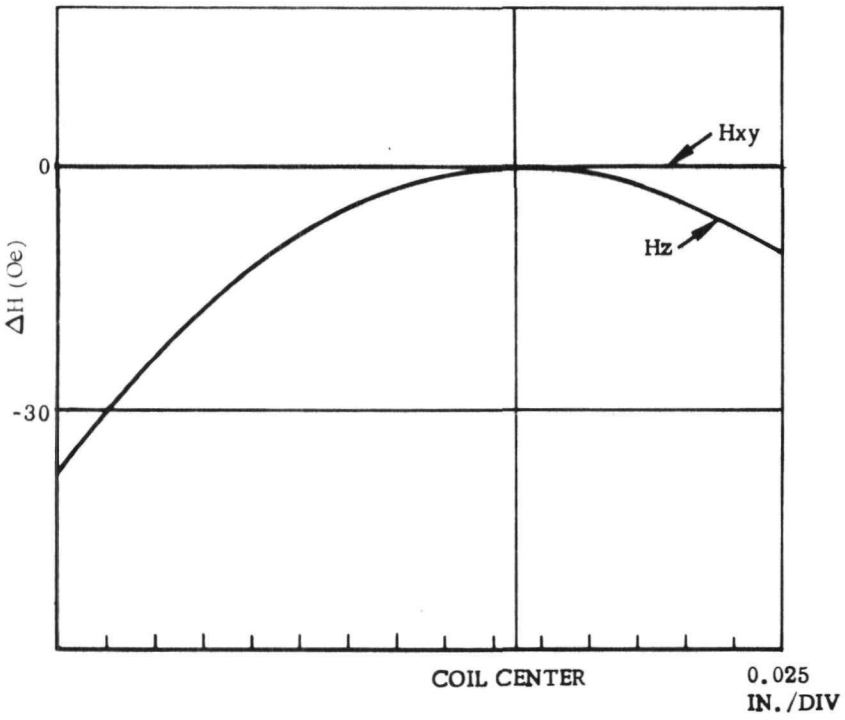

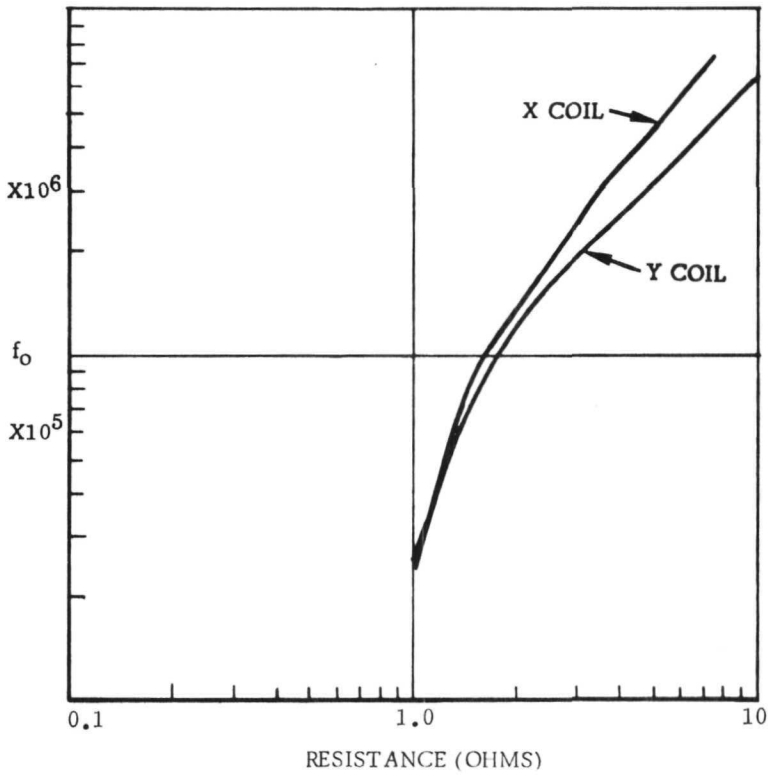

DC RESISTANCE

Rz = 15.345

Rx = 0.835

Ry = 0.846

Hz = 252 OE/AMP

Hx = 32 OE/AMP

Hy = 32 OE/AMP

RESONANCE RESISTANCE

Figure 33. – Field Characterization of Coil Set

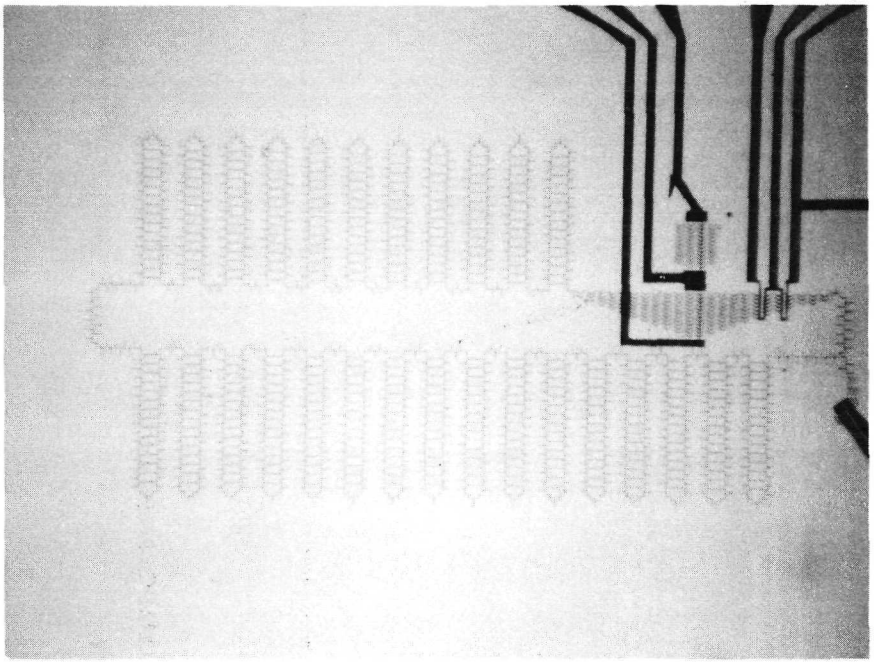

Figure 34. – 1024 Bit T-Bar Delay Line, 16 μm Period

to aid the processing of these devices to ensure accurate and uniform element separation. Figure 35 shows the operating margins for a T-bar overlay delay line mounted on a 75 mil square die of sample No. 6 (table 18). The margins are for operation at 25 kHz. The detector signal is 200 μv above the noise (figure 36) for a 0.75 ma dc current. The detector amplifier output is limited to 2 ± 2 vdc forming a 4 volt threshold window. Margins are for alternate bit configuration as this particular design will not support consecutive bit propagation through the angle type corners. The loop design generates reliably at 300 to 325 ma but will burn out at 350 ma, providing only the narrowest of safety margin.

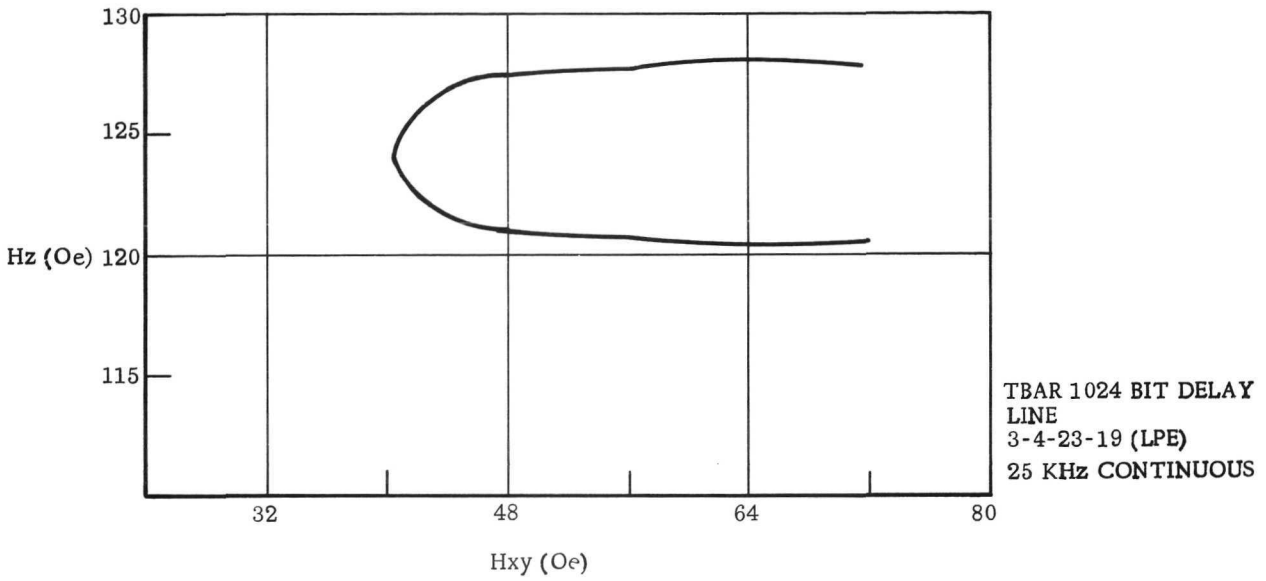

Figure 35. – Operating Margin, T-Bar Delay Line

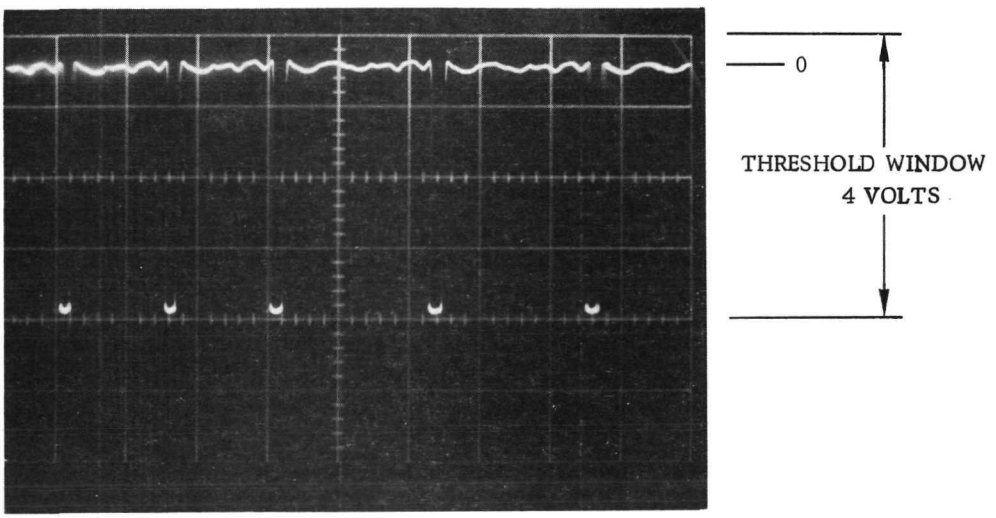

H_R = 25 KHz

VERT DEFLECTION = 1 VOLT/DIVISION

REPRESENTS BIT 10101001001

GAIN $\approx 10^4$

Figure 36. – Twelve-Element Chevron Detector Output

7.0 BUBBLE DOMAIN MEMORY EXERCISER
(B. J. Huffman)

7.1 General Description

The model 8VP1 Bubble Domain Memory Exerciser is a special purpose test instrument for exercising experimental field access bubble domain memory registers. A layout diagram of the exerciser control panel and chassis is shown in figure 37.

7.1.1 Z-field control. - The Z (bias) coil current is supplied by a constant current Kepco power supply in the exerciser and the current amplitude is controlled by a ten turn panel potentiometer. A panel calibration control is provided for setting a digital voltmeter (DVM) panel jack (labeled Oe/A) output in millivolts to equal the Oersted per ampere capability of the coil being used so that another DVM panel jack (labeled Oe) will provide a millivolt reading equal to the Z field magnitude in Oersted.

7.1.2 X-Y field control. - The exerciser supplies X-Y (propagation) coil currents which can be frequency and amplitude controlled from the panel and can be gated to provide controlled start-up and shut-down or to provide a preset number of cycles-either periodically (with panel controlled period) or each time the START pushbutton is depressed. Panel jacks (labeled Oe and Oe/A) are provided for DVM readout of the X and Y field magnitudes in Oersted and for DVM readout of Oersted per ampere for calibration. The X-Y field direction can be rotated manually to any desired position using a sine-cosine potentiometer or can be controlled by an external two-phase generator using input jacks on the panel or by an internal two-phase generator. The internal two-phase generator provides six frequency ranges each covering a decade with the lowest range covering 0.5 to 5 Hz and the highest range covering 50 to 500 kHz. Sine or square wave voltages can be selected to drive the X-Y coils. Symmetry controls are provided for the X and Y sine or square waves and an X-Y phase control is provided to permit adjustment of the relative phase between X and Y waveforms when using the internal two-phase generator. The separate 50K to 500K frequency control on the panel was necessary during initial development of the exerciser and may yet be needed as development continues but presently the .5 to 50K frequency control controls all ranges and the upper frequency limit is about 200 kHz. The field rotation direction can be made to reverse at alternate periods by setting the field rotation direction switch, which is set to the F position for forward rotation, to the F/R (forward/reverse) position. Manual control of the turn-off or stop phase-times for the X and Y coil + and - current switching transistors is provided to allow readjustment at different frequencies to cause each transistor to turn off just as the opposing one is turned on. This turn-off phase time occurs one coil current switching transistor storage period before the opposing transistor turn-on time and therefore varies with frequency. Panel jacks are provided for the X and Y coils and series tuning capacitors. For low frequencies, where series tuning is not needed to achieve the required coil voltages, jumper wires are used in place of the capacitors. Precharge controls are provided to adjust the dc voltages on the X and Y series tuning capacitors when the field is not rotating so that the first cycle current amplitude after rotating field start-up is the same as that of later cycles.

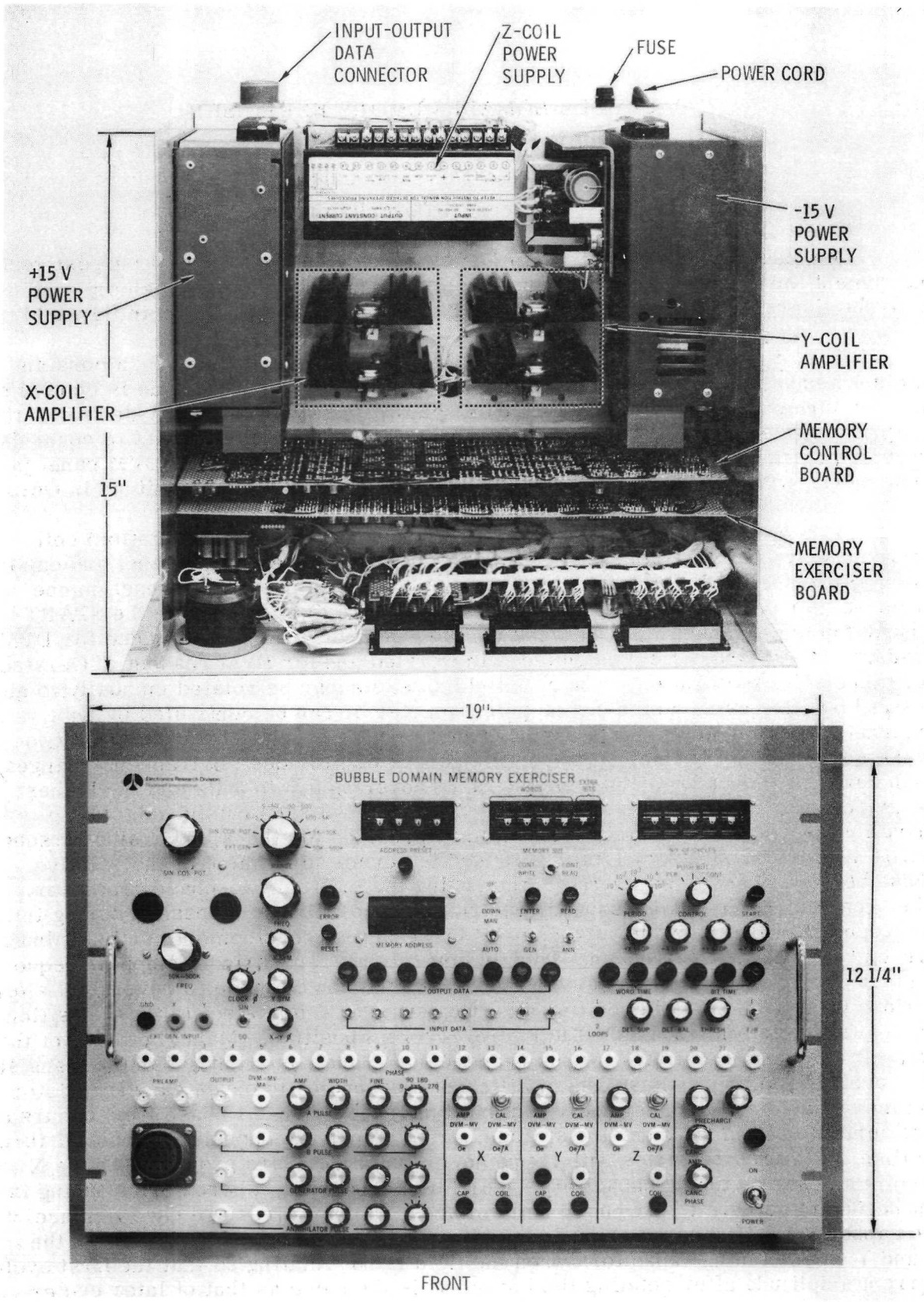

Figure 37.– Layout Diagram – Bubble Domain Memory Exerciser Model 8VP1

7.1.3 Conductor loop current control. - The exerciser allows addressed entry and readout of eight bit binary data. The memory size thumbwheel switches are used to set the memory timing counter period for register lengths from 0 to 9999 eight-bit words plus up to eight (0 through 7) extra bits. The correct memory size thumbwheel switch settings for several memory sizes are shown below:

Memory Size (Bits)	Memory Size Thumbwheel Switch Settings	
	Words	Extra Bits
8	0 0 0 0	7
9	0 0 0 1	0
10	0 0 0 1	1
32	0 0 0 3	7
33	0 0 0 4	0
64	0 0 0 7	7
1024	0 1 2 7	7
10999	1 3 7 4	6

The exerciser supplies current pulses to the bubble memory generator and annihilator loops which are phase and amplitude controlled from the panel and are gated on manually from panel switches or automatically by input data and data entry timing waveforms. Two additional general purpose pulse generators are provided with panel phase and amplitude controls for experimental work such as use of special switching loops. Control and output are from panel jacks. The pulse amplitude in milliamperes can be monitored at panel jacks using a DVM set to read millivolts.

The switch labeled to select one or two loops is intended for later use when circuitry is added to allow use of one conductor loop instead of two for generating and annihilating bubble domains.

The bit-time and the three least significant bits of the word-time are displayed for observation during slow and gated operation. At bit-time 1 (001) the data word corresponding to the displayed word time is in the input data shift register. Eight-bit binary data from panel switches or from the input/output data connector on the rear of the chassis can be entered or read one word at a time at the displayed four digit address by depressing the Enter or Read pushbuttons. The displayed address is incremented by one, up or down, at each entry or readout of data depending upon the setting of the up/down switch and data can be entered or read continuously using the CONT WRITE or CONT READ switch. Eight bit binary output data is displayed on the panel and is also available at the input-output data connector on the rear of the chassis. Each time an eight-bit word is read it is compared with input data and any difference causes the Error light to turn on. An error reset pushbutton is provided to reset the error light. A clock phase switch is provided to select any of the four phases of the clock generator for use as the system clock. The optimum setting of the clock phase switch depends on the detector location and X-Y coil connections.

Banana jacks on the panel are used for connecting the X, Y and Z coils to the exerciser. An MS type connector and two BNC jacks are used for connecting the memory conductor loops and detector circuitry to the exerciser.

7.1.4 Detector circuit control. - The exerciser provides control for the magnetoresistive detector bridge voltage and bridge balance and provides an amplifier and a threshold control for the amplifier which converts low-level (3 to 30 mv) pulses from the detector preamplifier to TTL level pulses. A cancelling phase and a cancelling amplitude control are provided for cancelling unwanted detector signals from the rotating field. Since the cancelling phase range is only 90 deg, the X-Y coil wires have to be connected in the particular order which will select an unwanted signal phase that can be cancelled.

7.2 Operating Procedure

A detailed operating procedure has been prepared under separate cover and delivered with the exerciser.

8.0 CONCLUSIONS

8.1 Film Growth and Characterization

(1) The CVD process is capable of producing low defect density films with excellent thickness and compositional uniformity.

(2) The film-to-film and day-to-day reproducibility of samples grown using individual metal halide sources is not adequate for bubble domain material requirements. The problem is traceable to the need to accurately control the relative transport rates of several different sources, both absolutely and relative to each other.

(3) Complex garnet compositions can be grown from a single metal alloy source over a wide range of deposition conditions. It has been possible to adjust the alloy composition and the deposition conditions to produce films closely matched to the substrate lattice constant so that they are uncrazed.

(4) It has not been possible within the time frame and level of effort of the contract to establish whether the key requirement of non-selective chlorination of the alloy source material constituents can be achieved. This condition is essential to achieving the required reproducibility.

(5) Even if reproducibility can be achieved the absence of evidence of growth induced anisotropy in the CVD films restricts the maximum wall energy in garnets to the range of 0.10 - 0.15 ergs/cm^2. Values of wall energy this low require special consideration in device design.

(6) It must be concluded that it has not yet been demonstrated that CVD is a suitable technique for the production of bubble domain material.

The factors which could alter this situation are the following:

a) Proof that day-to-day and film-to-film reproducibility can be achieved from an alloy source.
b) Development of device designs more compatible with low σ_w values.
c) CVD growth of garnets at lower temperatures to obtain some growth induced anisotropy.
d) Development of bubble materials having an intrinsic non-cubic anisotropy of the proper value.

There are unpublished reports that considerable progress on a) and c) has been made at Phillips Research Laboratories in Eindhoven, The Netherlands. (Ref. 52).

8.2 Delay Line

The 16 μm period device is feasible. The optimization of this device is not solely a design problem but is also a processing problem. Device processing can be improved by replacing the standard photolithographic and chemical etch techniques with projection alignment and ion milling and better mask definition by electron beam lithography. These new techniques are under investigation and/or evaluation at this laboratory.

(1) Small bubble detection with present detector designs is adequate for reliable operation and can be improved even further.

(2) Bit densities offered by the 4 μm bubble is 2.5 times that of the more common 6 μm bubble. Higher bit densities leads to larger bit capacities per chip and more efficient usage of bubble domain material.

APPENDIX

SUBSTRATE FACET REPLICATION BY EPITAXIAL MAGNETIC GARNET FILMS

H. L. Glass, P. J. Besser and T. N. Hamiltion
Research and Technology Division
North American Rockwell Electronics Group, Anaheim, CA 92803
and
R. L. Stermer
National Aeronautics and Space Administration
Langley Research Center, Hampton, VA 23365

ABSTRACT

Epitaxial ferrimagnetic garnet films were deposited on Czochralski grown single crystal gadolinium gallium garnet substrates containing faceted regions. Films grown by both chemical vapor deposition (CVD) and liquid phase epitaxy (LPE) were studied. Lattice parameter distributions were determined by the method of X-ray double crystal topography with rocking curve analysis. The demagnetized domain strip width, magnetization, and characteristic length were measured in a CVD film in regions inside and outside the substrate facets. It was determined that replication of the substrate facets by the epitaxial film is accomplished by a difference in film stress. This stress difference arises from the lattice parameter difference between the faceted and unfaceted regions of the substrate. These results lead to the establishment of a criterion for allowable lattice parameter variation in substrates to be used for magnetic bubble domain films with stress induced anisotropy.

Introduction

Czochralski grown GdGaG (gadolinium gallium garnet) crystals may contain faceted regions (cores) in which the lattice parameter is about 1 or 2 x 10^{-3} Å larger than in the unfaceted regions (1). In general, when these crystals are used as substrates for epitaxial ferrimagnetic garnet films, the films replicate the substrate facets (2, 3). This paper describes an X-ray topographic analysis of the replication mechanism. This analysis is correlated with measurements of magnetic domain characteristics which show that the faceted and unfaceted regions of the epitaxial films exhibit quantitative differences in magnetic properties. These results imply that the mechanism for replication of facets is the variation in film stress produced by the film/substrate lattice mismatch.

In materials whose magnetic anisotropy is partially stress-induced (4) this replication can result in an undesirable in-plane variation in the magnetic properties of the film. From our results the limits on substrate lattice constant variation required to suppress undesirable effects can be estimated.

Experiment and Results

Specimens consisting of thin epitaxial films of magnetic garnets on faceted GdGaG substrates were prepared and analyzed by X-ray double crystal topography as previously described (1-3). The films were grown either by LPE (liquid phase epitaxy) or by CVD (chemical vapor deposition).

Figure 1 shows a sketch of a $\{111\}$ specimen of GdYTmGaIG on GdGaG prepared by the LPE dipping method. The substrate was dipped only part way into the melt so that the epitaxial film was deposited only over the lower half (hatched area). The dip line cuts across the faceted region of the substrate. The facets on the left side are of $\{211\}$ type and are located near the center (axis) of the boule. The facet on the right is of $\{110\}$ type (1).

The double crystal FeKα (842) rocking curve of this sample is reproduced in Figure 2. There is no clear resolution of the film and substrate peaks (2) because the film/substrate lattice parameter mismatch is small. However, there is a shoulder on the low θ side of the peak. A series of double crystal reflection topographs was recorded using various values of rotation angle θ along the rocking curve peak. The letters (a)-(d) in Figure 2 show the positions at which the corresponding topographs in Figure 3 were obtained. The incremental change in rotation angle from one topograph to the next was about 25 seconds of arc.

Topograph (a) in Figure 3 was recorded at the smallest rotation angle (smallest Bragg angle). There are only two strongly diffracting regions: the faceted region of the bare substrate and an edge effect near the dip line. This edge effect, which appears in all four topographs, will not be discussed in detail.

Topograph (b) of Figure 3 shows that at a slightly larger Bragg angle the substrate facet is out of diffracting position but the unfaceted region diffracts strongly. This is exactly the result which was reported previously (1) and corresponds to the faceted region having a slightly larger lattice parameter than the unfaceted region. Except for edge effects, the epitaxial film does not diffract at this rotation angle. In both (a) and (b), the portion of the substrate which lies under the epitaxial film produces only a very faint topographic image because the X-rays suffer absorption in passing through the film.

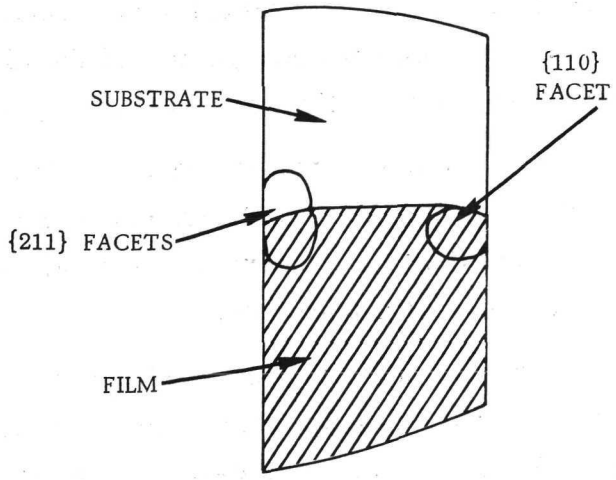

FIG. 1
Sketch of Faceted {111}
GdGaG Substrate Wafer With
LPE Film of GdYTmGaIG
Deposited on Lower Portion

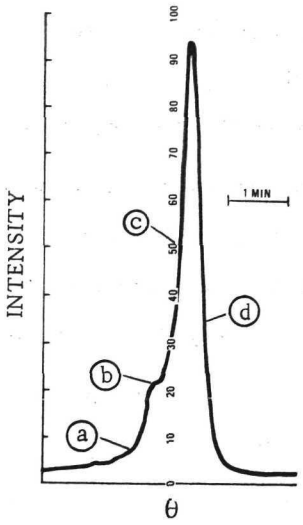

FIG. 2
FeKα (842) Double Crystal
Reflection Rocking Curve of
Specimen Shown in Fig. 1

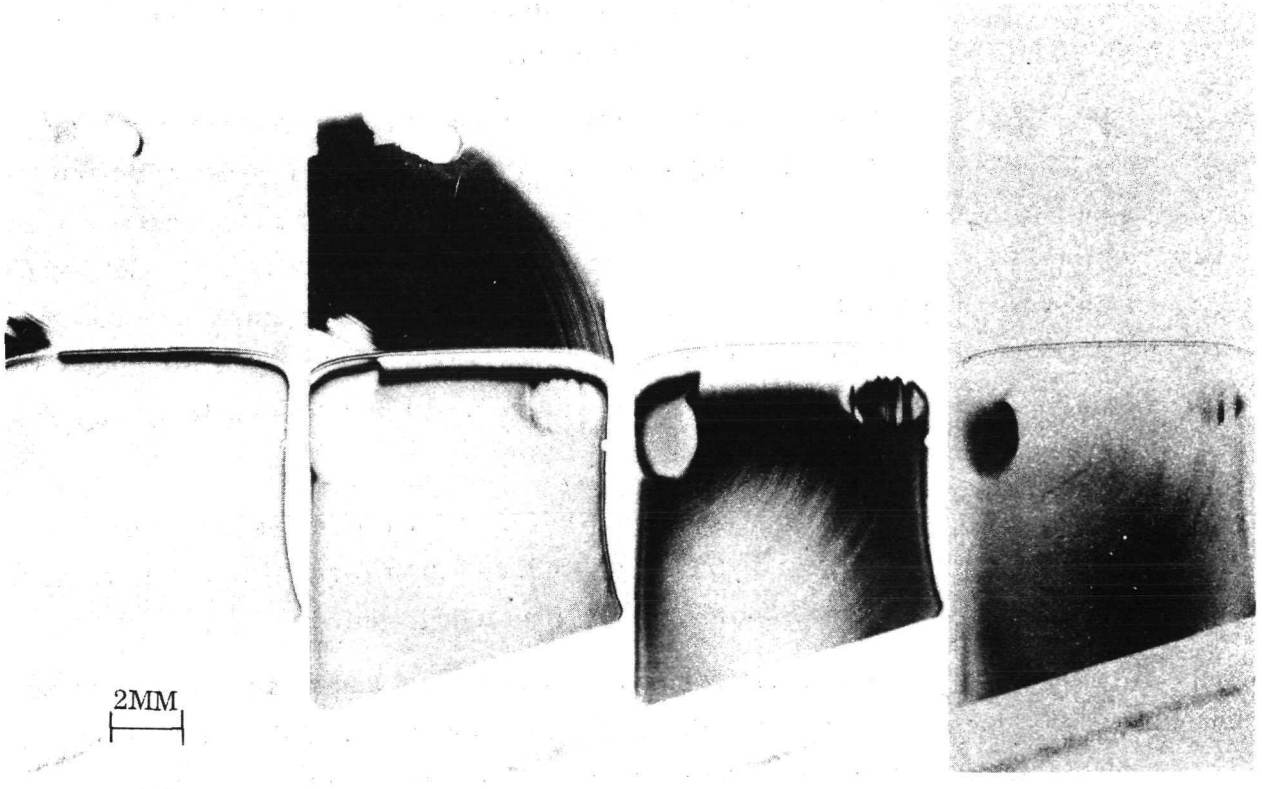

(a) (b) (c) (d)

FIG. 3
FeKα (842) Double Crystal Reflection Topographs Recorded at
Positions (a) - (d) on Rocking Curve Shown in Fig. 2

With a further increase in angle, topograph (c), the entire substrate is out of diffracting position. Now the epitaxial film diffracts strongly except for the central $\{211\}$ facet and portions of the outer $\{110\}$ facet. The unfaceted portion of the film is not imaged with uniform intensity, probably because of a slight compositional gradient.

In topograph (d) of Figure 3, corresponding to the largest Bragg angle, the central facet in the film and remaining portions of the outer facet have come into diffracting position while the unfaceted portion of the film is nearly out of position. This behavior is just the opposite of that observed in the substrate.

It is interesting that in Figure 3, the central facet of the film exhibits poor replication of the underlying substrate growth bands, although other regions of the film show very distinct replication. The reason for this is not completely understood. Another feature of these topographs is the existence of a strained region along the facet boundaries, particularly in the film.

The above example showed an LPE film; however, CVD films yield similar results. Figure 4 shows film and substrate topographs of a $\{111\}$ CVD sample of GdYGaIG on GdGaG. In this case there was a good separation of the film and substrate rocking curve peaks, so the topographs were obtained by the usual method (2) of setting the rotation angle to each of the two peak positions.

Since CVD samples have films on only one side, the film/substrate lattice parameter mismatch produces a slight specimen curvature. As a result, the entire specimen area is not uniformly imaged in the topographs. These topographs are somewhat similar to Renninger's zebra topographs (5), which are produced by deliberate misorientation of the specimen, and can be analyzed in a similar fashion. Topographs recorded at various positions along the rocking curve peaks show that the facet contrast in the film and substrate exhibits the same variation with rotation angle as was observed in the LPE sample of Figure 3.

The topographs in Figure 4 also show that the film replicates substrate growth bands and the strain field around an iridium inclusion (arrows). The strain along the facet boundary is extremely prominent in the film topograph.

In addition to the two specimens shown in Figures 3 and 4, several others have been examined including some with films in compression rather than in tension (4). In all cases the same variation of facet contrast with rotation angle was observed.

The demagnetized domain strip width, w, of the CVD film shown in Figure 4 was measured at the four locations indicated in the schematic diagram of Figure 5. The results of the measurements, shown in the figure, reveal a significantly higher strip

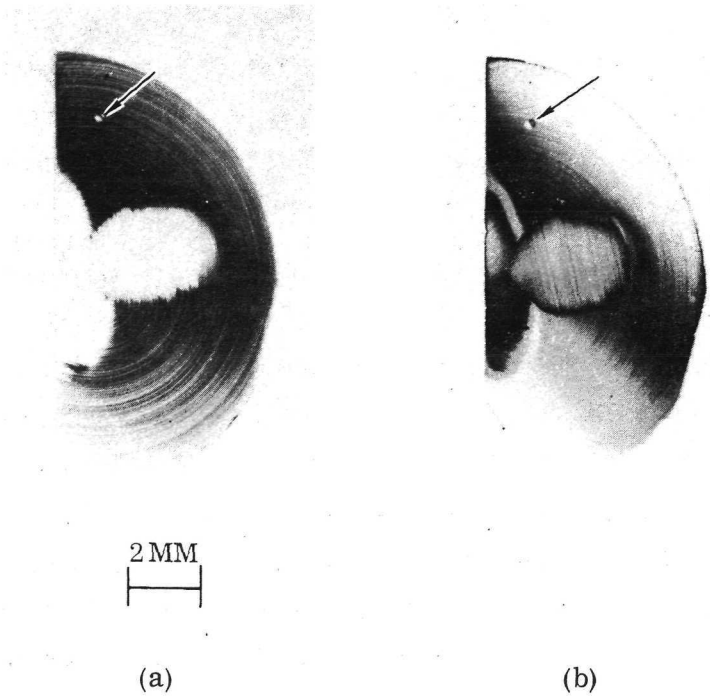

FIG. 4
FeKα (842) Double Crystal Reflection Topographs of {111} GdGaG Substrate With CVD Film of GdYGaIG; (a) Substrate, (b) Film

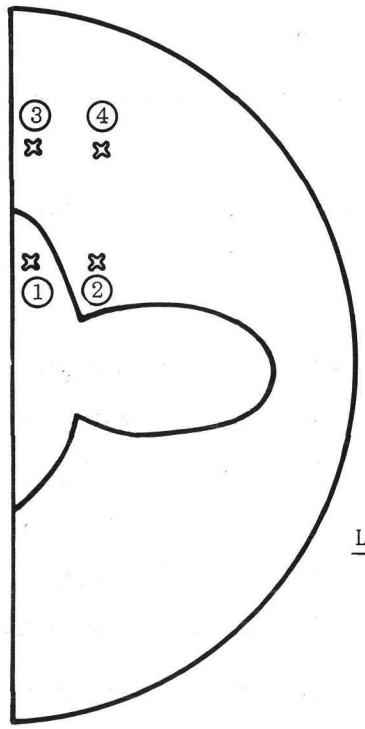

LOCATION	DOMAIN WIDTH
1	7.3 μm
2	6.2
3	6.4
4	6.3

FIG. 5
Domain Measurement Locations on Sample Shown in Fig. 4

width in the faceted region. Optical interferometry showed that the four points are in a region where the film thickness varies by less than 0.13 μm. Such thickness changes could not account for the observed domain size variation.

The magnetization, and characteristic length of the material were determined at the same four locations (6) and the domain wall energy was calculated. It was found that the magnetization was the same at all points but that the wall energy in the faceted region is 15 percent larger than its value outside.

Further evidence of the influence of the faceted region on the magnetic properties of the film was obtained by observing the domain pattern of the sample as it departs from a magnetically saturated state. As the bias field is reduced below the saturation value, reversal strip domains nucleate at the periphery of the sample due to the imperfections and thickness buildup there. The strip domains proceed into the interior of the disk in a random fashion as the field is further reduced. However, as the reversal domains approach the faceted region they appear to be repelled by the core boundary. Rather than penetrating into the faceted regions, the domains are deflected and follow the boundary so that the core region is outlined as a saturated region surrounded by a partially demagnetized region. Eventually the reversal domains do penetrate into the core region as the bias field is reduced still further. In the completely demagnetized state there is no evidence of preferential alignment of the domains in the plane of the film.

Discussion

The topographs showing the variation of core contrast with Bragg angle demonstrate that:

(a) In the substrate, the faceted region has slightly larger lattice parameter than the unfaceted region with the difference δa_s being 1 or 2 x 10^{-3} Å. This is the previously reported result (1).

(b) In the film the effect is just the opposite; the faceted region having a slightly smaller effective lattice parameter than the unfaceted region with the difference δa_f having a value approximating the substrate value δa_s.

In Figure 3, effect (b) was more clearly evident for the central $\{211\}$ facet than for the outer $\{110\}$. In part, this was due to the complications of the edge effects. However, it is also possible that δa_s is smaller for the $\{110\}$ facet than for the $\{211\}$.

The expression "effective lattice parameter" was used in (b) to emphasize the fact that the quantity actually measured was the difference in spacing of the (842) planes. This distinction is particularly significant in the film where it is necessary to give detailed consideration to the state of elastic strain. In the substrate, on the other hand, the faceted region is expanded in all directions with respect to the unfaceted region. This may be confirmed by diffraction measurements in other crystallographic

directions; however, the results of the magnetic measurements which will be discussed below demonstrate that the faceted region is expanded in directions parallel to the wafer surface.

The X-ray topography results, which are true for films in compression as well as for films in tension (as in Figures 3 and 4), are inconsistent with the earlier interpretation (3) that core replication is due to compositional adjustments in the film. The present results can be explained simply in terms of an elastic deformation of the film in response to the film/substrate lattice parameter mismatch. This may be understood with the aid of Figure 6 which shows the idealized lattice parameter distribution in the sample. Here a_s and a_f are the unstrained equilibrium values of the lattice parameters corresponding to the particular substrate and film compositions. The faceted region of the substrate has a slightly larger lattice parameter $a_s + \delta a_s$ due to a slight difference in composition (1).

Using a simple model in which the thick substrate is considered undeformed while the thin epitaxial film is strained isotropically and elastically to bring the film and substrate crystal lattices into registry across the interface (4,7,8), the perpendicular component of film strain e^{σ} is related to the parallel component e^{π} by

$$e^{\sigma} = -\frac{2\mu}{1-\mu} e^{\pi} \qquad (1)$$

where μ is the Poisson ratio of the film.

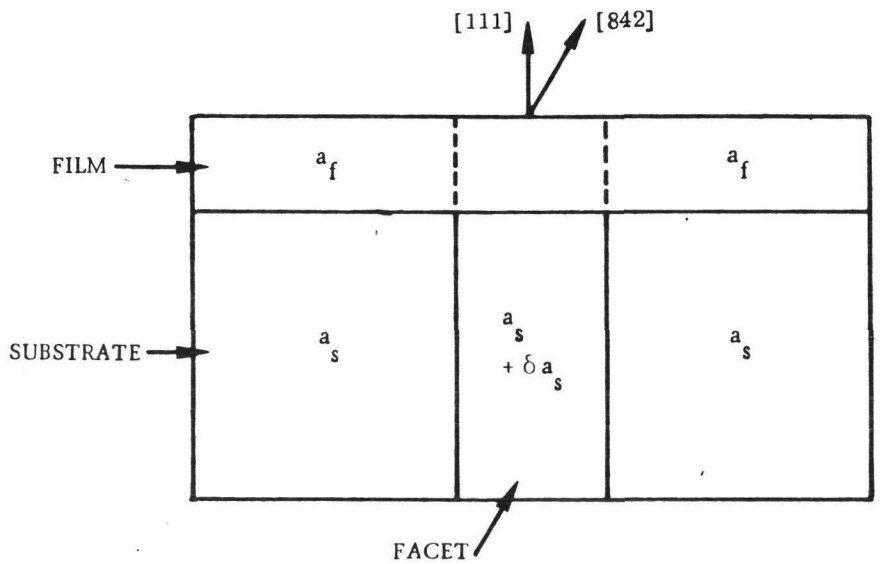

FIG. 6
Diagram of Lattice Parameter Distribution in Faceted Substrate with Epitaxial Film

In terms of the unstrained lattice parameters shown in Figure 6, e^{π} is $(a_s - a_f)/a_f$ in the unfaceted region and $(a_s + \delta a_s - a_f)/a_f$ in the faceted region. Similarly, e^{σ} is $(a_f^{\sigma} - a_f)/a_f$ in the unfaceted region and $(a_f^{\sigma} + \delta a_f^{\sigma} - a_f)/a_f$ in the faceted region; where a_f^{σ} is the lattice parameter of the film measured in the perpendicular direction and δa_f^{σ} is the perpendicular value of δa_f, the lattice parameter difference between faceted and unfaceted regions of the film. Assuming that Eq (1) is valid in the faceted region as well as in the unfaceted region, it follows that

$$\delta a_f^{\sigma} = -\frac{2\mu}{1-\mu} \delta a_s \tag{2}$$

Using the value $\mu = 0.29$ appropriate for yttrium iron garnet (9),

$$\delta a_f^{\sigma} = -0.82\, \delta a_s \tag{3}$$

Equation (3) shows that, for the perpendicular direction, the lattice parameter difference between the faceted and unfaceted regions of the film is determined by the corresponding lattice parameter difference in the substrate. Since δa_s is always positive (1), the faceted region of the film always has a smaller lattice parameter than the unfaceted region regardless of whether the film is in tension ($a_s > a_f$) or compression ($a_s < a_f$). Furthermore, δa_f^{σ} and δa_s are of the same order of magnitude.

In the present case Eq (3) is not directly applicable since lattice parameter differences were measured in the [842] direction rather than in the perpendicular direction. Qualitatively, the effects for [842] will be the same; however, the numerical factor in the equation will be less than 0.82. Furthermore, the earlier study of substrate facets (1) showed that, even apart from growth bands, it is not correct to treat a facet as a region of uniform lattice parameter.

Although certain approximations were made in deriving Eq (3), it does appear that this stress mechanism satisfactorily accounts for facet replication. This is supported by the magnetic domain observations.

The fact that the magnetization is the same at all four locations in Figure 5 strongly suggests that compositional differences between the faceted and unfaceted regions are not appreciable. The possibility that compensating changes in the Fe:Ga and Y:Gd ratios could occur to maintain a constant magnetization with varying composition cannot be ruled out; but this seems remote on the basis of the existing data. The differences in domain size and wall energy for the two regions are consistent with those expected from changes in the film stress. Indeed, the magnitude of these magnetic effects is in good agreement with that calculated by using a stress difference deduced from the measured lattice parameter differences (10). Since this film is in tension ($a_s > a_f$) and has negative magnetostriction, the fact that the wall energy is higher in

the faceted region shows that the substrate lattice parameter, parallel to the film surface, is larger in the faceted region than in the unfaceted region. Along with the X-ray results that $\delta a_s > 0$ in <842> directions, the magnetic data indicate that in all directions the substrate lattice parameter is larger in the faceted region than in the unfaceted region. The exclusion of the strip domains from the faceted region for the partially demagnetized film is also consistent with the higher wall energy in this region (11).

These observations have certain implications with regard to the use of the films in bubble domain memories. The differences in wall energy would have detrimental effects on bubble domain device operation since it would be harder to propagate a domain into the core than out of it. The operating margins of bubble generators presumably would also be different in the two regions. Furthermore, the growth bands in the substrate also produce wall energy variations in the films. This can result in an in-plane anisotropy associated with the growth bands; that is, it is easier to propagate domains parallel to the bands than perpendicular to them. However, if the bands are very diffuse and/or the variation in lattice constant associated with them is small these undesirable effects will be minimized.

If facet replication is accomplished directly by the varying stress exerted on the film due to the lattice parameter variations in the substrate, then a similar mechanism may be expected to play a role in growth band replication. This is presently under investigation. Recent results show that band replication is not sensitive simply to the lattice parameter difference between bands but to the gradient of this lattice parameter variation as well.

The earlier results which showed that certain YIG (yttrium iron garnet) films do not reproduce bands and facets (3) are in contradiction with the simple stress mechanism described above, since this stress should act without regard to the particular film composition. While it is possible that some compositional variations may accompany the stresses, for example a stress induced ordering or site preference involving the rare earth components, the YIG results must be considered inconclusive.

Conclusions

Previously it was shown that Czochralski grown garnet crystals may contain faceted regions which differ in lattice parameter from unfaceted regions. It was also shown that when epitaxial garnet films are deposited on faceted substrate crystals the facets are replicated by the films. The present study has demonstrated that this replication is brought about by the film stress which results from the film/substrate lattice parameter mismatch. Since there is a lattice parameter difference between the faceted

and the unfaceted regions of the substrate there is a difference in stress between the corresponding regions of the film. This stress difference results in differences in certain of the magnetic properties of the two regions of the film. For this reason the sources of substrate lattice constant variations, facets and bands, must be suppressed to obtain device quality samples. From the results obtained during this study it appears that restricting the variation in a_s to ≤ 0.0005Å across a substrate wafer is sufficient to avoid any undesirable magnetic effects.

Acknowledgements

LPE samples were provided by R. G. Warren. The support of NASA Langley Research Center, Hampton, Va. is acknowledged.

References

1. H. L. Glass, Mat. Res. Bull. 7, 1087 (1972).
2. H. L. Glass, Mat.Res. Bull. 7, 385 (1972).
3. H. L. Glass and T. N. Hamilton, Mat.Res. Bull. 7, 761 (1972)
4. P. J. Besser, J. E. Mee, P. E. Elkins and D. M. Heinz, Mat. Res. Bul. 6, 1111 (1971).
5. M. Renninger, J. Appl. Cryst. 5, 163 (1972).
6. D. C. Fowlis and J. A. Copeland, AIP Conf. Proc. No. 5, Magnetism and Magnetic Materials - 1971, p. 240 (1972).
7. R. Zeyfang, J. Appl. Phys. 41, 3718 (1970).
8. E. Klokholm, J. W. Matthews, A. F. Mayadas and J. Angilello, AIP Conf. Proc. No. 5, Magnetism and Magnetic Materials - 1971, p. 105 (1972).
9. T. B. Bateman, J. Appl. Phys. 37, 2194 (1966).
10. G. R. Pulliam and F. A. Pizzarello, in: Proc. 1972 Conf. on Magnetism and Magnetic Materials, to be published.
11. A. A. Thiele, Bell Syst. Tech. J. 50, 711 (1971).

REFERENCES

1. J. E. Mee, P. J. Besser, P. E. Elkins, H. L. Glass and E. C. Whitcomb, "Investigation of Single Crystal Ferrite Thin Film," Final Report NASA CR-112012, Contract NAS 12-522, Langley Research Center, National Aeronautics and Space Administration, Hampton, VA.

2. P. J. Besser, J. E. Mee, P. E. Elkins, and D. M. Heinz, "A Stress Model for Heteroepitaxial Magnetic Oxide Films Grown by Chemical Vapor Deposition," Mat. Res. Bull. 6, 1111 (1971).

3. P. J. Besser, J. E. Mee, H. L. Glass, D. M. Heinz, S. B. Austerman, P. E. Elkins, T. N. Hamilton and E. C. Whitcomb, "Film-Substrate Matching Requirements for Bubble Domain Formation in CVD Garnet Films," AIP Conf. Proc. 5, 125, (1972.)

4. L. K. Schick, J. W. Nielsen, A. H. Bobeck, A. J. Kurtzig, P. C. Michaelis, and J. P. Reekstin, "Liquid Phase Epitaxial Growth of Uniaxial Garnet Films: Circuit Deposition and Bubble Propagation." Appl. Phys. Letters 18, 89 (1971).

5. H. J. Levinstein, R. W. Landorf and S. Licht, "A Rapid Technique for the Heteroepitaxial Growth of Thin Magnetic Garnet Films," IEEE Trans. Magnetics, MAG-7, 470 (1971).

6. J. E. Geusic, H. J. Levinstein, S. J. Licht, L. K. Shick and C. D. Brandle, "Cylindrical Magnetic Domain Epitaxial Films with Low Defect Density," Appl. Phys. Letters 19, 93 (1971)

7. A. H. Bocheck, "Properties and Device Applications of Magnetic Domains in Orthoferrites," Bell System Tech. J. 46, 1901 (1967).

8. A. A. Thiele, "Theory of the Static Stability of Cylindrical Domains in Uniaxial Platelets," J. Appl. Phys. 41, 1139 (1970).

9. A. H. Bobeck, et al, "Uniaxial Magnetic Garnets for Domain Wall Bubble Devices," Appl. Phys. Lett. 17, 131 (1970).

10. J. E. Mee, D. M. Heinz, T. N. Hamilton and G. R. Pulliam, "Chemical Vapor Deposition of Epitaxial Magnetic Oxides," Invited paper at Symposium on Materials for Information Storage at Electrochemical Society Meeting, Los Angeles, May 1970.

11. J. E. Mee, G. R. Pulliam, D. M. Heinz, J. M. Owens and P. J. Besser, "Mobile Cylindrical Domains in Epitaxial Ga:YIG Films," Appl. Phys. Letters, 18, 60 (1971).

12. D. M. Heinz, P. J. Besser, J. M. Owens, J. E. Mee, and G. R. Pulliam, "Mobile Cylindrical Magnetic Domains in Epitaxial Garnet Films," Invited paper at 16th Annual Conference on Magnetism and Magnetic Materials, Miami Beach, Nov., 1970, J. Appl. Phys. 42, 1243 (1971).

13. M.D. Robinson, A. H. Bobeck, and J. W. Nielsen, "Chemical Vapor Deposition of Magnetic Garnets for Bubble Domain Devices, "IEEE Trans. Magnetics MAG-7, 464 (1971).

14. R. C. Taylor and V. Sadagopan, "Growth of Uniaxial Magnetic Garnet Films by a Simplified Methods of Chemical Vapor Deposition," Appl. Phys. Letters 19, 361 (1971).

15. S. T. Opresko, Jr. and H. L. Pinch, "Control of Product Phases in the Chemical Vapor Deposition of Garnet Films," Mat. Res. Bull. 7, 685 (1972).

16. B. C. McCollum, "The Growth of Complex Garnet Epitaxial Films with a Coaxially arranged CVD Reactor," AIP Conf. Proc. 10, 324 (1972).

17. A. I. Braginski, T. R. Oeffinger, R. W. Patterson and A. H. Charap, "Two Types of Bubbles in Garnet Films," AIP Conf. Proc. 10, 354 (1972).

18. Y. Sakurai, S. Ataka, S. Minagawa and F. Ishida, "Chemical Vapor Deposition of Epitaxial Aluminum-Substituted YIG for Bubble Domain Devices," IEEE Trans. Magnetics MAG-8, 298 (1972).

19. K. Kempter and W. Boegner, "Preparation of Epitaxial Magnetic Garnet Films by Chemical Vapor Deposition," Thin Solid Films 12, 35 (1972).

20. A. D. Milne, J. M. Owens, B. Solomons and S. J. Thornby, "The Effect of Structural Imperfections on Magnetic Properties of Epitaxial Garnet Bubble Films," AIP Conf. Proc. 10, 414 (1972).

21. R. L. Gentilman, "Chemical Vapor Deposition of YIG and Gallium: YIG--Growth of Epitaxial Films and a Thermodynamic Analysis," submitted to J. Appl. Phys.

22. L. K. Shick and J. W. Nielsen, "Liquid Phase Homoepitaxial Growth of Rare-Earth Orthoferrites," J. Appl. Phys. 42, 1554 (1971).

23. H. J. Levinstein, S. Licht, R. W. Landorf and S. L. Blank, "Growth of High-Quality Thin Films from Supercooled Melts," Appl. Phys. Letters 19, 486 (1971).

24. A. Rosencwaig, W. J. Tabor, F. B. Hagedorn and L. G. Van Uitert, "Noncubic Magnetic Anisotropies in Flux-Grown Rare-Earth Iron Garnets," Phys. Rev. Lett. 26, 775 (1971).

25. A. Rosencwaig, W. J. Tabor and R. D. Pierce, "Pair-Preference and Site-Preference Models for Rare-Earth Iron Garnets Exhibiting Noncubic Magnetic Anisotropics" Phys. Rev. Lett. 26, 779 (1971).

26. H. Callen, "Growth-Induced Anisotropy by Preferential Site-Ordering in Garnet Crystals," Appl. Phys. Lett. 18, 311 (1971).

27. A. J. Kurtzig and F. B. Hagedorn, "Noncubic Magnetic Anisotropies in Bulk and Thin Film Garnets," IEEE Trans. Magnetics, MAG-7, 473 (1971).

28. E. A. Giess, et al. "Europium-Yttrium Iron-Gallium Garnet Films Grown by Liquid Phase Epitaxy on Gadolinium Gallium Garnet," AIP Conf. Proc. 5, 110 (1972).

29. H. L. Glass, "X-ray Double Crystal Topography of Epitaxial Magnetic Bubble Domain Garnets," Mat. Res. Bull. 7, 385 (1972).

30. J. W. Matthews, E. Klokholm, V. Sadagopan, T. S. Plaskett and E. Mendel "Dislocations in Gadolinium Gallium Garnet ($Gd_3Ga_5O_{12}$) - I. Dislocations at Inclusions," Acta. Met. 21, 203 (1973).

31. H. L. Glass, "X-ray Topographic Analysis of Dislocations and Growth Bands in a Melt Grown Gadolinium Gallium Garnet Crystal," Mat. Res. Bull. 8, 43 (1973).

32. B. Cockayne and J. M. Roslington, "The Dislocation-free Growth of Gadolinium Gallium Garnet Single Crystals," J. Matls. Sci. 8, 601 (1973).

33. B. Cockayne, M. Chesswas and D. B. Gasson, "Faceting and Optical Perfection in Czochralski Grown Garnets and Ruby," J. Matls. Sci. 4, 450 (1969).

34. C. D. Brandle, D. C. Miller and J. W. Nielsen, "The Elimination of Defects in Czochralski Grown Rare-Earth Gallium Garnets," J. Crystal Growth 12, 195 (1972).

35. H. L. Glass, "X-ray Double Crystal Analysis of Facets in Czochralski Grown Gadolinium Gallium Garnet," Mat. Res. Bull. 7, 1087 (1972).

36. H. L. Glass, P. J. Besser, T. N. Hamilton and R. L. Stermer, "Substrate Facet Replication by Epitaxial Magnetic Garnet Films," Mat. Res. Bull 8, 309 (1973).

37. M. A. Zuegel, "Vapor Phase Equilibria in the Gallium-Chlorine and Gallium Arsenide - Chlorine Systems," J. Electrochem. Soc. 112, 1153 (1965).

38. R. W. Shaw, R. M. Sandfort and J. W. Moody, "Magnetic Bubble Materials - Characterization Techniques Study Report," MRC-SL-339, Final Report, Contract No. DAA H01-72-C-0490, Advanced Research Projects Agency, Washington, D.C.

39. D. C. Miller, "Chemical Polishing of Garnets with Phosphoric Acid." To be published in J. Electronic Matls.

40. J. A. Cape, "Dynamics of Bubble Domains," J. Appl. Phys. 43,3551 (1972)

41. W. A. Bonner, et al, "Characteristics of Stable Eu-Based Garnet Films for Magnetic Bubble Applications" J. Appl. Phys. 43,3226 (1972).

42. S. L. Blank, et al, "Kinetics of LPE Growth and Its Influence on Magnetic Properties," AIP Conf. Proc. 10, 256 (1973).

43. D. H. Smith and J. C. North, "Annealing of Magnetic Properties of Ion Implanted Garnet Epitaxial Films," AIP Conf. Proc. 10, (1973).

44. A. H. Bobeck, R. F. Fischer, A. J. Perneski, J. P. Remeika and L. G. Van Uitert, "Application of Orthoferrites to Domain Wall Devices," IEEE Trans. Magnetics, MAG-5, 544 (1969).

45. A. J. Perneski, "Propagation of Cylindrical Magnetic Domains in Orthoferrites", IEEE Trans. Magnetics Mag-5, 554 (1969).

46. M. Ohring, "Electromigration Damage in Thin Films due to Grain Boundary Grooving Processes" J. Appl. Phys. 42,2653, (1971).

47. Y. S. Lin, "Analysis of Permalloy Circuits for Bubble Domain Propagation," IEEE Trans. Magnetics Mag-8, 375 (1973).

48. C. H. Hsin, T. J. Matcovich and R. L. Coren, "Measurement of Bubble Drive Fields in a T-Bar Configuration," AIP Conf. Proc. 5, 244 (1972).

49. J. P. Jan, Solid State Physics, 5, p. 15, edited by F. Seitz and D. Turnbull, Academic Press (1957).

50. M. Prutton, Thin Ferromagnetic Films, Butterworths (1964).

51. R. F. Bailey and J. L. Williams, "Temperature Step Anneal Effects on the Physical and Magnetic Properties of Permalloy Films," Electrochemical Society Conference, Chicago, Ill. May 1973.

52. J. M. Robertson, private communication.

NEW TECHNOLOGY APPENDIX

A major accomplishment of this program was the demonstration that the CVD process is capable of producing low defect density films of epitaxial garnets with excellent uniformity of thickness and composition across a 1 in. diameter substrate. Other significant advances achieved on the program were:

1. Growth of uncrazed films of complex garnet compositions from a single metal alloy source.

2. Establishment of the lattice mismatch mechanism of film replication of substrate cores and bands and the implications that this has with regard to film magnetic properties.

3. Development of several substrate boule and wafer acceptance criteria.

4. The first 16 μm period shift register ever delivered to a government agency was fabricated on this contract.